第 65 回 ポーラログラフィーおよび電気分析化学討論会 要旨集

＜全講演＞

討論主題

「アジアへ拡がる電気分析化学の真髄」

2019 年 11 月 6 日（水）～ 8 日（金）

国立台湾大学　知武館　高坂記念講義室

2019 年 11 月 13 日　公開

SI1 Fundamentals and Applications of Redox Enzyme-functionalized Electrode Reactions

Kenji Kano (Division of Applied Life Science, Graduate School of Agriculture, Kyoto University, Kyoto, Japan)

Oxidoreductases (redox enzymes) are concerned with widespread biological electron transfers, *i.e.* processes of respiration, fermentation, and photosynthesis to catalyze electron transfer reactions across the tree of life and to facilitate biologically driven fluxes of several elements such as hydrogen, carbon, nitrogen, oxygen, and sulfur on Earth. The kinds of the redox enzymes are approximately one-quarter of all known enzymes based on enzyme nomenclature.

Redox enzymes use a palette of redox components called coenzymes, prosthetic groups, or cofactors: β-nicotine amide dinucleotides (phosphate) ($NAD(P)^+$), flavins, quinones, hemes, ion-sulfur clusters, copper, molybdenum, nickel, etc. NAD^+- and $NADP^+$-dependent enzymes catalyze hydride ion transfers in main streams of catabolism and anabolism, respectively. Core redox enzymes are ancient and highly diverse in amino acid sequence, and usually require specific transition metals in their active site to catalyze (multi-step) single-electron transfers. On the other hand, flavoproteins and quinoproteins can catalyze both two-step single-electron transfer and hydride ion transfer and link the electron transfer between several organic redox substances and inorganic redox-centers in metal-containing redox enzymes.

Over the last four decades, redox enzymes have received much attention for use in the coupling of the enzyme reactions in electrochemical reactions. The coupled reaction is known as bioelectrocatalysis. It has become an important technology that can be applied to a wide range of bioelectrochemical devices including biosensors, biofuel cells, and bioreactors.

In this lecture, electrochemistry of several quinone cofactors is briefed. An overview of the basic concepts of steady-state catalytic waves of mediated- and direct electron transfer (DET)-type bioelectrocatalysis is also presented. Several equations that can be used for the analysis of steady-state waves are introduced. The analysis may provide important thermodynamic and kinetic parameters that can be used not only for performance evaluation of the devices but also for fundamental research on the enzymes. Important progress made on how to tune electrode surfaces and enzymes for DET-type reactions are presented. Applications to bioelectrochemical devices are also summarized with emphasis on the achievements recorded in my research group.

S1 Spectroelectrochemical Study on Reduction Processes of Noble Metal and Actinide Ions

Akihiro Uehara (National Institute of Radiological Sciences, National Institutes for Quantum and Radiological Science and Technology, Chiba, Japan)

A fundamental analysis of a metal reduction process is of important for the development on metal plating, electric refining, and nanoparticle synthesis. Electrochemical and spectroelectrochemical methods have been applied for the mechanistic analysis of the noble metal nanoparticles formation as well as the actinide reduction. Ionic species and electron transfer reactions at the interface between aqueous and organic solutions were measured by charge transfer voltammetry at liquid|liquid interface. Chemical status and redox characteristics of actinide ions in various solutions such as water, organic solutions, molten salts, highly concentrated electrolytes were studied by electrochemical methods combined with in-situ X-ray absorption spectroscopy.

(1) Brust-Schiffrin nanoparticle synthesis The mechanism of the Brust-Schiffrin gold nanoparticle synthesis has been investigated through the use of ion transfer voltammetry at the water|organic solutions interface, X-ray absorption fine structure in the reaction between $[AuCl_4]^-$ and thiol in homogeneous organic solution. The species $[AuBr_4]^-$ is shown to be a preferable precursor in the method as it is more resistant to the formation of Au(I) thiolate species than $[AuCl_4]^-$. This new mechanistic understanding should enable nanoparticle synthesis with a higher yield and reduce particle size poly dispersity.

(2) Metal deposition at the liquid|liquid interface Electron transfer was observed voltammetrically at the interface between water containing both Au precursors and organic solution containing triphenylamine as reducing agent. Au particles, formed by constant potential electrolysis at the water|organic solutions interface, were examined by transmission electron microscopy. It was shown that deposit size was controlled via the applied potential and time, with specific conditions to form particles of less than 10 nm identified. Here, aqueous chloride ion concentrations and pH influence the interfacial reaction through the ligand exchange equilibria between $[AuCl_4]^-$, $[AuCl_3(OH)]^-$ and $[AuCl_2(OH)_2]^-$.

(3) Spectroelectrochemistry of uranium reduction The reduction mechanism of uranium U(VI) was investigated by in-situ X-ray absorption spectroscopy during controlled constant current electrolysis. Formal potential for the reduction of UO_2^{2+}/U^{4+} was determined based on equilibrium potential and radial distribution function of uranium.

S2 Bioelectrochemical studies on oxidoreductases and natural polyamino compounds

Kohei Uematsu (Department of Bioscience and Biotechnology, Fukui Prefectural University, Fukui, Japan)

It has been well known that electroanalytical methods are quite useful tools for analysis of biologically-relevant materials, such as quantification and evaluation of the redox potential, and elucidation of the biological functions and properties of the materials. As might be expected, some of the analytical works can only be performed by the electrochemical methods. I have conducted studies for revealing advantages of the electrochemical method, and studies for elucidating the function and property of biological materials using electrochemical methods, specifically (i) electrochemical method for analysis of enzymatic inhibition reaction, (ii) effect of polyamino compounds on enzymatic reactions of glucose oxidase, and (iii) ion transfer voltammetry of polyamino compounds at liquid | liquid interface. In this presentation, I will introduce some of interesting findings in the study of (ii).

Effect of polyamino compounds on enzymatic reactions of glucose oxidase

In the enzymatic reaction, ionic charges of substrates sometimes have a big influence on the enzymatic reaction rates. One of such reactions is the enzymatic reaction of glucose oxidase (GOx). In the enzymatic reaction, the general oxidant is oxygen. However, GOx can also react with various inorganic or organic oxidants, and the reaction rate tends to become slow as the oxidant is more negatively charged. The tendency of the reaction rate is interpretable by the electrostatic interaction between negatively charged GOx and oxidants. If the electrostatic interaction plays a critical role in the enzymatic reaction rate, a modifier of the electrostatic interaction may also be important for determining the reaction rate.

We investigated the effect of natural polyamino compounds, ε-poly-L-lysine (εPL) and its related compounds, on the GOx reaction. These compounds exist as polycation under acidic and neutral pH conditions, and are expected to interact with the negatively charged GOx. Interestingly, the effect of εPL on the GOx reaction dramatically changed depending on the charge of the oxidants. The GOx reaction with the negatively charged oxidant was significantly promoted by εPL, while the reaction with positively charged one was fairly suppressed by εPL. This result suggests that the effect of εPL is determined by the electrostatic interaction among GOx, εPL and oxidant. The promotion effect of polyamino compound became extremely large under a certain condition. Thus, the promotion effect is applicable to the improvement of the glucose biosensor and to the development of a sensitive analytical method for the polyamino compounds.

S3 Determination of Bioactive Compounds by Highly Sensitive Electrochemical Detection in Liquid Chromatography

Akira Kotani (School of Pharmacy, Tokyo University of Pharmacy and Life Sciences, Tokyo, Japan)

Various electrochemical detections (ECDs) for determining bioactive compounds were developed to hyphenate with liquid chromatography (LC-ECD) systems, and these LC-ECD systems were shown to have enough sensitivity and precision to apply for the analyses of biological and herbal medicine samples.

1. LC-ECD for determining femtogram levels of flavonoids

An LC-ECD is an attractive method for determining bioactive redox compounds, because ECD is highly sensitive and selective for the detection of redox compounds. And, the miniaturization of the entire system using capillary column (i.d., 0.2 mm) was especially contributed to establish highly sensitive LC-ECD, resulting in electrochemical determinations of catechins and baicalein at femtogram levels. [1] This LC-ECD was applied to examine the time courses of catechin concentrations in human plasma after green tea administration.

2. Multi-channel LC-ECD for analysis of herbal medicines

In order to simultaneously analyze the compounds that possess different hydrophobic properties with good separation, high sensitivity and efficiency, an LC with multi-channel isocratic elution ECD (LC-*n*ECD) was proposed using a new design of channel connections and the technique of alternate rotations of switching valves. Phenylethanoid glycosides in *Magnolia officinalis* roots and caffeoylquinic acids and flavonoids in *Chrysanthemum morifolium* flowers were determined by an LC-2ECD [2] and an LC-3ECD, [3] respectively, and quality assessment of herbal medicines were performed by these LC-*n*ECD systems.

3. LC-ECD for determining electro-inactive acids based on the reduction of quinone

Voltammetric acid sensing based on the reduction of 3,5-di-*tert*-butyl-1,2-benzoquinone (DBBQ) was applied to determine electro-inactive acid compounds, such as valproic acid (VPA) and polyunsaturated fatty acids (PUFAs). The present ECD was hyphenated with an LC system, and the LC-ECD system was provided as a quantitative analytical method for pharmacokinetic studies of VPA and PUFAs in plasma. [4,5] Moreover, a novel electroanalytical method for determining electro-inactive amino acids was proposed by the present method coupled with a concept of back neutralization titration. [6]

In conclusion, these LC-ECD systems with sensitivity produced a practically useful method for determining bioactive compounds in biological and herbal medicine samples.

Reference: [1] *J. Pharm. Biomed. Anal.*, 2008. [2] *J. Pharm. Biomed. Anal.*, 2018. [3] *Anal. Sci.*, 2015. [4] *J. Pharm. Biomed. Anal.*, 2014. [5] *Anal. Sci.*, 2016. [6] *Electroanalysis*, 2018.

K1 Structure and reactions at the liquid-liquid interface of ionic liquids

Naoya Nishi (Department of Energy and Hydrocarbon Chemistry, Graduate School of Engineering, Kyoto University, Kyoto, Japan)

Ionic liquids (ILs) are promising materials for electrochemical devices. To maximize the performance of such devices, it is important to understand and control the molecular-level structure of ILs at the electrochemical interfaces. Several unique features have been found at the IL interfaces. The most prominent one would be the spontaneous formation of ionic multilayers at the IL interfaces, revealed using interface-selective techniques such as x-ray reflectometry (XR) [1-4], neutron reflectometry (NR) [5], and molecular dynamics (MD) simulation [6,7]. From the electrochemical point of view, the behavior of ILs in the electrical double layer (EDL) is also unique due to excluded-volume and local-coulombic interactions between neighboring ions, leading to camel-shape potential dependence of the capacitance confirmed by NR [5], MD [7], and zero-frequency capacitance measurements [8-10]. In this presentation, I will focus on the structure at the liquid/liquid electrochemical interface of ILs, such as the IL/water, IL/mercury, and IL/oil interface. I will also introduce an application of such soft interfaces of ILs as formation sites for unique nanostructures of metals such as Au [11-14], Pt [15], and Pd [14,16].

References

[1] N. Nishi, Y. Yasui, T. Uruga, H. Tanida, T. Yamada, S. Nakayama, H. Matsuoka, T. Kakiuchi, *J. Chem. Phys.*, 132 (2010) 164705.
[2] N. Nishi, T. Uruga, H. Tanida, T. Kakiuchi, *Langmuir*, 27 (2011) 7531.
[3] N. Nishi, T. Uruga, H. Tanida, *J. Electroanal. Chem.*, 759 (2015) 129.
[4] S. Katakura, K. Amano, T. Sakka, W. Bu, B. Lin, M. Schlossman, N. Nishi, *to be submitted*.
[5] N. Nishi, J. Uchiyashiki, Y. Ikeda, S. Katakura, T. Oda, M. Hino, N.L. Yamada, *J. Phys. Chem. C*, 123 (2019) 9223.
[6] S. Katakura, N. Nishi, K. Kobayashi, K. Amano, T. Sakka, *J. Phys. Chem. C*, 123 (2019) 7246.
[7] S. Katakura, N. Nishi, K. Kobayashi, K. Amano, T. Sakka, *to be submitted*.
[8] N. Nishi, A. Hashimoto, E. Minami, T. Sakka, *Phys. Chem. Chem. Phys.*, 17 (2015) 5219.
[9] N. Nishi, S. Yasui, A. Hashimoto, T. Sakka, *J. Electroanal. Chem.*, 789 (2017) 108.
[10] N. Nishi, Y. Kojima, S. Katakura, T. Sakka, *Electrochemistry*, 86 (2018) 38.
[11] N. Nishi, T. Kakinami, T. Sakka, *Chem. Commun.*, 51 (2015) 13638.
[12] N. Nishi, I. Yajima, K. Amano, T. Sakka, *Langmuir*, 34 (2018) 2441.
[13] S. Takagi, N. Nishi, T. Sakka, *Chem. Lett.*, 48 (2019) 589.
[14] Y. Zhang, N. Nishi, T. Sakka, *Electrochim. Acta, in revision*.
[15] Y. Zhang, N. Nishi, K. Amano, T. Sakka, *Electrochim. Acta*, 282 (2018) 886.
[16] Y. Zhang, N. Nishi, T. Sakka, *ACS Appl. Mater. Interfaces*, 11 (2019) 23731.

K2 Hydrophobicity and Pseudo-Capacitance Control of Polyaniline for Solid-Contact Ion-Sensing

Yu-Fu Chen, Yi-Min Wu, and Lin-Chi Chen* (Department of Biomechatronics Engineering, National Taiwan University, Taipei, Taiwan)

Introduction: Solid-contact (SC) ion-sensing is an emerging solid-state ion sensor technology, which uses an electroactive SC layer (*e.g.*, a conducting polymer) to replace the bulky internal reference solution in an ion-selective electrode (ISE) and eliminates the use of silver electrodes. Thus, it has the advantages of size, cost, fabrication flexibility and miniaturization. In principle, an SC layer conducts ion-to-electron transduction (IET) to convert the concentration of a target ion (detected by an ion-selective membrane, ISM) into an electrical potential signal (measured at the electrode) through a field effect. Moreover, an ideal SC layer must be able to resist the permeation of a water layer from the sample solution to avoid interfering ions. Hence, an SC layer with high hydrophobicity and pseudo-capacitance is favored. Here, we report a novel idea for attaining high hydrophobicity and pseudo-capacitance of a polyaniline (PANI) SC layer at the same time via deposition control and demonstrate its benefits for SC ion-sensing.

Experimental: The PANI SC layer was electrodeposited on a screen-printed carbon electrode (SPCE) in a monomer bath via cyclic voltammetry (CV). The CV deposition rate (mV/s) was tuned to control the film thickness and surface morphology of PANI. SEM, contact angle (CA), and electrochemical measurements were done to characterize the PANI layers grown at different CV deposition rates. The SC-ISEs of Na^+, K^+, Cl^-, and Ca^{2+} were fabricated with different PANI SC layers and corresponding ISMs coated atop. The sensing performance factors of the SC-ISEs were then studied with respect to the hydrophobicity and pseudo-capacitance of PANI.

Results and discussion: The CV deposition is an effective method to tune the hydrophobicity and pseudo-capacitance of a PANI SC layer. When the CV deposition rate is slower than 20 mV/s, a thick film with a nano-fibrous surface is formed so that the quasi-superhydrophobicity (CA = 138^o) and high pseudo-capacitance (up to 4.61 mF) are attained. By contrast, the film grown faster (with the rate > 50 mV/s) has a decreased CA (< 85^o) and capacitance value (< 0.95 mF). Therefore, the SC-ISEs fabricated with the PANI layer grown slower show enhanced performance factors, including high sensitivity, high water layer resistance, low potential drift, and low detection limit as compared to those with the PANI layer grown faster.

K3 Nanoscale Electrochemical Imaging of Single Nuclear Pore Complexes

Shigeru Amemiya (Department of Chemistry, University of Pittsburgh, Pennsylvania, USA)

Introduction: In this presentation, the application of nanoscale scanning electrochemical microscopy (SECM) for the imaging of single nuclear pore complexes (NPCs) is discussed. The NPC solely transports both small molecules and macromolecules between the nucleus and cytoplasm of a eukaryotic cell to play imperative biological and biomedical roles. The NPC is crucial to the regulation of gene expression and is linked to many human diseases including cancers and neuronal diseases. In this work, we enable SECM permeability imaging of single NPCs with a spatial resolution of ~30 nm. The spatial resolution is high enough to distinguish "plugged" and "unplugged" states of NPC. We determine the impermeability of "plugged" NPC to unambiguously conclude that plugs are not permeable central transporters of the NPC but are impermeable cargos, e.g., ribonucleoproteins, captured during translocation through the NPC. These two origins have been debated for decades because they cannot be distinguished by structural imaging of plugged NPCs using cryoelectron tomography and atomic force microscopy.

Experimental: Permeability imaging by nanoscale SECM was established for single solid-state nanopores by our group[1,2] and applied for single NPCs in this work. Nanopipet-supported interfaces between two immiscible electrolyte solutions were employed as nanotips with diameters of ~30 nm. A homebuilt SECM instrument with an isothermal chamber was used to image the nuclear envelope of the *Xenopus* oocyte nucleus in buffer solutions after the nuclear envelope was spread on a glass plate and fixed by glutaraldehyde.

Results and discussion: SECM images of individual NPCs were obtained successfully by scanning ~30 nm-diameter nanopipet tips to electrochemically detect small probe ions, i.e., tetrabutylammonium. The tip current decreased as the tip moved over each NPC, which hindered the diffusion of probe ions to the tip. The density of NPCs in the SECM images agreed with that determined by AFM. The cross-sections of SECM images of plugged NPCs fitted well with finite element simulation of an impermeable pore to indicate that the plug is a captured macromolecule, which blocks the NPC, not a transporter, which is highly permeable to small probe ions.[3]

[1] M. Shen, R. Ishimatsu, J. Kim, and S. Amemiya, *J. Am. Chem. Soc.* **2012**, *134*, 9856.

[2] R. Chen, R. J. Balla, A. Lima, and S. Amemiya, *Anal. Chem.* **2017**, *89*, 9946.

[3] P. Pathirathna, R. J. Balla, G. Meng, Z. Wei, and S. Amemiya, *Chem. Sci.* **2019**, *10*, 7929.

K4 More than a Liquid Junction: Effect of Stirring, Flow Rate, and Inward and Outward Electrolyte Diffusion on Reference Electrodes with Nanopore and Capillary Junctions

Evan L. Anderson, Blair K. Troudt, and Philippe Bühlmann (Department of Chemistry, University of Minnesota, Minneapolis, USA)

Introduction: As electroanalytical sensors based on novel materials have reached exceptional stabilities with drifts in the low uV/h range and long-term and calibration-free measurements gain more and more attention, reference electrode designs that used to be satisfactory for most users do not satisfy the needs of new challenging applications.

Nanoporous Glass Frits: The Henderson equation is usually used to calculate liquid junction potentials between miscible electrolyte solutions. However, the potentials of reference electrodes that comprise an electrolyte-filled nanoporous glass frit may also be affected by charge screening. When the Debye length approaches or surpasses that of the glass pore diameter, reference potentials depend on the composition of the bridge electrolyte, the pore size of the frit, and the concentration of electrolyte in the sample. Stirring of samples may alter the reference potential as it affects the electrolyte concentration in the section of the nanoporous glass frits that is facing the sample solution. When the flow rate of bridge electrolyte into the sample is small, convective mass transport of sample into the nanoporous frit occurs. The depth of penetration into the frits is only a few nanometers but—despite the use of concentrated salt bridges—this is enough to affect the extent of electrostatic screening when samples of low ionic strength are measured. Importantly, because flow through nanoporous frits is slow, mass transport through such frits is dominated by diffusion. Consequently, reference electrode frits with low flow rates become contaminated with sample components.

Capillary Junctions: Commonly used reference electrodes with free-flowing junctions often suffer either from experimental difficulties in assuring a minimum flow rate or from excessive flow rates that require frequent replenishing of bridge electrolyte. To this end, we developed a reference electrode which contains a concentrated electrolyte that contacts samples through a 10.2 μm capillary. By applying a minimal pressure of 10.0 kPa, a flow rate of 100 nL/h is achieved. This maintains a constant liquid junction potential, as evidenced by a potential stability of 0.7 ± 4.8 μV/h.

K5 Mechanism of Emulsion Formation in an Organic Solvent in the Presence of Hydrated Ions

○ Vladimír Mareček
J. Heyrovský Institute of Physical Chemistry of ASCR, v.v.i., Prague, Czech Republic

A two-electrode cell comprising a liquid/liquid interface has been used to study the water clusters formation in the organic solvent phase following the tetraalkylammonium chloride (TAACl) transport from the aqueous phase. The partition of chloride ions is controlled by the interfacial potential difference induced by the distribution of a common TAA^+ ions in both phases. The transfer of hydrated chloride ions is accompanied by the transfer of TAA^+ ions which concentration

at the aqueous side of the interface can be monitored by the open circuit potential (OCP) measurement. The amount of TAACl transported at a given potential to the organic phase exceeds amount of TAACl which could be dissolved. It results in the water clusters formation in the organic solvent phase. The presented mechanism of this process involves an additional water transport to the organic phase completing dissolved water consumed by the water clusters formation. At higher concentration of TAACl in the aqueous phase this process leads to the formation of emulsion in the organic phase.

The analysis of OCP transients lead to the following mechanism of the water clusters formation In the first step the TAACl is transported to the organic phase to fulfill the partition of chloride anions. In the next step the chloride ions dissolved in the organic phase form the water clusters utilizing the initial presence of water in the organic phase and water transported by chloride ions. The expended water in the organic phase is replenish by its diffusion from the aqueous phase to fulfill the equilibrium. At any distance from the interface the partition of TAACl between the organic phase and the water clusters must be fulfilled. It can be expected that the partition of TAACl will be influenced by the water cluster size.

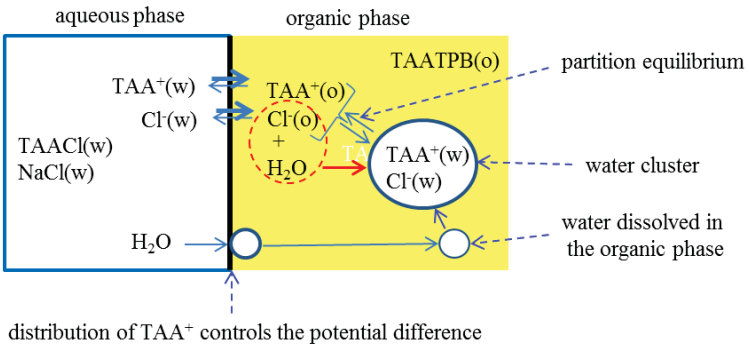

Figure 1: A cartoon depiction of the mechanism of water clusters formation at a water/organic solvent interface associated with the superfluos extraction of TAACl into the organic phase.

The financial support from the Czech Science Foundation (project number 17-09980S) is gratefully acknowledged.

[1] V. Mareček, Electrochem. Commun., 88 2018, 58–60.
[2] K. Holub, Z. Samec, V. Mareček, Electrochim. Acta, 306 2019, 541-548.

K6 Extracellular Electron Transfer: How about Different Mechanisms Run in Parallel?

Shiue-Lin Li[1] ([1]Department of Environmental Science and Engineering, Tunghai University, Taichung City, Taiwan)

Introduction:

In order to reduce solid-state electron acceptor, microorganisms need to carry out extracellular electron transfer (EET) mechanisms to facilitate respiration. Bacterial nanowires are specialized appendages that provide a larger surface area and a possible way for non-motile cells to attach to the desired solid-state electron acceptors over a long distance. In addition to bacterial nanowires, it has been found that some bacteria are capable of secreting flavins that can boost current generation. It is undoubted that EET capable bacteria are versatile, which is possibly carry out multi mechanisms simultaneously to implement a smooth respiration with solid-state electron acceptor. Since it is a booming era for EET study, in this talk, I will collect the results people have found in these year to point out that there are still something unclear about EET-capable microorganisms.

Experimental:

Atomic force microscopy was used to explore bacterial nanowires, and cyclic voltammetry was used to understand the electrochemical characteristics of microbial electrodes.

Results and discussion:

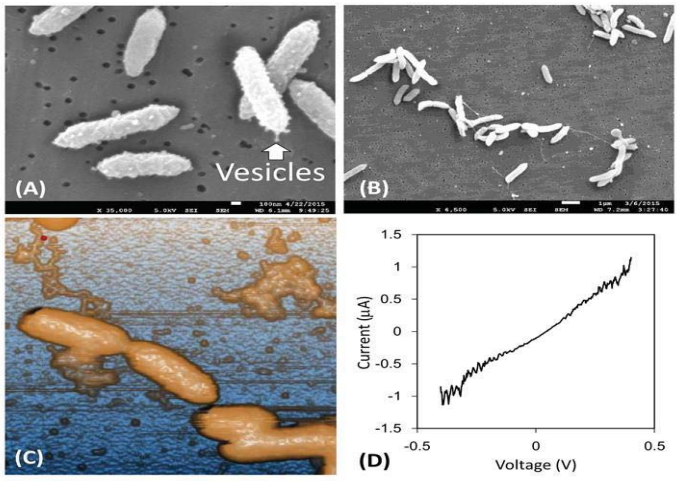

Figure. *Geobacter sulfurreducens* PCA growth pattern in a chemostat (A) a vesicle-like structure formation; (B) a bacterial nanowire structure observed; (C) bacterial nanowire observation using contact atomic force microscopy; (D) conductance measurement of the bacterial nanowire.

K7 Carbon Nanotube Platform for Bioelectrochemistry

Masato Tominaga
Graduate School of Science and Engineering, Saga University, Saga, Japan
masato@cc.saga-u.ac.jp

Carbon nanotubes have some advantages as an electrode such as high electric conductivity and high surface area. On the other hand, there are some disadvantages such as defects (carbon oxidized functional group), impurity compounds and bundled structure, which would relate to a lack of repeatability. I would introduce my previous researches [1] and discuss the advantage and disadvantage of carbon nanotubes in bioelectrochemistry.

1. Preparation of single-walled carbon nanotube modified electrode

We synthesized single-walled carbon nanotubes (SWCNTs) ourselves because of repeatability. The SWCNTs were directly synthesized on a metal and a carbon surface by using CVD method. For bioelectrochemistry, the SWCNTs were synthesized on a gold electrode. The SWCNT synthesis was perfectly controlled the synthesis conditions, especially humidity, which produces exactly same SWCNTs each synthesis in the viewpoint of the defect, diameter and bundled structure of the SWCNTs. Our synthesized SWCNTs were 1~2 nm in a diameter, and very few defect from results of TEM and Raman spectroscopy.

2. Bioelectrochemisty at SWCNT

Cytochrome c: Cytochrome c is one of the typical standard redox protein to understand the surface condition. The redox reaction of cytochrome c was not observed at as-grown, high-quality SWCNTs. Well-defined diffusion-controlled redox wave of cytochrome c was observed at SWCNTs with oxidized carbon species such as C-O, C=O and O-C=O induced by UV-ozone treatment. The redox reaction was inhibited immediately by SWCNT surface contamination when the SWCNT was exposed under atmosphere.

NADH: Two main oxidation peaks of β-nicotinamide dinucleotide (NADH) at the SWCNTs were due to adsorbed and diffused species, which was strongly related to the SWCNT surface defect.

Laccase: The interface between laccase and SWCNTs was improved by modification with the steroid biosurfactant, especially sodium cholate, resulting in obtaining large catalytic O_2 reduction current at starting from a potential very close to the redox equilibrium potential of the oxygen/water couple.

References

[1] M. Tominaga et al., *Colloids and Interfaces*, **2**, paper No. 33 (2018); *J. Electroanal. Chem.*, **800**, 156 (2017); *New J. Chem*., **41**, 231 (2017); *Anal. Chem.*, **87**, 5417 (2015).

K8 Improvement of optical properties for cadmium-free quantum dot fluorophores

Taro Uematsu (Graduate School of Engineering, Osaka University, Japan)

Introduction: Semiconductor nanoparticles (quantum dots, QDs) are photoluminescent (PL) materials represented by cadmium selenide (CdSe), and they have recently been applied to the color conversion materials used in display devices due to prominent monochromaticity of their PL. Unfortunately, the use of cadmium compounds is no longer allowed for commercial products and alternative materials have been proposed. Silver indium sulfide ($AgInS_2$) QDs are one of the cadmium-free candidates that our group have contributed to development, but the lack of PL monochromaticity deriving from multiple defect levels was the largest problem. Recently, we have successfully generated a narrow band-edge PL from the $AgInS_2$ QDs and solved the problem over ten years. The key factor for the observation of band-edge emission was surface passivation by III-VI semiconductors, indium and gallium sulfides (InS_x and GaS_x) to form core/shell structure. Unlike the famous zinc sulfide shell, III-VI semiconductor shells had an amorphous nature that is unusual as QDs' shell. Probably, the amorphous nature helps to create a defect-free interface between the $AgInS_2$ cores, as well as a better matching of valences (In^{3+} vs. Zn^{2+}) at the interface. More recently, we attempted to improve the $AgInS_2$ cores that are as important as GaS_x shells. Synthesis of ternary compound semiconductor nanoparticle materials are more difficult than binary materials because two kinds of metals with different reactivity are involved in the reaction. A dropwise addition of reactive sulfur precursors into a preheated metal solution created monodispersed $AgInS_2$ nanoparticles by the two-step reaction through Ag_2S nanoparticle intermediates.

Experimental: Silver acetate and indium acetate was mixed with oleylamine and a small amount of 1-dodecanethiol was added to the mixture to stabilize Ag^+ species. The solution was heated to 140 °C in Ar and an oleylamine solution of 1,3-dimethylthiourea was slowly injected by using a syringe pump.

Results and discussion: Figure 1 shows PL spectra for $AgInS_2$ cores having tetragonal and orthorhombic phases; the tetragonal cores emitted more strongly than the orthorhombic cores. These tendencies have not been changed after the formation of GaS_x shells, where tetragonal $AgInS_2/GaS_x$ QDs showed narrow band-edge emission (fwhm = 31 nm) which is still narrower than our recent report.

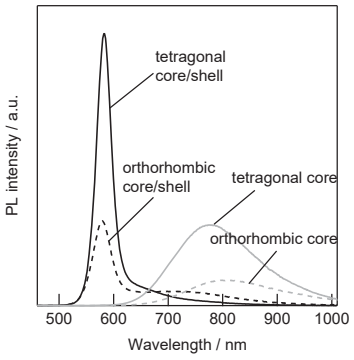

Figure 1. PL spectra for tetragonal- and orthrhombic $AgInS_2$ core QDs and the corresponding $AgInS_2/GaS_x$ core/shell QDs (ex = 450 nm).

I 1 Electrochemical quantitative evaluation of bacterial activity

Maki Saito, Kengo Ishiki, Nguyen Dung, Hiroshi Shiigi,
(Department of Applied Chemistry, Osaka Prefecture University, Sakai, Japan)

Introduction: A better understanding of the biological functions of microorganism is required to reduce their threats and increase their usefulness. Therefore, an importance of real-time evaluation of bacterial activity increase for various purposes such as hygiene management, development of antibacterial agents, and effective utilization of bacterial resources.[1] This necessitates a quantitative assessment of metabolic processes, including growth and respiration. Here we would like to introduce the development of electrochemical methods for assessing bacterial activity.

Results and discussion: Electrochemical detection of viable bacterial cells was performed using cell membrane permeable electron mediator and redox active pigment. *Shewanella oneidensis* MR-1 transfers electrons generated within the cell to the extracellular environment via the cytochrome complex in the inner/outer membranes and is one of the most useful bacteria for the recovery of metals, treatment of wastewater, and preparation of microbial fuel cells. By using potentiometric measurements, we have examined intracellular electron generation in bacterial suspensions of *S. oneidensis* supplemented with different carbon sources or ferricyanide, which was almost completely reduced to ferrocyanide during the incubation without affecting bacterial cell viability.[2] On the other hand, a tetrazolium salt (MTT), which was converted to an insoluble reduction form (formazan) through the respiration of microbial cells.[3] The insolubility of this formazan was effectively exploited as a surface-confined redox event. The electrochemical detection of formazan was effectively coupled with the thermal lysis of microbes. The sensitivity of the present technique is up to 10,000-fold higher than that of MTT colorimetry and requires an incubation time of only 1 h, which is approximately 1/4 of that required for other metabolism-based techniques. Furthermore, the measurement of the reduction current of dissolved oxygen provides an effective mean for assessing the respiratory activity of bacteria in suspension.[4]

1) T. Kinoshita, K. Ishiki, D. Q. Nguyen, H. Shiigi, T. Nagaoka, *Anal. Chem.*, **90**(6), 4098 (2018).
2) K. Ishiki, H. Shiigi, **submitted**.
3) K. Ishiki, D. Q. Nguyen, A. Morishita, H. Shiigi, T. Nagaoka, *Anal. Chem.*, **90**(18), 10903 (2018).
4) M. Saito, K. Ishiki, D. Q. Nguyen, H. Shiigi, *Anal. Chem.*, **in press**.

I2 Selective retrieval of single cells with a secretory ability of a target antibody in cell−based arrays using a microwell array electrode

Tomoyuki Yasukawa, Misaki Hata, Masato Suzuki (Graduate School of Material Science, University of Hyogo, Ako, Japan)

Introduction: This study demonstrates proposed manipulation techniques for retrieving target hybridomas from cell−based arrays selectively by the novel device with microwell arrays that employs dielectrophoresis (DEP) after hybridomas with the secretion of antibodies were discriminated. Individual cells trapped in microwells can be selectively retrieved by regulating the generation of electric fields in individual microwells. The development of series of these techniques could be useful to recover hybridomas producing antibodies with high affinity in large populations of cells without repeated steps of a culture and a limiting serial-dilution.

Experimental: The device comprises the upper substrate with indium-tin-oxide (ITO) microband electrodes and the lower substrate with microwell arrays on ITO microband electrodes. Hybridomas producing an anti-rabbit serum albumin (RSA) antibody suspended in the DEP medium were introduced in the channel. AC signal (3 MHz, 2 Vpp) was then applied to the upper and lower microband electrodes with opposite phase to form a cell-based array. Anti-RSA antibodies secreted from hybridomas trapped in the microwells were captured by RSA immobilized on the electrodes. Cell arrays were then treated with anti-mouse IgG antibody conjugated with Alexa 488 (a secondary antibody). Thereafter, a repulsive force of negative dielectrophoresis (n-DEP) was employed to retrieve the target hybridomas from the microwell array. To retrieve the target hybridoma, an AC signal in the n-DEP frequency region was applied to a pair of microband electrodes above and below the microwell with the target hybridoma.

Results and discussion: Cell−based arrays were formed with the occupancy efficiency of over 90% in a few seconds by p-DEP. Antibodies secreted in microwell arrays were captured to discriminate target hybridomas in a few hours without repeated steps of a culture and a limiting serial-dilution. Furthermore, hybridomas trapped in microwells were retrieved from the cell−based array by applying an AC signal to band electrodes. The sequential system for forming cell−based arrays, discriminating hybridomas secreting specific antibodies, and retrieving target hybridomas was developed by using the novel microwell array device comprising 3-D microband array electrodes with an orthogonal arrangement.

I3 Application of Electrochemical Measurement Technique in Cell study and Oxidative Stress

Shigenobu Kasai
(Department of Electrical and Electronic Engineering, Tohoku Institute of Technology, Sendai, Japan)

Abstract

Oxidative stress is induced by imbalance in redox state in living body and associated with ROS related diseases, for example, inflammation, allergy, allergy, aging and various adult diseases. Visualization of oxidative stress is indicative of a significant for diagnostic purpose visualization techniques of oxidative stress, which leads to a practical diagnostic device that contributes to the social demands on health and welfare. In this research, we introduce the following two electrochemical measurement cases.

Mastitis is a generic term for biological reactions leading to damage of mammary gland tissue, which occurs when intestinal microbes invade into mammary glands. Currently, Somatic cell count (SCC) is widely used as mastitis diagnosis method utilizing the fact that a large number of somatic cells are present in the milk of mastitis cattle. However, it is difficult to know whether the immune cells increase at the early stage of mastitis and early diagnosis is difficult. We have evaluated respiratory activity and respiratory burst of immune cells by Scanning electrochemical microscopy (SECM). In this study, attention was paid to the fact that neutrophils are particularly likely to increase among somatic cells, and evaluation of respiratory activity can be used as a marker for the diagnosis of mastitis.

Cell sheets have been studied for the purpose of regenerating dysfunctional tissue, and it has also been reported that whole-body transplantation of autologous cultured epidermis was actually successful. However, there are few simple methods to test activity after cell sheet preparation. In this study, we aimed to reproduce the sunburn condition on a part of normal human epidermal keratinocyte sheet by ultraviolet irradiation and to evaluate its activity using Bio-LSI. We monitor the oxygen reduction current of the epidermal cell sheet in real time, and report the results of imaging the respiratory burst phenomenon similar to that of immune cells as the area irradiated with ultraviolet light.

References

1) A. Prasad et al. Frontiers in Physiology 7, 109, 1-10 (2016)
2) S. Kasai et al. Scientific Reports 9, Article number: 12234 (2019)

I4 Preparation of glucose sensor using electrodeposition method and its application to in vivo measurement

Mikito Yasuzawa* and Masashi Kurashina (Department of Applied Chemistry, Tokushima University, Japan)

Introduction: Development of implantable glucose sensors for a continuous glucose monitoring system (CGMS) has provided significant benefit, since it not only provide instant glucose level but also its continuous trend, which help to provide effective treatment. However, commonly 1 cm in length is requested to be injected in the tissue for the sensor placement and the development of lower invasive CGMS is longed to improve the patients quality of life. We have previously reported that the sensor response of a fine tapered needle type glucose sensor, which has a sensing region at the tip, showed good correlation with blood glucose value, even though the sensor device was implanted in the skin for a length of 1.0 mm[1)]. This result indicate that the glucose measurement in dermis have potential to provide valuable information for blood glucose management. Nevertheless, low-invasive sensor require sensing region miniaturization and improvement of sensor sensitivity is indispensable. Here, we report various procedures to increase the sensitivity of the glucose sensor based on the immobilization of enzyme using electrodeposition method.

Experimental: Glucose oxidase (GOx) was used as the enzyme for sensor fabrication. Carbon nanomaterials, such as carbon nanotube (CNT) and graphene, were introduced and Gallen gum powder was employed to obtain dispersed aqueous electrodeposition solution containing GOx. GOx was electrodeposite on Pt electrode by applying a constant potential of 1.3 V (vs. Ag/AgCl). Electropolymerization of o-phenylenediamine was carried out at a constant potential of 0.7 V (vs. Ag/AgCl) to form a polymer film, which increase the stability of the enzyme film. Response current measurement was performed at a constant potential of 0.60 V (vs. Ag/AgCl) for hydrogen peroxide detection.

Results and discussion: Stable dispersed solution containing GOx and CNT was prepared using gellan gum and was applied successfully for the electrodeposition on Pt electrode. The obtained GOx and CNT immobilized electrode performed good glucose sensor response and its sensor sensitivity was two times higher than that without CNT.

References

1) J. Li, P. Koinkar, Y. Fuchiwaki, M. Yasuzawa, *Biosens. Bioelectron.*, **86**, 90 (2016).

I5 Different Chemistry of Li- and Na-ion toward Carbon Electrode

Yasuyuki Kondo[1], Yuko Yokoyama[2], Yuto Miyahara[3], Kohei Miyazaki[1,3], and Takeshi Abe[1,3] ([1]Graduate School of Global Environmental Studies, Kyoto Univ., [2]Office of Society Academia Collaboration for Innovation, Kyoto Univ., [3]Graduate School of Engineering, Kyoto Univ.)

Introduction: It has been well-recognized that lithium-ion batteries (LIB) are the main secondary batteries for portable devices, electric vehicles, etc. Storage of renewable energies has been of great importance for their effective use, and LIB also plays an important role for the storage systems. The storage of renewable energies will be rapidly increased and therefore, other secondary battery systems must be developed because of the resources' limitation. In this sense, sodium-ion batteries have attracted much attention. Graphite has served as a negative electrode of LIB for more than 25 years mainly because of its high capacity (theoretical 372 mAh/g), low potential identical with Li metal, and low cost. The use of graphite is one of the key issues for the success of LIB. Then, we have focused sodium-ion chemistry toward carbon electrode and compared it with lithium-ion.

Intercalation of Li- and Na-ion into graphite: While graphite accepts lithium-ion to form Li-graphite intercalation compound (GIC), reactivity of sodium-ion with graphite is quite low. Little reactivity of sodium-ion with graphite has been a mystery for ca. 50 years. We tried to solve this mystery and the details will be shown in the conference [1, 2].

Insertion of Li- and Na-ion into hard carbon: When organic compounds are heat-treated up to 3000 ^{o}C under inert atmosphere, most of them will become graphite. However, some compounds will be still amorphous, and the resultant carbons are called non-graphitizable carbon (or hard carbon). Glassy carbon is one the hard carbons. Hard carbons heat-treated by 1200 ^{o}C possess many open pores, and the carbons heat-treated exceeding 1500 ^{o}C possess almost no open pores but closed pores. Sodium-ion can easily insert into the hard carbons with closed pores, but lithium-ion cannot [3, 4]. These results have become the second mystery between lithium-ion and sodium-ion.

References

1, Y. Kondo et al. Chem. Lett., in press (2019).
2. Y. Kondo et al. J.Electrochem. Soc., 166, A5323 (2019).
3. G. Hasegawa et al. ChemElectroChem 2, 1917 (2015).
4. G. Hasegawa et al. J. Power Sources 318, 41 (2016).

I6 A Simple EIS Model to Describe Diffusion and Migration inside a Porous Electrode

Zyun Siroma (Research Institute of Electrochemical Energy, National Institute of Advanced Industrial Science and Technology (AIST), Osaka, Japan)

The use of an equivalent circuit is helpful to interpret electrochemical impedance spectroscopy (EIS). Transmission-line model (TLM) is a kind of equivalent circuits with a ladder-like structure and several rows of infinitesimally small elements. Usually the values of the elements in a row do not depend on the position in the ladder (uniform model). Impedance values of several uniform TLMs are mathematically obtained [1]. If the analytical solution is not available for the assumed model, such as a non-uniform model or even a uniform model with a highly complicated structure, the model is usually transformed to a discrete model with finite-length ladder steps to obtain the impedance values with the aid of some simulation software. Generally there are two different types of the TLMs used in the field of EIS: One is to reflect spatial distributions of the ionic and/or electronic resistances, and the other is to describe diffusion of the active species. As an example in the former meaning, an expansion of the Randles-type circuit for a porous electrode is shown in Fig. 1. However, since the arrayed Warburg elements in Fig. 1 are isolated with each other, there is a limitation that the model can describe only a locally terminated diffusion. The diffusion inside the active material (usually a powdery material) is applicable, whereas that inside the electrolyte solution is not, since the concentration perturbation propagates spatially successively throughout the porous electrode.

On the other hand, it is known that a kind of TLMs can describe the diffusion and migration in an electrolyte solution containing several ionic species [2]. Therefore, an incorporation of such a TLM into Fig. 1 becomes a powerful equivalent circuit to describe the effects of diffusion, migration, and electronic resistance on the faradaic impedance inside a porous electrode. A difficulty lies in the fact that all of the ionic species, not only the active species, contribute the electric double-layer charge/discharge process. An exact modeling of the double-layer capacitance will be discussed.

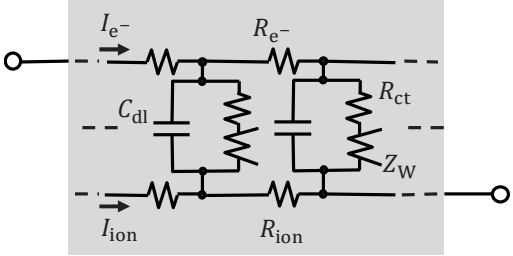

Fig. 1. A TLM for a porous electrode based on a Randles-type equivalent circuit.

References

1) Z. Siroma et al., *Electrochim. Acta*, **160** (2015) 313.

2) T.R. Brumleve, R.P. Buck, *J. Electroanal. Chem.*, **126** (1981) 73.

I7 *operando* X-ray Absorption Spectroscopic Study on Oxygen Reduction Reaction Kinetics of Pt Monolayer on Pd Core-shell Catalyst

Yoshiharu Uchimoto (Kyoto University)

Introduction: Considering the practical application in PEFCs, more and more researches start focusing on the catalytic properties under moderate temperature as the working temperature of PEFCs is over 70 °C. In this study, we measured ORR activities and coverage of oxygenated species on Pt monolayer-shell Pd-core catalyst from 25 ºC to 60 ºC. The core-shell catalyst was synthetized by Pt monolayer deposition on Pd/C with the galvanic displacement of Pt from a Cu monolayer obtained by under-potential deposition. *Operando* XAS also used to observe Pt-Pt bond distance of the catalyst, trying to illustrate the ORR activity temperature dependence of Pt shell-Pd core catalyst.

Experimental: Pd/C catalyst (30wt%) made from ISHIFUKU Metal Industry Co., Ltd. was used as core metal. The core-shell catalyst was prepared by depositing Pt monolayer involving the galvanic displacement by Pt of underpotentially deposited (UPD) Cu monolayer. *Operando* XAS measurements for Pd K-edge of Pt/Pd/C core-shell catalyst and Pt L_{III}-edge of Pt/C catalyst and Pt/Pd/C core-shell catalyst were carried out by using synchrotron radiation at the beamlines BL37XU and BL01B1 at SPring-8, Hyogo, Japan.

Results and discussion: The apparent rate constant (k_{app}) in Pt/Pd/C core-shell catalyst possessed the higher ORR activity than Pt/C catalyst at 25ºC but the ORR activity started to decrease at 60ºC. The coverage of Pt/Pd/C core-shell catalyst was much lower than Pt/C catalyst at 25ºC but it dramatically increased with the rising temperature, which could be a part reason of the ORR activity decrease. *Operando* XAS study showed the Pt-Pt bond length of Pt/Pd/C core-shell catalyst was shorter than that of Pt/C catalyst, in the case of the compressive surface strain on the Pd core. As the summarize in Figure 6, the Pt-Pt bond length extension was more significant for Pt/Pd/C core-shell catalyst than Pt/C catalyst at 60ºC, which cause the decrease of ORR activity. This structural change of the catalyst was caused by the lager thermal expansion of Pd core as well as the particle size effect of thermal expansion coefficient.

Acknowledgements
This research is based on results obtained from a project commissioned by the New Energy and Industrial Technology Development Organization (NEDO).

1P1 Boosting Bioelectrocatalysis of Multicopper Oxidase from Hyperthermophilic Archaea Induced by SWCNT immobilization

Masato Tominaga[1]* and Shino Nakao[1], Takenori Satomura[2], Shin-ichiro Sue[2]
([1] Graduate School of Science and Engineering, Saga University, Saga, Japan,
[2] Graduate School of Engineering, University of Fukui, Fukui, Japan)
*masato@cc.saga-u.ac.jp

Introduction

Multicopper oxidase (MCO) of hyperthermophilic archaeon has ability of catalytic reduction of oxygen at a high-temperature more than 80 ℃, and the activity can be maintained long term. This characteristic advantage would be useful for a biocathode of enzymatic biofuel cell. However, at a room temperature, the MCO shows very small activity. The catalytic oxygen reduction current of the MCO-modified electrode was much smaller than that of fungal laccase at a room temperature, even when a mediator was used. In the present research, we investigated the electrocatalytic reduction of oxygen of archaea MCO immobilized on a single-walled carbon nanotube (SWCNT) under wide range of pH and temperature, compared to that of fungal laccase (Lac).

Experimental

Fungal laccase from *Trametes sp.* was obtained from Amano Enzyme and purified before use it. Hyperthermophilic archaea MCO, *Pyrobaculum aerophilum* was expressed in *E. coli* BL21-Codon-Plus (DE3)-RIL and was purified from soluble extract, anion-exchange chromatography and gel filtration chromatography. SWCNT-modified gold electrode was synthesized by CVD method, which was used for electrode to immobilize archaea MCO and Lac.

Results and discussion

The archaea MCO immobilized onto the SWCNT showed large bioelectrocatalysis current from ca. 0.4 V, which was more negative potential than that of Lac (Fig. 1). The oxygen reduction current for archaea MCO was observed pH range of 2 - 9, although that for laccase was not observed at pH 9. The reduction current for archaea MCO was observed at 25 - 75 ˚C, although that for laccase was not observed at 75 ˚C.

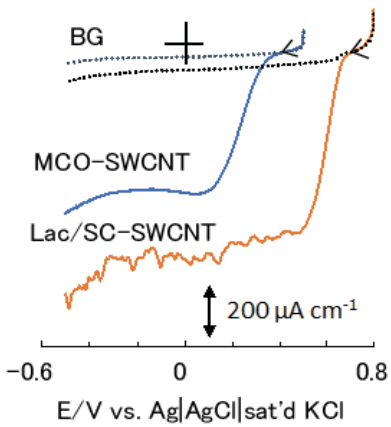

Fig. 1. Voltammograms at fungal Lac and archaea MCO immobilized SWCNT electrode in B&R buffer (pH 5). Potential scan rate: 10 mV s^{-1}.

1P2 Kinetics of Intracellular Electron Generation in *Shewanella oneidensis* MR-1

Kengo Ishiki, Hiroshi Shiigi (Department of Applied Chemistry, Osaka Prefecture University, Osaka, Japan)

Introduction: Efficient utilization of bacterial bioresources requires quantitative evaluation of metabolic activity in living bacterial cells. *Shewanella oneidensis* MR-1 transfers electrons generated within the cell to the extracellular environment via the cytochrome complex in the inner/outer membranes and is one of the most useful bacteria for the recovery of metals, treatment of wastewater, and preparation of microbial fuel cells. Here, we performed a potentiometric evaluation of electron generation based on individual enzyme reactions in *S. oneidensis* MR-1.

Experimental: Potentiometry was performed as follows: two electrodes were immersed in 10 mL of the purified bacterial suspension that included an organic source (e.g., formate, lactate pyruvate, or acetyl-CoA). Oxygen was removed by bubbling the suspension with nitrogen (99.99%) for 5 min before ferricyanide addition. The time at which ferricyanide reduction by *S. oneidensis* was complete was determined from the equivalent point in the potential profile.

Results and discussion: The potential (E) in the bacterial suspension containing 10 mM formate changed from +0.05 V (vs. Ag|AgCl) to +0.30 V immediately after an addition of ferricyanide (Fig. 1A) and gradually decreased throughout the incubation, reaching the quantity potential ($E^{o'}$) of ferricyanide. Then, the potential drastically dropped, indicating a terminal point, whereas the yellowish color of ferricyanide-containing suspension based on ferricyanide disappeared.

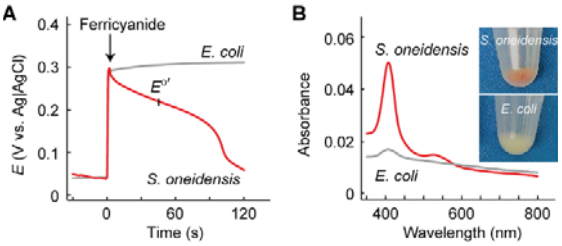

Fig. 1 (A) Potential profiles in bacterial suspensions (3.0×10^9 cells) of facultative anaerobic *S. oneidensis* and *Escherichia coli*. Ferricyanide (0.10 mM) was added into the suspension at t = 0 s. (B) UV-vis spectra of bacterial suspensions. The inset represents photographs of bacterial pellets of *S. oneidensis* and *E. coli*

These observations indicated that ferricyanide was almost completely reduced to ferrocyanide without affecting cell viability (>99%) during the incubation. No potential change was observed in other bacterial species with FDH. A previous study suggested that metal nanoparticles formed on the bacterial surface, whereas no particles were observed in the extracellular environment (K. Ishiki et al, *Anal. Sci.* 33(2), 129, 2017). Therefore, the reducing reaction occurred directly at the numerous electron outlets formed by the cytochrome complex (Fig. 1B).

1P3 A photosynthesis-mimetic solar cell based on bioelectrocatalysis

Taiki Adachi[1], Yuki Kitazumi[1], Osamu Shirai[1], Kunishige Kataoka[2], Kenji Kano[1] ([1]Division of Applied Life Sciences, Graduate School of Agriculture, Kyoto University, Japan, [2]Division of Material Sciences, Graduate School of Natural Science and Technology, Kanazawa University, Japan)

Introduction: The light reactions of photosynthesis proceed in the thylakoid membrane in photosynthetic organisms. Electrons produced by H_2O oxidation are transferred via photosystem II (PSII), cytochrome b_6f, and photosystem I (PSI), and the two photon excitation reactions occur at PSII and PSI (called the Z-scheme). Recently, mimicking natural photosynthesis has been expected to be a fundamental technology to realize a sustainable energy economy. We focused on the thylakoid membrane as a photo-bioelectrocatalyst for H_2O oxidation and bilirubin oxidase (BOD) as a direct-electron-transfer-type bioelectrocatalyst for O_2 reduction, and constructed a bio-solar cell, which is a photosynthesis-mimetic device and extracts excited electrons to an electric circuit outside the photosynthetic system.

Experimental: The photo-driven bioanode was prepared by applying the mixture of thylakoid membranes from spinach and multi-walled carbon nanotubes on a gold-spattered indium tin oxide electrode. $[Ru(NH_3)_6]Cl_3$ was used as a soluble mediator. The biocathode was prepared by applying a BOD solution on Ketjen Black-modified waterproof carbon cloth. A bio-solar cell was constructed by combining the bioanode and the biocathode with a variable resistor. The light was illuminated from the backside of the bioanode. Electrochemical measurements were carried out under quiescent conditions at 25 °C and pH 7.0.

Results and discussion: The bioanode exhibited a photocurrent density of 180 μA cm^{-2} at 0 V vs. Ag|AgCl|sat. KCl. This value is better than one reported previously (with NQ as a mediator: 100 μA cm^{-2} at 0.2 V),[1] in spite of reducing the overpotential. It seems to be due to fast electrode kinetics and suitable water solubility of $[Ru(NH_3)_6]^{3+/2+}$. The cell exhibited an open-circuit voltage of 0.61 V and a maximum power density of 50 μW cm^{-2} at a cell voltage of 0.42 V (Figure 1). To the best of our knowledge, the power density of our cell unit is the highest among those reported for the bio-solar cells to date.

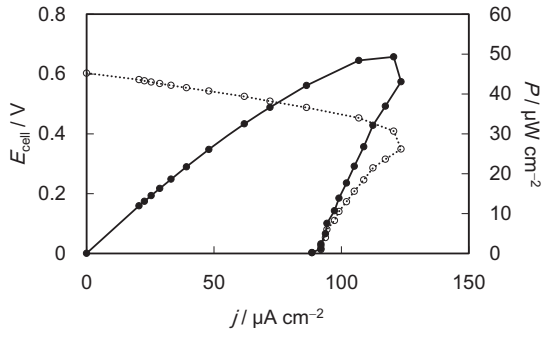

Figure 1. The cell voltage (E_{cell}, open circles) and the power density (P, closed circles) are plotted as a function of the current density.

(1) R. Takeuchi, A. Suzuki, K. Sakai, Y. Kitazumi, O. Shirai, K. Kano, *Bioelectrochemistry*, **122**, 158 (2018).

1P4 Evaluation of respiratory burst of immunocyte in bovine milk using SECM

Ryoma Kumagai[1], Saya Saito[1], Haruka Takanashi[1], Masashi Kumagai[2], Shigenobu Kasai[1]
([1]Tohoku Institute of Technology, [2]Morinokuma Animal Hospital)

Introduction: Mastitis is a generic term for biological reactions leading to damage of mammary gland tissue, which occurs when intestinal microbes invade into mammary glands[1)]. Currently, the somatic cell count (SCC) is widely used as a mastitis diagnosis method. However, this method cannot determine the cell type. Therefore, it is difficult to know whether the immune cells increase during the early stage of mastitis, thus early diagnosis is difficult. We have electrochemically evaluated the respiratory burst (Fig.1) when neutrophils and monocytes are triggered by phorbol 12-myristate 13-acetate (PMA)[2)]. In this study, we describe the results of examining the respiratory burst evaluation of neutrophils and monocytes contained in bovine milk using a scanning electrochemical microscopy (SECM).

Experimental: We centrifuged the bovine milk and removed the cell suspension(1.8×10^5 cells/mL). We inserted 8 μL of this cell suspension into an inverted conical well (both the radius and height are 2 mm). The respiration activity was measured by scanning a Pt microelectrode in the Z direction between 20 μm (the cell suspension surface) and 1020 μm (the bulk) from the cell suspension while measuring the oxygen reduction current, and the measurement solution was PBS buffer containing 11.4 mM glucose. We injected PMA at a final concentration of 100 nM and measured similarly. The scanning distance, scanning speed and sampling time are 1000 μm, 20 μm/s and 100 msec, respectively.

Results and discussion: Fig.2 shows the results using a Pt microelectrode moving back and forth in the Z-direction to determine the difference of oxygen reduction current at a distant position and in the cell suspension surface by SECM during ordinary respiration (dashed line) and during respiratory burst (solid line). We normalized the oxygen reduction current value at the bulk to 0 nA. We use a dissolved oxygen concentration of 209 μM in PBS at 37 ℃, and an oxygen reduction current value based on this at -3.0 nA[2)]. We calculated the oxygen consumption of the cells from the difference in the peak current value. The oxygen concentration during ordinary respiration was determined to be approximately 2 μM, and the oxygen concentration during respiratory burst was determined to be approximately 13 μM. This result was suggested that the respiration activity of immunocyte is increased by the respiratory burst. In the future, we plan to compare mastitis bovines and healthy bovines.

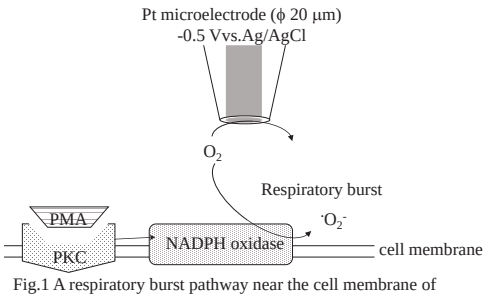

Fig.1 A respiratory burst pathway near the cell membrane of immunocyte and its electrochemical measurement conceptual diagram.

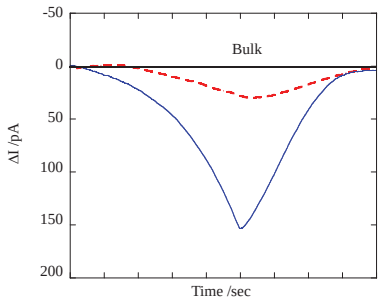

Fig.2 Evaluation of respiration activity: comparison of the magnitude of oxygen reduction current using SECM in the presence of milk

References

(1) M. Damm, C. Holm, M. Blaabjerg, M. N. Bro, D. Schwarz: *J.Dairy Sci.*100, 4926-4940(2017)
(2) H. Kikuchi, A. Prasad, R. Matsuoka, S. Aoyagi, T. Matsue, S. Kasai: *Frontiers in Physiology* 7, 25, 1-6 (2016)

1P5 Excimer Formation of Pyrene in Electrogenerated Chemiluminescence

Ryoichi Ishimatsu[1], Koji Nakano[1] ([1]Department of Applied Chemistry, Graduate School of Engineering, Kyushu University, Fukuoka, Japan)

Introduction: It is well-known that electrogenerated chemiluminescence (ECL) of pyrene, which generated by the ion annihilation of the radical anion and cation of pyrene, shows the excimer emission at relatively low concentrations. As far as we know, no monomer ECL of pyrene has been reported clearly so far. It is believed that the formation of a contact pair of the radical anion and cation leads to a direct formation of excimer for pyrene. This proposed mechanism is known as E-rout (E represents excimer or exciplex).

Here we report time-dependent ECL spectra of pyrene. The ECL was generated by applying a square wave voltage. We found that structured ECLs derived from the monomer emission of pyrene were quickly disappeared within a few ten ms after the applied potential was switched from negative to positive. We discuss the electron transfer distance with a framework of Marcus theory, and propose a mechanism of the excimer ECL of pyrene, *i.e.*, the formation of the monomer S_1 state of pyrene through the electron transfer between the radical ions at ~ 1 nm is followed by the excimer formation.

Experimental: A there-electrode system composed of a Pt disk (d =3 mm), Pt coil and Ag wire as working, counter and reference electrodes, respectively was employed for the electrochemical measurements. ECL was collected with an optical fiber connected to an EMCCD camera with a spectrophotometer. The potentials of square wave were set beyond the peak potential of the oxidation and reduction waves (E_p(Ox) and E_p(Red), respectively. Acetonitrile (MeCN) and tetrabutylammonium hexafluorophosphate ($TBAPF_6$) were used as a solvent and supporting electrolyte, respectively.

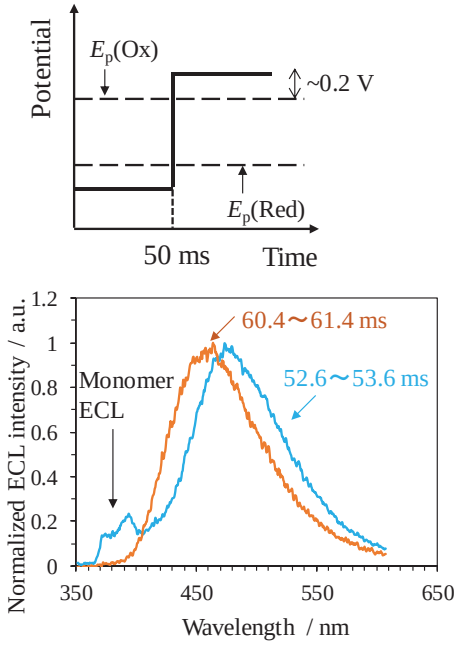

Fig. 1. Schematic representation of square wave voltage (top) and time-dependent ECL spectra of 1 mM pyrene (bottom).

Results and discussion: Fig. 1 shows ECL spectra of pyrene at different time. The monomer ECL was only seen at an early stage of the potential step. The appearance of the monomer ECL suggests that the electron transfer between the radical ions occurs at a separated distance, but not “contact ion pair”. We performed kinetic analysis based on a framework of Marcus theory, and found that the electron transfer can kinetically take place at < ~ 1 nm.

1P6 Inevitability of peak potential shift – dedicated to late Prof. Ichimura-

Koichi Jeremiah Aoki (Electrochemistry Museum)

Introduction: Prof. Ichimura used to say that voltammetric peaks in any case shifted at fast scan rates, but that the shift had been explained with heterogeneous kinetics without sufficient reasons. His enthusiastic devotion to experimental results has motivated me to apply the negative capacitance associated with any redox reactions observed by ac-impedance. The concept of the negative capacitance is used here for cyclic voltammetry in the light of variation of peaks with scan rates.

Experimental: Voltammetry was made for a ferrocenyl derivative in aqueous solution at a platinum wire electrode at scan rates up to 5000 V s^{-1}.

Results and discussion: The peak currents at fast scan rate, v, showed two linear term of $v^{1/2}$ and v. The coefficient of the last term was negative (-64 μF cm^{-2}). The peak potential exhibited linearity to log v, of which slopes ranged ±55 mM for the anodic and the cathodic scans. Both results cannot be explained by the Butler-Volmer kinetics. A possible reason is the capacitance caused by the charge generated by the electrode reaction. The generated charge density σ decreases the applied electric field by a fraction of σ/ε_0, which should decrease the voltage required for the redox reaction to yield the negatively capacitive current density, $j_{rc} = d\sigma/dt$. Since the diffusion-controlled Faradaic current density j_F and j_{rc} are logically in series conjunction, the inverse of the observed capacitive current density, j_c, is a sum of the inverse of the two: $1/j_c = 1/j_F + 1/j_{rc}$. Then the observed current density is given by $j = j_F - j_F j_{rc}/(j_F + j_{rc})$. The dimensionless current density was calculated for several values of the parameter $(\sigma^*/c^*)^2 v/RTFD$ to be shown in Fig. 1. The potential shift is caused by j_{rc} (see (B) in Fig), which shifts the diffusion-controlled peak (A) to (C).

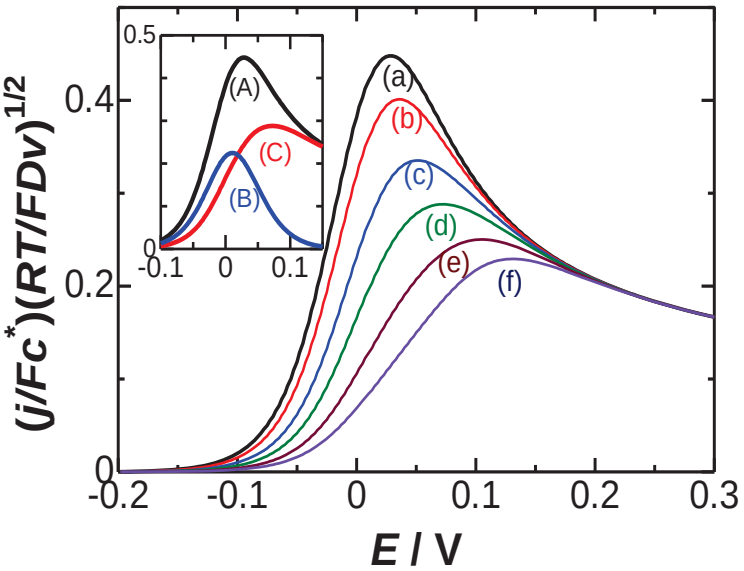

Fig. 1. Calculated voltammograms for $(\sigma^*/c^*)^2 v/RTFD$ = (a) 0.0, (b) 0.09, (c) 1.0, (d) 4., (e) 16. and (f) 49. The inset shows voltammograms of (A) j_F, (B) j_c and (C) j, calculated for $(\sigma^*/c^*)^2 v/RTFD = 4$.

1P7 Formation of Self-organized Film Composed of Graphene Oxide/ Melamine on Electrogalvanized Steel Plate and its Anticorrosion Activity

Takeru Yamamoto[1], Ryo Saito[1], Wataru Sugimoto[2], Masa-aki Haga[1]([1]Applied Chemistry, Chuo University, Tokyo, Japan, [2]Department of Chemistry and Materials, Shinshu University, Nagano, Japan)

Introduction:

Graphene oxide (GO) has been paid much attention to apply various fields such as energy storage, catalysts, and biotechnology, etc. because of easy handling as a GO-dispersed aqueous solution. We have been studying the application of GO as a surface modification materials[1], in particular to replace the chromate treatment in corrosion protection of an electrogalvanized steel plate (EG plate). Recently, we found that the self-accumulation of GO and melamine (MA) aggregates[2] on an EG plate took place by a simple contact of the aqueous dispersion of the mixture of GO and MA with EG plate under stirring condition. In this study, we investigated how the self-accumulation occurs and whether the anti-corrosion ability improves by the coating of GO and MA composites (GO/MA) on the EG plate.

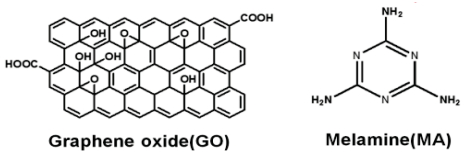

Fig. 1 Chemical structures of GO and MA

Experimental:

GO was prepared by the Hammers method, and average size and zeta potential were 2.5 μm and -31 mV. The mixed ratio of GO and MA were varied from GO : MA=1:1 to 1:5. An EG plate was immersed in the aqueous dispersion of the mixture of GO and MA with stirring. The transmittance and pH of the solution were monitored, during which time the initial brown suspension became clear only by stirring for 8 h. The resulting GO/MA aggregates on the EG plate was studied by the SEM, and XPS measurements. However, the GO/MA aggregates on the EG plate were easily peeled off from the EG plate, several additives such as glutaraldehyde or the electrodeposition on EG plate by an applied voltage were investigated for the improvement of anticorrosion coating on EG plate.

Results and discussion:

The XPS spectra of the GO/MA aggregate film showed the Zn 2p signals, indicating the Zn^{2+} ion bound the GO and MA strongly to form the Zn^{2+}-GO-MA network composites on the EG surface. The corrosion potential (E_{corr}) and corrosion current density (I_{corr}) were determined from Tafel plots of linear sweep voltammetric measurements. The I_{corr} for EG plate with GO/MA aggregates is slightly higher, but E_{corr} is anodically shifted compared to bare EG plate. From these results, the anti-corrosion ability has been improved for the electrodeposited GO/MA aggregates film.

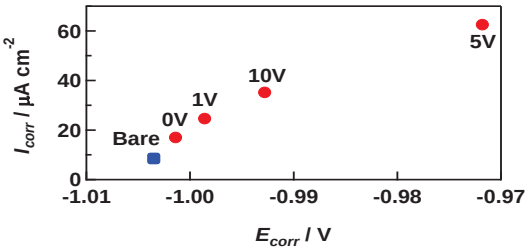

Fig. 2 Plots of E_{corr} vs I_{corr} for the EG plate covered by electrodeposited GO/MA aggregates

References:

[1] H. Ozawa, S. Kusaba, M. Matsunaga, and M. Haga, *Langmuir*, **34**, 2952 (2018)
[2] X. Wang *et al*., *New J. Chem*., **41**, 10899 (2017)

1P8 Interfacial properties of a binary ionic liquid composed of a potential-determining and a highly hydrophobic salts in contact with water

Takumi Kawamoto, Takashi Kakiuchi, Masahiro Yamamoto, Ryo Murakami (Konan Univ.)

Introduction: Moderately hydrophobic ionic liquid (IL) has been shown to function as a salt bridge[1]. However, in recent research of our laboratory group, it has been found that the potential deviated upward by ca. 5 mV from the Debye-Hückel Limiting law (DHLL) by saturating the sample aqueous solution with IL, and spontaneous emulsification took place at the IL | water interface[2,3]. In the present study, we examined the stability and reproducibility of the interfacial potential at the IL|water interface using an IL salt bridge in which a highly hydrophobic IL, trioctyldecylphosphonium tetrakis[3,5-bis(trifluoromethyl)phenyl]borate)([P_{88810}][TFPB]), was mixed with a moderately hydrophobic and potential-determining IL, tributyl (2-methoxyethyl)phosphonium bis(pentafluoroethanesulfonyl)-amide([TBMOEP][C_2C_2N]) to reduce water dissolution in the IL phase.

Experimental: The composition of the electrochemical cell used for the potentiometric measurement is: .

Ag | AgCl | 10 mmol kg^{-1}NaCl (W_{ref}) | ILSB | m mmol kg^{-1}NaCl (W_1)| AgCl| Ag (I)

where ILSB stand for the IL salt ridge. When the mixed IL was brought into contact with water, water dissolved into the IL phase by spontaneous emulsification. For the ILSB for potentiometric measurements, the transparent portion of the IL after centrifugation at 18000 rpm for 180 min was employed. The electrochemical cell was immersed in the water bath at 25.0 ºC.

Results and Discussion: Figure 1 shows the plots of $-E-(F/RT)\ln m_{Cl^-}$ vs. $I^{1/2}$, where E is the cell voltage, m_{Cl^-} the molality of Cl^-, and I the ionic strength at four ILSBs of different mixing ratios, the fraction of [P_{88810}][TFPB], x, being 0, 0.1, 0.2, and 0.3. The straight and curved lines represent the DHLL and the Debye-Hückel-Smaller-ion shell model, respectively. The reproducibility of varied considerably in the lower concentration range. Decreasing solubility of [TBMOEP][C_2C_2N] in water with increasing x seems to give rise to the greater variability of E.

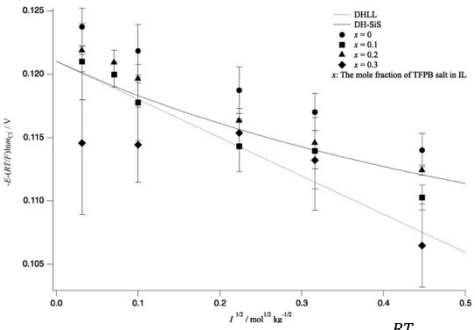

Fig.1 Ion strength dependence of $-E-\frac{RT}{F}\ln m_{Cl^-}$

References

1. Kakiuchi, T.; Yoshimatsu, T., Bull. Chem. Soc. Jpn. 2006, 79, 1017−1024.

2. Nakamura, R.; Hashimoto, R .; Yamamoto, M.; Kakiuchi, T.; Murakami, R., 82nd Annual Meeting of the Electrochemical Society of Japan.

3. Onishi, Y.; Yamamoto, M.; Kakiuchi, T.; Murakami, R., The 63rd Annual Meeting of Polarographic Society of Japan.

1P9 Mechanism of the ion transfer through a bilayer lipid membrane analyzed by an electrochemical method combined with fluorometry

Terumasa Omatsu, Kisho Hori, Naoto Ishida, Hotaru Minato, Yumi Yoshida, Kohji Maeda (Faculty of Molecular Chemistry and Engineering, Kyoto Institute of Technology, Kyoto, Japan)

Introduction: Analyzing the ion transport through biomembranes and bilayer lipid membranes (BLMs) is important for understanding biological activities (such as neurotransmission, respiration, and metabolism) and for artificial introductions of bioactive ionic substances (such as peptides and nucleic acids) to a cell. The mechanism of ion transport through a BLM is studied conventionally by electrochemical methods[1]. However, the transported ion cannot be easily identified on the basis of the transmembrane current. In this study, a novel analytical method, which combines the electrochemical method with fluorometry, was developed for analyzing ionic transport through a BLM.

Experimental: In this method, the transmembrane current and fluorescent intensity of a fluorescent ion crossing the membrane are simultaneously measured as a function of a scanning membrane potential with a potentiostat and the confocal fluorescent microscope. The horizontal BLM was formed by using the lipid solution of 1,2-dioleoyl-*sn*-glycero-3-phosphocholine and cholesterol.

Results and discussion: When the membrane potential E was changed in the range of ±100 mV, the transmembrane current and the change of fluorescence intensity f was observed simultaneously. Transmembrane current was converted into the transmembrane charge Q. The Q and f are synchronized with E and increased with increasing concentration of $R6G^+$ in water phase, indicating that the transport of $R6G^+$ was detected as f. In increasing the aqueous phase concentration of a relatively hydrophobic counter ion, BF_4^-, both of Q and f increased in spite of the constant concentration of $R6G^+$. The results suggest that the transport of $R6G^+$ through a BLM is enhanced by the presence of BF_4^-. However, Br^- of a relatively hydrophilic counter ion, did not enhance the membrane transport of $R6G^+$. Therefore, we concluded that distribution of $R6G^+$ with the counter anion into the BLM causes the increase in the ionic conductivity of the BLM.

[1] Shirai, O., Kihara, S., Yoshida, Y. & Matsui, M. *J. Electroanal. Chem*. 389, 61–70 (1995).

1P10 Electrocatalytic Properties of Noble Bimetal Modified Nickel Microparticles

Daiki Terazawa, Munetaka Oyama (Department of Material Chemistry, Graduate School of Engineering, Kyoto University, Kyoto, Japan)

Introduction: Since noble metal nanoparticles exhibit high electrocatalytic activity, they can be used for the electrocatalysts of fuel cells and electrochemical analysis. Our group is studying modifications of Au and Pd nanoparticles on nickel surfaces via the galvanic replacement reactions. As a preliminary result, we found that the surface modification was promoted by treating nickel wire in a mixed aqueous solution containing both tetrachloroaurate ($AuCl_4^-$) and tetrachloropalladate ($PdCl_4^{2-}$). On the basis of this result, in the present work, PdAu bimetal modified nickel microparticles (PdAu/NiMPs) are prepared by treating NiMPs in a mixed aqueous solution of $AuCl_4^-$ and $PdCl_4^{2-}$, or stepwise modifications of $AuCl_4^-$ and $PdCl_4^{2-}$ to explore the changes in electro catalytic properties.

Experimental: PdAu/NiMPs were prepared by dispersing NiMPs in an aqueous solution of noble metal precursors. Actually, in a 200-mL conical flask, 50 mL of an aqueous solution of 1.0 mM noble metal precursors was heated at 60 ^oC, 100 mg of NiMPs were dispersed in the solution, and the particles were separated and dried. To prepare modified electrodes, 10 mg of dried PdAu/NiMPs was added into a mixed solution of 100 μL of 5% Nafion solution and 900 μL of ethanol, and a portion of 5.0 μL was dropped on a glassy carbon (GC) disk electrode (diam. 3.0 mm). Thus-fabricated PdAu/NiMPs modified GC electrode was used as a working electrode for recording CVs of 1.0 M ethanol in 1.0 M NaOH aqueous solutions.

Results and discussion: At first, we prepared PdAu/NiMPs by treating NiMPs in a mixed aqueous solution of $AuCl_4^-$ and $PdCl_4^{2-}$. As the result, the CVs of the ethanol oxidation showed that the electrocatalytic property came from Pd. However, compared with the case of the same modification of nickel wire, the electrocatalytic current per surface area was apparently smaller, with indicating less promotion of the modification. This would be due to the differences in the preparation conditions. Therefore, we next examined stepwise modifications of Au and Pd. When Au was modified after Pd, the electrocatalytic response of Pd was observed with some increase in the electrocatalytic current. On the other hand, when Pd was modified after Au, the electrocatalytic response was that of Pd even when the concentration of $PdCl_4^{2-}$ was as low as 0.01 mM $PdCl_4^{2-}$ after the modification of 1.0 mM $AuCl_4^-$. From these results, it was found that the influence of Pd is dominant for the electrocatalytic oxidation of ethanol regardless of the order of the modification of Pd.

1P11 The effect of oxygen coverage and ionomer on oxygen reduction activity of Pt/C

Tomoki Uchiyama[1], Chen Liu[1], Kentaro Yamamoto[1], Naoki Takao[2], Hideto Imai[2], Seiho Sugawara[3], Kazuhiko Shinohara[3], Yoshiharu. Uchimoto[1] ([1] Kyoto University, [2] Nissan ARC, [3] FC-Cuibc)

Introduction: For wide spread of Polymer Electrolyte Fuel Cell (PEFC), It is necessary to improve the oxygen reduction reaction (ORR) activity of cathode catalyst. While the Ionomer (e.g., Nafion®) have been used in commercial PFEC to improve the triple-phase boundary and the effect of side-chain in perfluoro-sulfonic acid ionomers adsorbing on the surface of Pt has been discussed. For the terminal sulfonate group is adsorbed on Pt by one or two oxygen atom(s) and the oxygen atom of ether group also interaction with the Pt, it's shown that the existence of ionomer will block the oxygen reduction reaction. In this study, the weight ratio of Ionomer and carbon which was used in the catalyst (I/C) has been changed to control the degree of specific adsorption in order to analysis the effect of specific activity and construct a model of specific adsorption on the surface of Pt.

Experimental: Catalyst ink is made by mixture Catalyst powder(6.446mg) with ultrapure water (7.6ml), isopropanol (2.4ml) and 5wt% Nafion® solution (quantity is changed with I/C) then bath sonicated in ice bath for 20 mins to obtain well-dispersed ink. Thin-film Rotating Disk Electrode technique is used to get a homogeneous catalyst layer. Finally, 10 ul aliquots of the ink were subsequently casted on to the GC disk. For ORR activity measurements, the limiting current is calculated from the raw currents at 0.90V and analyzed to determine the specific activity. Pt L-edge X-ray absorption spectra were collected at BL37XU, SPring-8.

Results and discussion: Figure 1 shows the I/C dependence of ORR activity for Pt/C. It indicated the decrease along with I/C increasing. The more Nafion® was mixed in the ink, the more catalyst will be covered by ionomer which lead to more specific adsorption. For the specific adsorption occurs only at the interface of ionomer and the catalyst, ORR activity of Pt/C might not be changed over I/C=0.2. According to XAS results the Pt 5d orbital vacancy was lower for I/C=0 than I/C=1 even at 0.9 V vs RHE, which suggested that the direct evidence of specific adsorption.

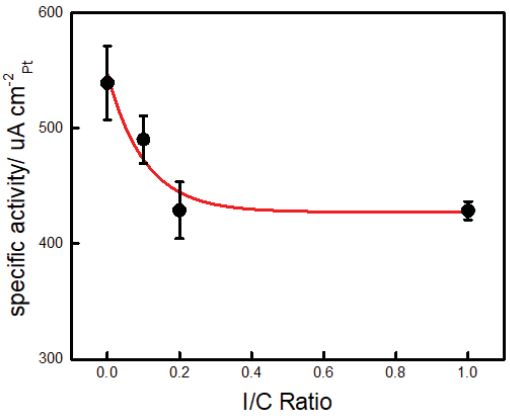

Figure 1. I/C dependence of specific activity for Pt/C

Acknowledgements

This research is based on results obtained from a project commissioned by the New Energy and Industrial Technology Development Organization (NEDO).

1P12 Morphological effect to proton conductivity Nafion thin-film on platinum cathode for polymer electrolyte fuel cell

Gao Xiao[1], Kentaro Yamamoto[1], Tomoyasu Hirai[2], Tomoki Uchiyama[1] Naoki Takao[3] Hideto Imai[3] Shota Katayama[4] Seiho Sugawara[4] Kazuhiko Shinohara[4] Yoshiharu Uchimoto[1] ([1]Graduate School of Human and Environmental Studies, Kyoto University, Kyoto, Japan [2] Department of Applied Chemistry, Osaka Institute of Technology, Osaka, Japan [3] Nissan Analysis and Research Center, Kanagawa, Japan, [4] Fuel Cell Cutting-Edge Research Center Technology Research Association, Tokyo, Japan)

Introduction: Herein, we examined the correlation between morphology and proton conductivity under humidity of Nafion thin-film with annealing treatment via grazing incidence small angle X-ray scattering (GISAXS) and electrochemical impedance spectroscopy. The glass transition temperature strongly dependent on film thickness, which demonstrate that the presence of interaction between ionomer/substrate.

Experimental: Nafion thin-films were prepared on interdigitated array electrodes on Pt substrate and sputter Pt substrate by spin-cast method. Annealing treatment was conducted at 120-240^{o}C under N_2 atmosphere for 1 h. GISAXS measurements were performed under beamline BL40B2 at SPring-8, Japan.

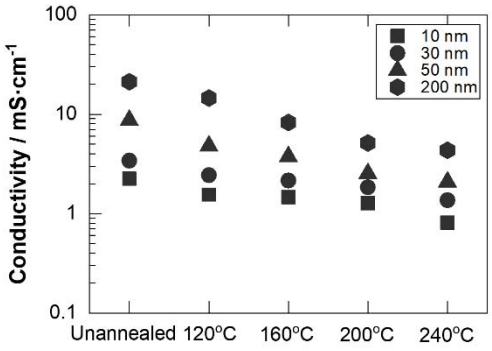

Figure 1. Proton conductivity of Nafion thin films with various thickness and annealing treatment.

Results and discussion: In case of 200 nm, proton conductivity decreased with increasing annealing temperature and significantly reduced after 160^{o}C. As thickness decreased to 50 nm, similar tendency was also observed while the temperature that conductivity obviously reduced become 200^{o}C. Furthermore, in case of 10, 30 nm, both of them apparently decreased after 240oC. These results evidently indicate that the glass transition temperature various with thickness due to ionomer/substrate interaction and confinement effect.

1P13 Electric double layer capacitance in mixtures of dimethyl sulfoxide and water

Peng Tang[1,2], Sousuke Taniguchi[1,2], Koichi Jeremiah Aoki[2], Jingyuan Chen[1,2],
([1] Dept. Appl. Phys. Univ. Fukui, [2] Electrochemistry Museum)

Introduction: A double layer capacitance represents a measure of relaxation of external electric field by solvent dipoles on the electrode rather than ionic distributions. The capacitance in mixtures of acetonitrile|water is mainly controlled by water because of the dipole moment of water larger than that of acetonitrile. The variation of the capacitance with the molar ratio was obeyed by the Langmuir-like adsorption equation with strong interaction of water-Pt[1]. Since dimethyl sulfoxide (DMSO) has interaction similar to water, it is predicted to reveal Langmuir-type adsorption. It is examined here.

Experimental: Mixtures of DMSO-water and methanol-water were prepared including 1 mM tetrabutylammonium perchlorate. The working electrode and counter electrode were platinum wires. Ac impedance was used for determine the capacitances at various molar rations.

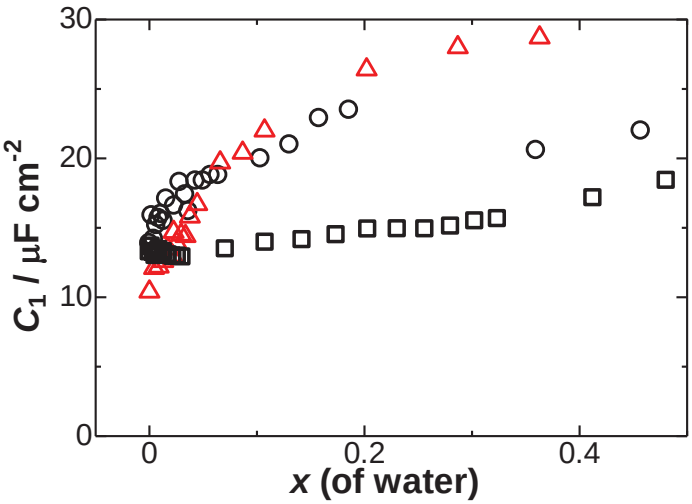

Fig. 1 Variations of C_1 with molar ratio for acetonitrile (△), methanol (○) and DMSO (□).

Results and Discussion: The ac currents were confirmed to be obeyed by the equation for the power-law, $I = \mathrm{d}(CV)/\mathrm{d}t = (\lambda+i)\omega CV_0\, \mathrm{e}^{i\omega t}$ at any molar ratio. A critical capacitance is at 1 Hz, C_1, of which values are plotted against various molar ratio for acetonitrile, methanol and DMSO in Fig. 1. DMSO exhibits a linear relation, indicating that the mixture with water is close to be ideal.

1. K. J. Aoki, J. Chen, P. Tang, Double Layer Impedance in Mixtures of Acetonitrile and Water, *Electroanalysis* 30 (**2018**) 1–9

1P14 Diffusion analysis of TEMPO derivatives in a viologen-type ionic liquid by CV and EPR

Wataru Imura, Akira Kitagawa, Hironobu Tahara, Takamasa Sagara
(Graduate School of Engineering, Nagasaki University)

Introduction: Viologen-type ionic liquids (VILs) have larger cation size and greater viscosity than typical ionic liquids such as imidazolium- and quaternary ammonium-type ionic liquids. In addition, the cations are of an asymmetric molecular shape. Therefore, the diffusion of a solute in them can show an anisotropy and behave beyond the hydrodynamic model. To understand the kinetic behavior of VILs as a medium, we have investigated cyclic voltammetry (CV) and electron paramagnetic resonance of TEMPO (2,2,6,6-tetramethylpiperidine 1-oxyl) derivatives as a redox and spin probe in a VIL solvent.

Experimental: Commercial products of electroneutral TEMPO derivatives were used without further purification. Electrically charged TEMPO derivatives and a viologen-type ionic liquid ($[C_4VC_7][TFSI]_2$) were synthesized in our group. Cyclic voltammetry was conducted at a Au microelectrode in a two-electrode system. EPR measurements were conducted by X-band frequency. All measurements were performed under temperature control.

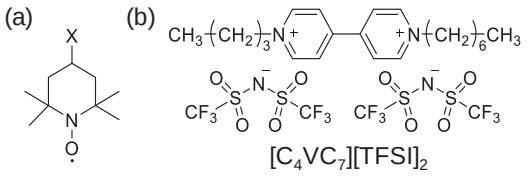

Fig.1. Chemical structures. (a) TEMPO derivatives, X is an electroneutral or a charged substituent, (b) a viologen-type ionic liquid.

Results and discussion: Fig. 2 shows typical CV and EPR spectrum of a TEMPO derivative (X = -OH), abbreviated as TEMPOL, in $[C_4VC_7][TFSI]_2$ at 60 °C. The rotational diffusion coefficient of TEMPOL obtained from EPR was 2.1×10^{8} s^{-1}. The translational diffusion coefficient by the limiting current of the CV was 6.0×10^{-8} cm^2 s^{-1}. These diffusion coefficients are larger than the values calculated by Stokes-Einstein hydrodynamic theory. This is because the molecular size of TEMPOL is smaller than that of $[C_4VC_7][TFSI]_2$. Therefore, the diffusion of TEMPO derivatives in $[C_4VC_7][TFSI]_2$ should be carefully analyzed taking into consideration of the microenvironment of the solvent and size correction of the solute and solvent.

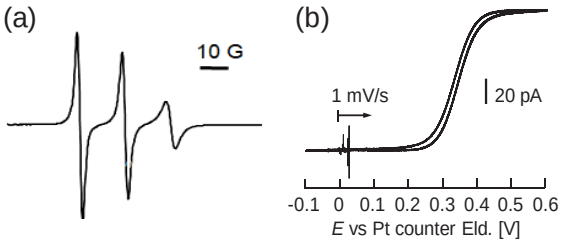

Fig.2. (a) EPR spectrum and (b) CV of a TEMPO derivative (X = -OH) at 60 °C.

1P15 Analytical applications of closed bipolar electrode array and consideration of its operating principle

Kumi Y. Inoue[1], Siti Masturah Fakhruddin[1], Tomoki Iwama[1], Miho Ikegawa[1], Hitoshi Shiku[1], Tomokazu Matsue[2] ([1]Graduate School of Environmental Studies, Tohoku University, Sendai, Japan, [2]Center for Promotion of Innovation Strategy, Tohoku University, Sendai, Japan)

Introduction: A bipolar electrode (BPE) is an electrically conductive material that promotes electrochemical reactions at its poles even in the absence of a direct ohmic contact. During the past 20 years, many interesting bipolar electrochemical experiments have been presented. We will present our applied study of bipolar electrochemistry to liquid-junction-free substitutional stripping voltammetry system, a sensor chip with liquid-junction-free reference electrode system for simultaneous multiple amperometric sensing, and high spatial-temporal electrochemical imaging system combined with electrochemiluminescent (ECL) detection, as well as our consideration of its operating principle

Experimental: Prototype sensor chips were fabricated with photolithography. For consideration of operation principle, we set a closed BPE (cBPE) system with a sample cell and a reference cell connected with a BPE. A pair of driving electrode was inserted into the sample cell and the reference cell connected to a WE terminal and a CE terminal of a potentiostat, respectively. A Ag/AgCl electrode connected to RE terminal of a potentiostat was inserted into the reference cell. To ensure that the reaction at the BPE pole in the sample cell was the rate-limiting process of entire system, an Au disc electrode (1.6 mm in diameter) was used in the sample cell that was sufficiently small relative to the other electrodes. In the sample cell, 0.5 mM ferrocenemethanol (FMA) was added as a model analyte. In the reference cell, a mixture solution of 2.5 mM $K_4[Fe(CN)_6]$ and 2.5 mM $K_3[Fe(CN)_6]$ with 100 mM KCl was placed.

Results and discussion: Using our experimental setup for consideration of operation principle, we obtained cyclic voltammograms (CVs) of FMA consistent with the conventional cyclic voltammetry. When using a same material (Au or Ag/AgCl) for both driving electrodes, CVs showing the same apparent formal potential were obtained, while when using Au and Ag/AgCl for two driving electrodes respectively, the formal potential was shifted 0.250 V from the previous CVs. From this result, we propose the driving principle based on the Kirchhoff's law. The devices also successfully worked and quantitatively measured the samples.

1P16 Electrochemical Evaluation of Metabolic Activity of Bacteria Immobilized on conducting bioplatform

Maki Saito, Kengo Ishiki, Hiroshi Shiigi, (Department of Applied Chemistry, Osaka Prefecture University, Osaka, Japan)

Introduction: Although pathogenic bacteria pose a threat to human life, some strains find application in areas such as sewage purification and microbial fuel cell construction. A better understanding of the biological functions of bacteria is required to increase the usefulness of these microorganisms, which, in turn, necessitates the quantitative evaluation of bacterial metabolic processes including growth and respiration. In this study, we tracked *Escherichia coli* growth on the polypyrrole (PPy) by dark-field microscopy and electrochemically evaluated the respiration of a single cell focusing on the consumption of dissolved oxygen.

Experimental: Pyrrole was added to the as-prepared *E. coli* suspension in a phosphate buffer. An ITO electrode was used as the working electrode. A polymerization was carried out at +0.98 V (vs. Ag|AgCl) for 100 s to obtain a cell-doped PPy film. Cyclic voltammograms (CVs) were recorded between −0.8 V and +0.6 V at 10 mV s^{-1} using a laboratory-made thin-layer cell [1].

Results and discussion: The dark-field image shows the cells as light, rod-shaped bodies, and the cell density is 1.5×10^6 cells cm^{-2}. Fluorescence observation indicates the cell viability to be greater than 99%. The growth of *E. coli* in PPy was examined by dark-field microscopy. We found that the typical growth pattern suggests that *E. coli* maintain metabolic activity in the PPy matrix as well as in the liquid medium. We evaluated the respiratory activity of *E. coli* in a PPy film using a thin-layer electrochemical cell. There was no discernible difference in the CVs recorded with and without glucose at 0-min incubation time. However, the oxygen reduction current decreased dramatically in the presence of glucose after 30 min. The decrease in the Faradaic current between −0.3 V and −0.8 V is attributed to the consumption of oxygen dissolved in electrolyte solution by *E. coli*. When the accumulated charge estimates from the difference in the current responses obtained before and after incubation, the quantity of oxygen were calculated to be 0.11 nmol. The estimated oxygen consumption by *E. coli* cells is 1.8×10^{-17} mol min^{-1} per cell.

The conducting polymer matrix is a useful platform for evaluating the metabolic activity of facultative anaerobic bacteria. In addition, its biocompatibility and electrical conductivity facilitates quantitative evaluation of oxygen consumed by bacterial cells.

[1] M. Saito, K. Ishiki, D. Q. Nguyen, H. Shiigi, *Anal. Chem.*, in press. DOI: 10.1021/acs.analchem.9b02350.

1P17 Detection and characterization of AGEs produced from immune cells using electrochemical techniques

Yutaro Takahashi[1], Hoshi Hiroyoshi[2], Shigenobu Kasai[1]
(Graduate Department of Electronics Tohoku Institute of Technology, Miyagi, Japan[1],
Research Institute for the Functional Peptide[2])

1. Introduction

Advanced Glycation End Products (AGEs) are substances produced by non-enzymatic reaction of reducing sugars and protein (amino groups) in the body. AGEs are associated with various pathological conditions such as accumulation with aging, diabetes and arteriosclerosis. Studies aimed at developing AGEs production inhibitors has been conducted, but the mechanism of action *in vivo* has not been elucidated [1]. Cytokines production has been previously monitored from cells using electrochemical ELISA [2].
In our current study, we first examined whether AGEs can be measured using electrochemical ELISA, and then report the results of examining the amount of AGEs produced from immune cells.

2. Experimental

In this experiment, competitive wells were formed using AGEs Competitive ELISA kit (Cell Biolabs, Inc.). First, the electrochemical measurement was performed using a 3 electrode method, and an experiment was performed using a phosphate buffer solution (pH 7.4) containing 4 mM Ferrocenemethanol (FcMeOH) and 2 mM hydrogen (H_2O_2) as a measurement solution. The Au electrode scanned 500 μm in the Z-axis at a scan rate of 10 μm/ s and FcMeOH was used as an electron mediator. AGEs were detected electrochemically by horseradish peroxidase (HRP) activity as shown in figure 1. Further, using a competitive method well fabrication process, the AGEs amount was compared in the presence or absence of phorbol 12-myristate 13-acetate (PMA) in the THP-1 cell suspension.

3. Results and discussion

Figure 2 shows the results of THP-1 cell count and AGEs production by PMA stimulation. The horizontal axis shows the number of THP-1 cells and the vertical axis shows the reduction current value and the AGEs amount. An increase in the AGEs amount was confirmed by the cell number and PMA stimulation. As a part of the study, we will also present results of an electrochemical study of the effects of AGEs on immune cells.

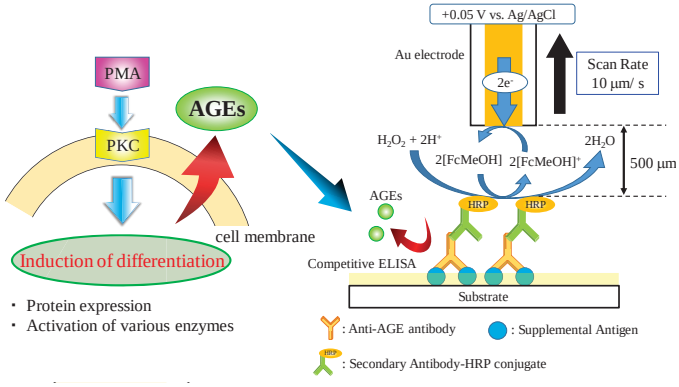

Fig. 1. Schematic diagram of electrochemical measurement of AGEs produced from THP-1 cells

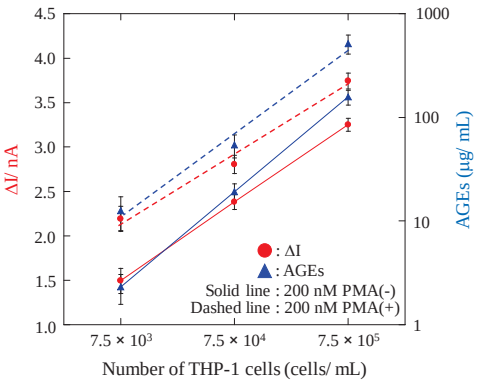

Fig. 2. Characterization of AGEs in THP-1 cell by PMA stimulation (n = 3)

References

[1] Y. Fujiwara, et al., Free Radical Biology and Medicine, 50, 883-891 (2011)
[2] S. Kasai, et al., Analytica Chimica Acta, 566, 55-59 (2006)

1P18 Direct Electron Transfer-Type Bioelectrocatalysis by Downsized and Axial-Ligand Exchanged Variants of D-Fructose Dehydrogenase

Yuya Kaida, Yuya Hibino, Yuki Kitazumi, Osamu Shirai, Kenji Kano (Kyoto Univ.)

Introduction: Direct electron transfer (DET)-type bioelectrocatalysis, in which the electrode reaction and the catalytic function of the redox enzyme are directly coupled, plays a significant role in constructing mediator-free, simple bioelectrochemical devices such as biofuel cells and biosensors with minimum thermodynamic energy loss. A membrane-bound heterotrimeric D-fructose dehydrogenase (FDH) from *Gluconobacter japonincus* NBRC3260, which contains a flavin adenine dinucleotide (FAD) in subunit I and three heme *c* moieties (1*c*, 2*c*, and 3*c* from N-terminus) in subunit II, shows strong activity in DET-type bioelectrocatalysis. FDH catalyzes an oxidation of D-fructose to 5-keto-D-fructose at the catalytic site FAD and transfers the electrons to the electrode via heme 3*c* and 2*c*, in this order. In order to improve the DET-type bioelectrocatalysis of FDH, two FDH variants were constructed: one that lacked 143 amino acid residues involving the heme 1*c* moiety and the sixth axial ligand of heme 2*c* was replaced with glutamine (M450QΔ1*c*FDH), and one that lacked 199 amino acid residues involving the heme 1*c* and 2*c* moieties (Δ1*c*2*c*FDH).

Experimental: Electrochemical measurements were performed using Au electrode on which each FDH variant was adsorbed.

Results and discussion: M450QΔ1*c*FDH-adsorbed electrode provided a larger catalytic current density at potentials more negative than that of recombinant FDH-adsorbed due to the downsizing of the enzyme and the negative shift of the formal potential of heme 2*c*. The Δ1*c*2*c*FDH variant transferred the electrons to the electrode at potentials more negative than that of rFDH due to its shortcut electron transfer pathway (Fig. 1).

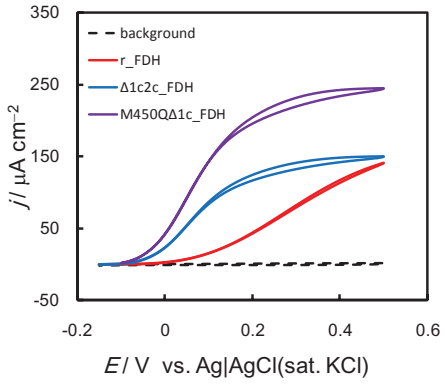

Figure 1. CVs of D-fructose oxidation at each FDH-adsorbed Au electrode.

1P19 Analysis of reaction products of polyphenols with DPPH radical

Kenji Matsumoto[1], Hiroki Hotta[1], Yukihiro Kimura[2], Toshiyuki Osakai[3], ([1]Graduate School of Maritime Sciences, Kobe University, Hyogo, Japan, [2]Graduate School of Agricultural Science, Kobe University, Hyogo, Japan, [3]Graduate School of Science, Kobe University, Hyogo, Japan)

Introduction: Polyphenols are a group of antioxidants characterized by the presence of several hydroxyl groups on an aromatic ring. Antioxidants are preferentially oxidized by oxidants such as radicals, therefore protect living tissues from the oxidation. 2,2-Diphenyl-1-picrylhydrazyl (DPPH) is an organic radical used to evaluate antioxidant activity. Since the antioxidant activity measurement by DPPH is performed by the changes in absorbance due to the reduction of radicals, detailed reaction mechanisms such as structural changes of antioxidants and DPPH cannot be observed. So far, we have reported that antioxidants can be classified into three groups by observing the time course change of this reaction by cyclic voltammetry (CV) measurement. The purpose of this study is to clarify the reaction mechanisms by separation and analyzing the reaction products of antioxidants with DPPH.

Experimental: The oxidation products of antioxidant was analyzed by HPLC. Antioxidant sample solutions were oxidized by injecting into DPPH solution (MeCN-aqueous mixed solvent containing Tris buffer (pH 7.4)), or by flow complete electrolysis.

Results and discussion: In CV measurements, the reaction between antioxidants and DPPH was classified into three patterns. In the first group, the reactants (antioxidants and DPPH radical) showed reversible electron transfer. The both reaction products of antioxidant and DPPH were stable, and they showed reversible electron transfers. *p*-Hydroquinone, one of this group, DPPH adducts or dimers were not detected, and only *p*-quinone was detected. The same result was obtained by an electrolytic oxidation. In the second group, DPPH undergoes reversible electron transfer, on the other hand antioxidants undergo irreversible oxidation by subsequent reactions. Regeneration of reductant, multimer formations, and re-oxidation of these products of caffeic acid were observed by HPLC analysis of electrolysis products. It was found that the similar reaction proceed in the chemical oxidation by DPPH. In the third group, the both reactants behave irreversibly. As for catechin, many oxidation products were detected. Some of which appeared only in the reaction with DPPH. These are considered to be addition products of DPPH. From these results, we consider that there is a need to analyze not only the change in absorbance but also the reaction products in the DPPH measurement.

1P20 Distribution of ionic species into the bilayer lipid membrane

[1]Koji Murakami, [1]Kisho Hori, [1]Terumasa Omatsu, [1]Masahiro Miyagi, [1]Naoto Ishida, [1]Hotaru Minato, [1]Kohji Maeda, [2]Mao Fukuyama, [1]Yumi Yoshida ([1]Kyoto Institute of Technology, Kyoto, Japan, [2]Tohoku University, Sendai, Japan)

Introduction: The distribution constant of the ionic species between the aqueous phase and the bilayer lipid membrane (BLM) is the parameter expressing the direct transport of the ionic species through the BLM. However, it is difficult to evaluate the distribution constant experimentally, which strongly depends upon the concentration of the coexisting electrolyte or the presence of the hydrophobic coexisting ion. Moreover, the BLM is an ultrathin membrane of nanometer thickness and has functional groups on the membrane surface, and not only distribution into the membrane but also adsorption of ionic species on the membrane surface takes place. In the present work, the distribution of the target ion between the aqueous phase and the BLM was analyzed based on the partition model of ions and the distribution constant of the target ion was evaluated from the dependence of the apparent distribution ratio of the target ion upon the concentration of the coexisting counter ion.

Experimental: A fluorescent ion (rhodamine 6G$^+$: R6G$^+$) or an ionic peptide modified with fluorescent probe (arginine peptide modified with fluorescein: FL-R8^{8+}) were utilized as the target ion. The extraction of the target ion with various anions (X$^-$: Cl$^-$, Br$^-$, BF_4^-, ClO_4^-, or Pic$^-$) into liposomes was carried out based on the dialysis membrane method[1)].

Results and discussion: The extraction of R6G$^+$ by liposomes was explained by the following equilibria: the adsorption equilibrium on the BLM surface (K_{ad}), the ion distribution equilibrium in the BLM (K_D), and the ion-pair formation equilibrium in the BLM (K_{ip}). The adsorption equilibrium was confirmed to be unaffected by the coexisting counter ion. The apparent distribution ratio (R) can be expressed by a quadratic equation of $[X^-]^{1/2}$, and the equilibrium constants were estimated from the curve fitting as shown in Table 1.

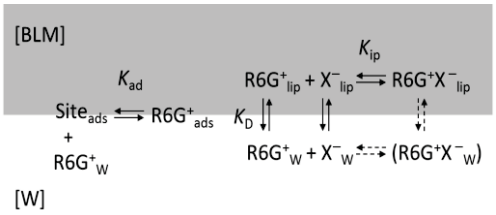

Figure 1 Equibria at the BLM interface

Table 1 The estimated values

X^-	K_{ip} /mol^{-1} L	K_D	K_{ad} /mol^{-1} L
Cl^-	N.D.	N.D.	16000
Br^-	2800	0.12	13000
BF_4^-	2300	1.4	11000
ClO_4^-	15000	3.0	13000
Pic^-	76000	40	14000

1) K. Murakami, K. Hori, K. Maeda, M. Fukuyama and Y. Yoshida, *Langmuir*, 32 (2016) 10678, *Langmuir*, 35 (2019) 6492.

1P21 Toxicity evaluation of chemical substances based on the monitoring of oxygen consumption of zebrafish by Bio−LSI

Kazuki Terao[1], Masato Suzuki[1], Ryota Kunikata[2], Atsushi Suda[2], Kumi Y. Inoue[3], Kosuke Ino[4], Tomokazu Matsue[3], Tomoyuki Yasukawa[1]
([1] Graduate School of Material Science, University of Hyogo. [2] Japan Aviation Electronics Industry.[3] Graduate School of Environmental Science, Tohoku University. [4] Graduate School of Engineering, Tohoku University.)

Introduction:

We have developed an estimation method of the effect of chemicals. A zebrafish was arranged on a chip of large scale integration based amperometric sensors (Bio-LSI) [1], which can be detected the current responses of 400 microelectrodes integrated on the chip. The reduction current of oxygen around a zebrafish was monitored after adding the valinomycin. A zebrafish was embedded in a thin layer of agarose gel to restrict the motion. The layer with the zebrafish was then arranged on the chip to determine the oxygen concentration at neighboring zebrafish.

Experimental:

A Zebrafish was arranged on the chip filled with the low melting point agarose solution containing artificial seawater. We added the seawater containing valinomycin over the gel layer. Voltage of –0.5 V at which oxygen was sufficiently reduced was applied to all 400 electrodes to obtain the images of the reduction currents of oxygen.

Results and discussion:

Fig .1 shows optical and current images of zebrafish embryo on Bio-LSI chip. The region with low reduction current of oxygen (white area) coincided with the location of the embryo in the optical image. The embryo absorbs oxygen around the embryo and, therefore, the concentration of oxygen around the embryo becomes low compared to the remainder. We investigated the effect of valinomycin on cellular image. The addition pales the current image of the cells, indicating that valinomycin lowers the respiration activity. We can trace cellular activity by monitoring the reduction current of oxygen with Bio-LSI systems.

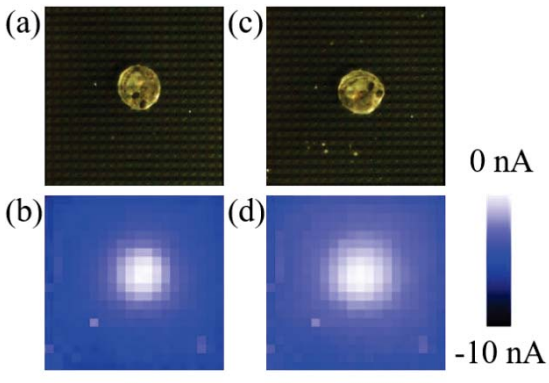

Fig .1 Optical and current images on Bio-LSI chip before ((a), (b)), and 10 minutes after adding the solution containing valinomycin ((c), (d)).

[1] Inoue, K. Y., et al., *Lab Chip*, **2012**, *12* (18), 3481-3490.

1P22 Catalytic reduction of Uranyl ion by metal hydroxide nanoparticles

Y. Kitatsuji, K. Ouchi, T. Yomogida, H. Otobe (Japan Atomic Energy Agency)

Introduction: Since the migration of radioactive elements in environment is affected by the solubility of them in a water, understanding chemical states and chemical reactions of the ions is necessary to evaluate the safety of the radioactive waste dispersal Redox reactions of actinide ions such as U, Np and Pu in a low-acid solution are often accompanied by the formation of hydroxide complexes, colloids and precipitates. Therefore voltammetric studies of these ions have been limited. The authors have studied the electrode reactions of actinide ions with coupled chemical reactions, and they have reported the autocatalysis of the U(V) reduction to U(IV) in a weak acid solution where U(IV) forms hydroxide nano particles[1]. The formed U(IV) nano particles facilitate the reduction of U(V). In the present study, possibility of catalysis of some kinds of metal hydroxide analogous to U(IV) hydroxide is investigated in order to elucidate the reaction mechanism of U(V) reduction.

Experimental: The colloidal nano particles of Zr(IV) and Ce(IV) hydroxide were prepared by neutralization of $HClO_4$ solution containing those perchlorate. After hydroxide particle was aged, U(VI) ion was added in the solutions. Electrolysis was performed by using bulk electrolysis cell at the constant potential to reduce uranyl ion and time course of reduction current was recorded.

Results and discussion: When the U(VI) in a solution of pH 3.0 was electrolyzed at a constant potential of -0.35 V vs silver/silver chloride electrode, the electrolysis current decreased rapidly and exponentially due to reduction of U(VI) to U(V). After the almost steady-state current was observed for several min, increase of current was observed. Increase in current is due to autocatalysis by U(IV) particle formed both in a solution and on the electrode surface[2]. In the case of the solution containing Zr(IV) hydroxide, the larger reduction current of U(VI) was observed in initial stage of bulk electrolysis. This result indicates that U(VI) was reduced further to U(IV) with catalysis of Zr(IV) hydroxide before forming U(VI) hydroxide particle. Zr(IV) is redox inactive. Thus, in the catalytic reduction of U(V) ion, the metal hydroxide particle does not participate directly in electron transfer. The metal hydroxide catalyst seems to provide reaction field to reduction of U(V). The results of chemical state analysis of the U particles are also discussed.

[1] Y. Kitatsuji, H. Otobe, T. Kimura, S. Kihara, Electrochim. Acta, 141(2014)6-12.

1P23 Design of Carbon Nanotube-based Non-precious Metal Electrocatalysts with High Performance Title

Jin Nishida[1], Jun Yang[1], Shunsuke Uchimura[2], Jun Matsuda[3], ○Naotoshi Nakashima[1]

[1]International Institute for Carbon Neutral-Energy Research (WPI-I2CNER), Kyushu University, Fukuoka, Japan
[2]Graduate School of Engineering, Kyushu University, Fukuoka, Japan
[3]International Research Center for Hydrogen Energy, Kyushu University, Fukuoka, Japan

E-mail: nakashima.naotoshi.614@m.kyushu-u.ac.jp

Introduction: In recent years, a sustainable and low-carbon emission energy chain has attracted much attention. Toward the goal, the development of non-precious metal electrocatalysts for fuel cells, water splitting and batteries with high performance, durablity, and scalability is a strong social demand for the next-generation eco-friendly energy society[1].

Experimental & Results and discussion: In this meeting, we summarize our recent studies on i) seven different nanocarbons /iron phthalocyanine (II) hybrids with well-defined nanostructures that show excellent efficiency and durability for oxygen reduction reaction[2,3], ii) decorating unoxidized-carbon nanotubes with homogeneous Ni-Co-spinel nanocrystals that show superior performance for oxygen evolution and oxygen reduction reactions[4], and iii) nanocarbon-Fe-Ni-based catalyst with high oxidation evolution reaction performance, in which we used several kinds of nanocarbon including multi-walled carbon nanotubes and carbon black as a carbon support and compared the performance of oxidation evolution reaction.

References

[1] N. Nakashima (Editor), "Nanocarbons for Energy Conversion-Supramolecular Approach-", Springer, **2018**, pp. 1-564.
[2] J. Yang, J. Tao, T. Isomura, H. Yanagi, I. Moriguchi, N. Nakashima, *Carbon*, **2019**, *145*, 565-571.
[3] J. Yang, F. Toshimitsu, T. Fujigaya, N. Nakashima, *J. Mater. Chem. A*, **2017**, *5*, 1184-1191
[4] J. Yang, T. Fujigaya, N. Nakashima, *Sci. Rep.*, **2017**, *7*, art.no.45384.

1P24 A strategy for in silico prediction of the membrane permeability of drugs

Yuri Nagai, Erina Yoshida, Yu Fujii, Toshiyuki Osakai
(Department of Chemistry, Kobe University, Kobe, Japan)

Introduction: The membrane permeability is a key element in drug discovery. Previously our group determined the standard ion-transfer potential ($\Delta_O^W\phi^\circ$) of cationic amine drugs by using ion-transfer voltammetry (ITV), showing that $\Delta_O^W\phi^\circ$ could be a useful index for the membrane permeability [1]. Also, we developed a digital simulation technique [2] for the recently/frequently used parallel artificial membrane permeation assay (PAMPA), and then revealed that the permeability coefficient in PAMPA (P_{pampa}) could be estimated from the distribution coefficient ($K_{\mathrm{D,M}}$) of the neutral form of a drug molecule to the artificial lipid membrane. It was also found that there is a liner relationship between $\log K_{\mathrm{D,M}}$ and $\Delta_O^W\phi^\circ$ for the cationic drugs [3]. In addition, we have recently developed a non-Bornian solvation model [4], which enables us to estimate accurately the ion-transfer energy $\Delta G_{\mathrm{tr}}^{\circ,\mathrm{W}\to\mathrm{O}}$ ($=zF\Delta_O^W\phi^\circ$) based on DFT calculation. Accordingly, from the thus estimated value of $\Delta_O^W\phi^\circ$, we can predict $\log K_{\mathrm{D,M}}$ by using the empirically obtained liner relationship. Then, we can use the digital simulation method to predict P_{pampa} for ionic drugs. In the previous paper [3], we used experimental data to suggest that such perfect in silico prediction could be done for cationic drugs. In this study, we have extended PAMPA measurements to anionic drugs.

Results and Discussion: For anionic drugs including ketoprofen, indomethacin, proxicam, and sulfadimethoxine, experimental $\log P_{\mathrm{pampa}}$ vs. pH plots showed a reverse sigmoidal curve, as shown in the right figure for piroxicam. This indicates that the lower the pH, the higher the concentration of the membrane-permeable neutral form of anionic drugs, and thus the higher the drug permeation rate. Using the digital simulation method, we could determine the values of $\log K_{\mathrm{D,M}}$ for the anionic drugs to find their liner relationship with those of $\Delta_O^W\phi^\circ$ determined by ITV. From these experimental data, it has been confirmed that the perfect in silico prediction of membrane permeability was also possible for anionic drugs.

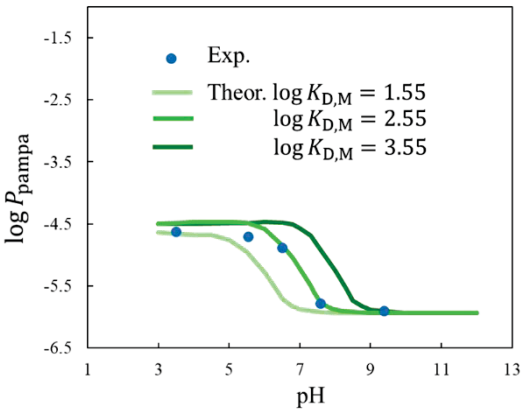

[1] M. Nakamura, T. Osakai, J. Electroanal. Chem. 779 (2016) 55. [2] M. Nakamura, T. Osakai, Eur. J. Pharm. Sci. 91 (2016) 154. [3] Y. Fujii, et al., Bull. Chem. Soc. Jpn. 91 (2018) 1618. [4] A. Yamada, et al., Anal. Sci. 34 (2018) 919.

1P25 Phase transition behavior of $MgMn_2O_4$ cathode during magnesium ion insertion/extraction reactions

Saeko Otani[1], Kentaro Yamamoto[1], Hiroaki Imai[2], Toshihiko Mandai[3], Tomoki Uchiyama[1], Toshiyuki Matsunaga[1], Kiyoshi Kanamura[4], Yoshiharu Uchimoto[1] ([1]Graduate School of Human and Environmental Studies, Kyoto University, [2]Department of Applied Chemistry, Faculty of Science and Technology, Keio University, [3]National Institute for Materials Science, Ibaraki, [4]Department of Applied Chemistry for Environment, Graduate School of Urban Environmental Sciences, Tokyo Metropolitan University)

Introduction: Magnesium rechargeable batteries are deemed the next-generation secondary battery systems because of their high theoretical capacity and the terrestrial abundance of magnesium. However, in terms of cathode materials, major problems are the strong polarization effect and slow diffusion of Mg^{2+}. In this study, we examine phase transition behavior of $MgMn_2O_4$ cathode during Mg^{2+} insertion/extraction reactions using electrochemical and synchrotron radiation measurements.

Experimental: $MgMn_2O_4$ composite electrode was used as a working electrode, magnesium metal was used as a counter and reference electrode. 0.3 M $Mg[B(HFIP)_4]_2$/triglyme was used as an electrolyte solution. Galvanostatic charge/discharge measurements were performed at rate of 1/20 C rate at 50 °C. *operando* x-ray absorption spectroscopy measurements for Mn K-edge were performed at BL14B2 in SPring-8, Japan.

Results and discussion: The $MgMn_2O_4$ composite electrode exhibits 75 mAh/g discharge capacity and 60 mAh/g charge capacity during first charge/discharge cycle. *operando* Mn K-edge XAS measurements shows that XANES shifted to lower energy during discharge process and shidted to higher energy during charge process. These results indicate that Mn in the $MgMn_2O_4$ contributes to the charge compensation for Mg^{2+} insertion/extraction reactions.

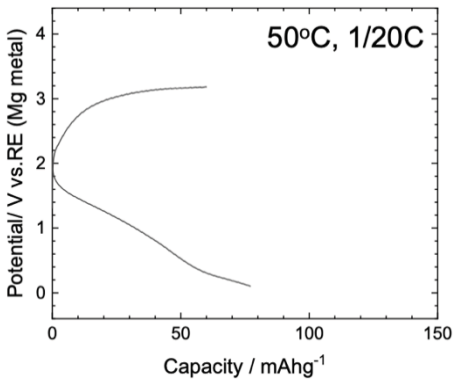

Figure 1. Charge/discharge curves of $MgMn_2O_4$ composite electrode.

Acknowledgement: This research was financially supported by JST, ALCA-SPRING Project.

1P26 Electrochemical property of Cu nano-composite cathode for all-solid-state fluoride ion battery

Datong Zhang[1], Yuya Kitaguchi[1], Kenji Tojigamori[2], Kazuto Ide[2], Shinji Nakanishi[2], Hideki Iba[2], Kentaro Yamamoto[1], Tomoki Uchiyama[1], Toshiyuki Matsunaga[1], Koji Amezawa[3], Koichi Tsuchiya[4], Yoshiharu Uchimoto[1]* ([1]Graduate School of Human and Environmental Studies, Kyoto University, Kyoto, Japan, [2]Battery Research Div., Higashifuji Technical Center, Toyota Motor Corporation, Shizuoka, Japan, [3]Institute of Multidisciplinary Research for Advanced Materials, Tohoku University, Sendai, Japan, [4]Research Center for Structural Materials, NIMS, Ibaraki, Japan)

Introduction: Herein, we introduce nanocomposites and high-pressure torsion (HPT) as effective optimizing methods for the Cu cathodes materials of all-solid-state fluoride ion batteries (FIBs), which leads to ideal electrochemical properties compared with previous reports, with the X-ray absorption fine spectroscopy (XAFS) being proposed to understand the details of phase transition and reaction procedures.

Experimental: The nanocomposites with Pb was tested in thin-film type all-solid-state batteries and prepared by the RF Sputtering using LaF_3 substrates. The Cu K-edge XANES measurements of the batteries at various state of charge (SOC) were conducted at BL01B1 beamlines (SPring-8, Hyogo, Japan). The effects of HPT processing were evaluated by bulk cells using $PbSnF_4$ as electrolytes.

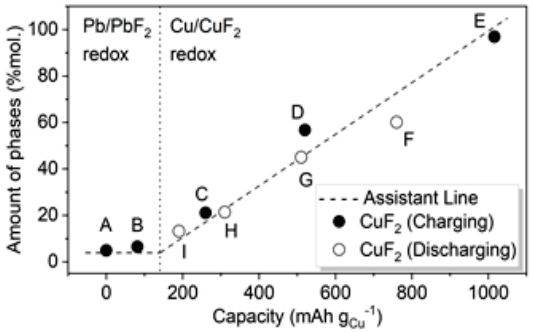

Figure 1. Amount of CuF_2 upon charging and discharging, fitted from XANES data.

Results and discussion: After being composited with Pb nanolayers, the electrochemical properties of Cu-Pb nanocomposites greatly exceeds those of Cu metal at 25°C. The extra electrochemical behaviors of Pb/PbF_2 redox near 0.5 V could be observed on the charge-discharge curves of Cu-Pb nanocomposites. The PbF_2 generates in advance and acts as F fast ion conductor, which is beneficial to realize the deep (de)fluorination of Cu. The HPT processing could also improve the electrochemical performances by inducing more defects into cathode bulks, and thus improving the kinetics of F ion transportation.

1P27 The state of Ni and O in Li doped NiO for oxygen evolution reaction

Yadan Ren, Tomoki Uchiyama, Kentaro Yamamoto, Toshiyuki Matsunaga, Yoshiharu Uchimoto (Kyoto University, Kyoto, Japan)

Introduction: Investigating the electronic states on the electrode surface under applying potential is necessary to understand oxygen evolution activities. As the contribution of catalyst is limited to near-surface region, surface sensitive *in-situ*/*operando* measurements are required for understanding the behavior of the catalyst. Among many recently reported catalysts, $LiNiO_2$ exhibits the high oxygen evolution reaction (OER) activity in water electrolysis [1]. In this study, we investigated $LiNiO_2$ thin film as electrocatalyst for oxygen evolution in alkaline media. Coupled with Total reflection *operando* X-ray absorption spectroscopy, the initial valence state of Ni and O in $LiNiO_2$ was also investigated by *ex-situ* soft X-ray absorption spectroscopy.

Experimental: NiO and $LiNiO_2$ thin film was synthesized on $SrTiO_3$ (100) substrate by pulsed laser deposition (PLD). The surface roughness was evaluated by atomic force microscope (AFM). The electrochemical tests were performed using Bio-Logic VMP-300 with a three-electrode cell comprising a thin-film fixed rotating disc electrode (HOKUTO DENKO) as the working electrode, a counter electrode (Pt wire), and reversible hydrogen electrode (RHE, reference electrode) under 0.1M KOH aqueous solution. Total reflection *operando* XAS was conducted by using home-made electrochemical cell at BL37XU, SPring-8 under 0.1M KOH aqueous solution.

Results and discussion: Figure 1 shows OER activity curves for $LiNiO_2$ and NiO. The onset potential of OER was smaller for $LiNiO_2$ than NiO. This tendency was consistent with the previous report [1]. According to AFM, the surface roughness of thin films wer under 10 nm, which was small enough for total reflection XAS. Total reflection Ni K-edge XAS indicated the shift of absorption edge for $LiNiO_2$. This suggested that the surface of Ni in $LiNiO_2$ had a higher oxidation state at 1.5 V as compared to NiO.

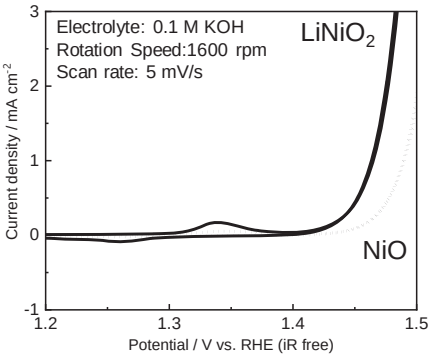

Figure 1. OER activity of $LiNiO_2$ and NiO

Acknowledgements

This research is based on results obtained from a project commissioned by the New Energy and Industrial Technology Development Organization (NEDO).

References

[1] G. Fu, X. Wen, S. Xi, Z. Chen, W Li, J.Y. Zhang, A Tadich, R. Wu, D.C. Qi, Y. Du, J. Cheng, K.H.L. Zhang, *Chem. Mater.*, **31** (2019) 419-428.

1P28 Chronoamperometry for double layer capacitances obeying the power-law

Ridong He[1,2], Koichi Jeremiah Aoki[2], and Jingyuan Chen[1,2] ([1]Univ. Fukui, [2]Elecrochemistry museum)

Introduction: A current-time curve of an ideal capacitance responding to a voltage step should theoretically exhibit an impulse, but that of a double layer (DL) capacitor shows a decay however small is a solution resistance. The decay may be cause by a relaxation included in DL capacitors in the form of the power-law of the ac-frequency. Potential-step chronoamperometry was made here at a Pt wire electrode in KCl solution at the aim of finding a role in the power law of the time or the constant phase element.

Experimental: A working electrode was a platinum wire 0.5 mm in diameter without any seal in order to avoid floating capacitance. It was treated with mixed acids. The test solution, 0.5 M KCl, was deareated for 20 min before chronoamperometry.

Results and Discussion: The current decayed, and the values were recognized even at 2 s (in the inset of Fig. 1). The logarithmic current at short times represents the well-known exponential decay (exp(-t/RC)), where R is the solution resistance. In contrast, the variation had a linear relation of the logarithmic time at the long time. The linearity indicates the power law ($I = C_{1s}t^{\lambda}$: λ being constant close to 0.1, C_{1s} being a value of C at t = 1 s). The intercept provides the capacitance value, regardless of the resistance. This prediction was demonstrated experimentally for KCl solutions of which concentrations ranged from 1 mM to 1 M. Therefore, the capacitance can be evaluated simply by the chronoamperometry on a second order time scale without considering any resistance effect.

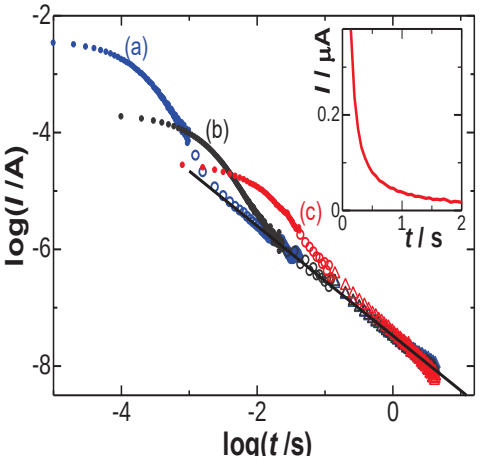

Fig. 1 Double logarithmic plots of the current-time curves observed at the 0.1 V voltage step in the solution of concentrations of (1) 0.1 M, (b) 0.2 M and (c) 0.3 M KCl.

References: 1) K Aoki, J Chen, X Zeng, Z Wang. RSC Adv.,7 (2017) 22501; 2) K Aoki, J. Chen. Faraday Discuss. 210 (2018) 219-234.

1P29 Transport characteristics of a CT ionic liquid consisting of a viologen and a carbazole

Yudai Tanaka, Shoko Yamamoto, Hironobu Tahara, Takamasa Sagara
(Graduate School of Engineering, Nagasaki University)

Introduction: Physicochemical properties, e.g. viscosity and conductivity, of ionic liquids can be modulated by a combination of the anion and cation. A charge transfer (CT) interaction between donor and acceptor has been attracted for photochemistry and electrochemistry to introduce extra functions that neither the donor nor acceptor show individually. To expand the variety of ionic liquids, particularly for functional ionic liquids, we have synthesized a mixed ionic liquid with CT interaction consisting of a carbazole as a donor and a viologen as an acceptor and investigated the physicochemical and electrochemical properties.

Experimental: A CT ionic liquid (CT-IL) was prepared as equimolar mixture of a carbazole-based RAIL ([CzC$_4$ImC$_1$][TFSI]) and a viologen-based RAIL ([C$_4$VC$_7$][TFSI]$_2$) (Fig.1(a)). UV-vis absorption spectra, viscosity, conductivity and CV measurements were performed under temperature control.

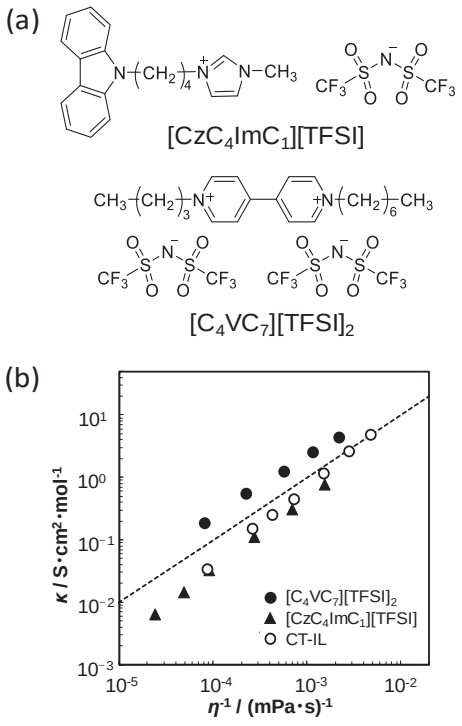

Fig. 1. (a) Chemical structures of the RAILs, (b) Walden plot of three RAILs. Broken line is the ideal Walden line.

Results and discussion: A new absorption band at 427 nm of CT-IL appeared by mixing faint yellowish [CzC$_4$ImC$_1$][TFSI] and the colorless [C$_4$VC$_7$][TFSI]$_2$. The absorption band indicates that CT complex between the carbazole and the viologen formed in CT-IL without a solvent. The slope in the Walden plot (Fig.1(b)) of CT-IL was greater than [CzC$_4$ImC$_1$][TFSI] and [C$_4$VC$_7$][TFSI]$_2$. This is likely due to the equilibrium of the formation and dissociation of the CT complex. The redox behavior of CT-IL was different from that of [CzC$_4$ImC$_1$][TFSI] and [C$_4$VC$_7$][TFSI]$_2$. We will discuss the electrochemical and physicochemical properties of CT-IL based on some temperature dependent experiments.

1P30 Electroporation by concentric-type needle electrodes and arrays

Yi Kung[1,5], Alexey Lihachev[2], Saulius Šatkauskas[3], Keng-Li Lan[4], Wen-Shiang Chen[1,5] ([1]Department of Physical Medicineand Rehabilitation, National Taiwan University Hospital, Taipei city, Taiwan. [2]Institute of Atomic Physics and Spectroscopy, University of Latvia, Riga, Latvia. [3]Biology Department, Faculty of Natural Science, Vytautas Magnus University,VKaunas, Lithuania. [4]Cancer Center, Taipei Veterans General Hospital, Taipei city, Taiwan. [5]National Taiwan University College of Medicine, Taipei city, Taiwan.)

Introduction: The efficacy of genomic medicine depends on gene transfer efficiency. In this area, electroporation has been found to be a highly promising method for physical gene transfer. However, electroporation raises issues related to electrical safety, tissue damage, and the number of required wounds.

Experimental: Concentric-type needle electrodes seek to address these issues by using a lower bias (10 V), a single wound, fewer processing steps, and a smaller working area (≈ 10 mm^3), thus offering greater accuracy and precision. Moreover, the needle can be arrayed to simultaneously treat several target regions.

Results and discussion: The proposed concentric-type electroporation needle electrode and array (NTUH 1) can be used with a lower bias, fewer wounds, fewer processing steps, and a smaller working area to provide significantly improved accuracy and precision (as shown in Table 1). Moreover, the proposed solution can be arrayed to simultaneously treat several target regions.

Due to the limitation of customized resources, the proposed needles-electrodes were all made using commercial products, as such imposing restrictions on prototype design (e.g., bevel size, needle shaft length). Nonetheless, once manufacturing issues are resolved, the proposed approach will provide a new tool for improving the efficacy of genomic medicine in terms of electrical safety, human factor and usability engineering.

Table 1. Comparison between NTUH 1 and BTX 533

	NTUH 1	BTX 533
Process steps of electroporation	1	2
Minimal transfer bias (V) [40 μg DNA]	10	50
Arrayed-possibility	Yes	No
Wound number	1	3
Required working area (mm^2)	2.4	113.1
Accuracy	High	Low
Precision	High	Low

2P1 Electrical double layer across semiconductor (S) | electrolyte soution(E), metal(M) | S, S | S interfaces

Masahiro Yamamoto (Konan University, Kobe, Japan)

Introduction: The theory of the electrical double layer across the metal electrode | electrolyte solution has 100 years history and Gouy, Chapman, Stern, Grahame (GCSG) model is widely used. The basic equation of the GCSG model is Poisson-Boltzmann (PB) equation which combine the one of the Maxwell equations and the charge density profile which is given by Boltzmann distribution. For the one-dimensional PB equations for the *z*:*z*, 1:2, and 2:1 electrolyte solutions, we have the analytical solutions. To investigate the double layer at micropore and rough surfaces we should solve the 3D PB equations by numerically.

In this study we reformulated the PB equation in semiconductor and to check the numerical solution is right we apply the method for the metal(M) | semiconductor (S) interfaces which gives the Schottky barrier across the interface. It is believed that the potential dependence of the capacitance of the Schottky barrier follows the Mott-Schottky relationship.

Method: The PB equation in semiconductor is given by[1]

$$\Psi = (e\,\phi + \mu - \mu_i) / (k_B T), \quad d^2\psi/dz^2 = K^2(\sinh\psi(z) - \Delta N(z)/2n_i), \quad K^2 = 2e^2 n_i/(\varepsilon_0 \varepsilon k_B T)$$

where e is elementary charge, ϕ is the potential, μ is the chemical potential (Fermi energy) of the system and set to be constant, μ_i is the chemical potential of intrinsic semiconductor, k_B is Boltzmann constant, T is absolute temperature, z is the distance from the metal electrode, $\Delta N(z) = N_d(z) - N_a(z)$, $N_d(z)$ is donor number density distribution, $N_a(z)$ is acceptor number density, n_i is carrier number density on intrinsic semiconductor, ε_0 is permittivity of vacuum, ε is dielectric constant. The fourth order Runge-Kutta method is used to solve the PB equation.

Results and discussion: In the present study the n-type semiconductor with 10^{16} cm^3 P dopant in Si (ε=11.8, E_{gap} = 1.12 eV, 6.55×10^9 cm^{-3}) is considered. The potential profile across the Schottky barrier is shown in the figure. We also calculated the parabolic potential profile which can be obtained with the approximations that the charge carrier density is zero. The PB numerical solution gives the longer-range double layer at the Schottky barrier.

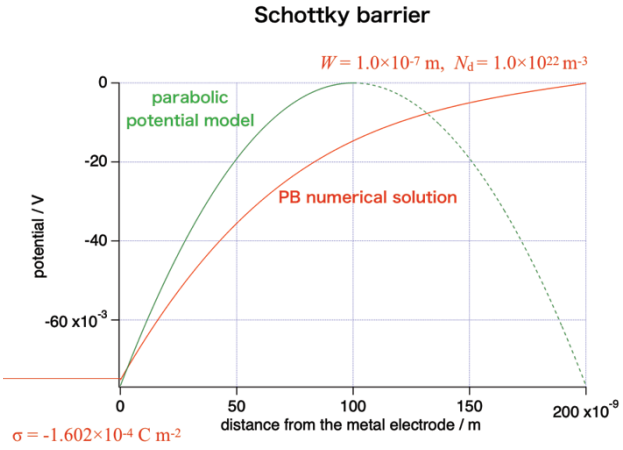

Reference [1] N. W. Ashcroft and N. D. Mermin, Solid State Physics, Chap. 29, 1976

2P2 Electrocatalytic Oxidation of Ethanol on PtAu Modified Nickel Wire Electrodes

Sota Funo, Munetaka Oyama (Department of Material Chemistry, Graduate School of Engineering, Kyoto University, Kyoto, Japan)

Introduction: As an easy method for preparing nanostructures of noble metals, such as Au, Pd and Pt, our group is interested in galvanic replacement reactions between noble metal precursors and common base metals. We tried to modify several common base metals, and consequently, found that Ni would be suitable for the purpose of noble metal modifications. Thus, our group reported the modification of Ni wire with Au for the application of electroanalysis [1], and the modification of Ni wire with Pd for electrocatalytic oxidation of ethanol [2]. The Pd modification is also possible on Ni microparticles via the galvanic replacement reaction [3]. As the next stage, we are trying to elucidate the modification of noble bimetals on Ni wire, so that the co-modifications of PdAu, and PtAu are carried out.

Experimental: The modification of Ni wire was performed by immersing a piece of Ni wire (diam. 3.0 mm) into an aqueous solution containing both $AuCl_4^-$ and $PdCl_4^{2-}$ (or $PtCl_4^{2-}$). By change the concentration of metal precursors, several modifications were carried out and the electrocatalytic properties were evaluated by observing cyclic voltammograms (CVs) of ethanol in an alkaline aqueous solution.

Results and discussion: In the modification of PdAu on Ni wire, it was found that the modification was significantly promoted by immersing an aqueous solution containing $AuCl_4^-$ and $PdCl_4^{2-}$, compared with single modifications of Pd or Au. Thus, the lower concentrations and shorter immersion time were enough to obtain higher electrocatalytic current. However, the observed electrocatalytic responses were that of Pd. On the other hand, in the modification of PtAu, unique electrochemical responses that are remarkably different from the responses of Au or Pt were observed. The electrochemical responses showed larger oxidation waves in the positive going scans, but the oxidation waves in the negative going scans were quite smaller. In addition, the oxidation current in the positive going scans significantly decreased with the scan cycles. While 1/100 of $PdCl_4^{2-}$/ $AuCl_4^-$ was too small to change the electrocatalytic responses to those of Pd, 1/100 of $PtCl_4^{2-}$/ $AuCl_4^-$ caused the impressive changes in the responses to the unique ones. We are now studying the details of the electrocatalytic responses.

1. Y. Umeya et al., *Electroanalysis*, **30**, 1370 (2018),
2. Y. Kobayashi et al., *ACS Appl. Energy Mater*, **2**, 2337 (2019)
3. Y. Kobayashi et al., *ACS Appl. Energy Mater*, in press.

2P3 Electrochemistry of cofactor F430 as a methane generation catalyst

Shota Harakawa[1], Seiya Tsujimura[1], Masanori Kaneko[2]
([1]Graduate School of Pure and Applied Sciences, University of Tsukuba, Ibaraki, Japan, [2]Geomicrobiology Research Group, National Institute of Advanced Industrial Science and Technology, Ibaraki, Japan)

Introduction: Coenzyme F430 is the hydrocorphinoid nickel complex which is contained in the enzyme, methyl coenzyme M reductase (MCR). MCR is responsible for the final step of the methanogenic reaction in the methanogenic archaea. F430 is known to be involved in the reduction of methyl coenzyme M to methane as active center of MCR. F430 resides at the end of the hydrophobic channel in the MCR. Due to the hydrophobic channel, MCR has strict reaction selectivity and can utilize only methyl coenzyme M (CH3-S-CoM) as a substrate.

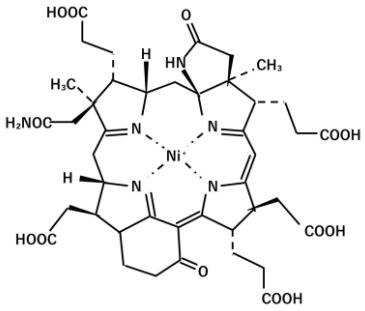

Fugure1. Coenzyme F430

The reduced form of F430 has Ni(+1), whereas oxidized form has Ni(2+). F430(ox) is known to be reduced by using a reducing agent such as titanium citrate (III). In this study, we utilized purified F430 as an electrocatalyst to produce methane from a variety of substrate which contains methyl group. The electrochemical methane production allows continuous methane production without any reducing agent.

Experimental and Result: We investigated the electrochemical reduction of CH_3-S-CoM using F430 as an electrocatalyst in pH 10 CAPS buffer solution. However, the CV did not change when we added F430 into the CH_3-S-CoM solution. Even the redox response of F430 on the electrode surface was not observed. We introduced redox mediator to facilitate the electron transfer between F430 and electrode. An increase of reduction current, starting at −1 V vs. Ag|AgCl was observed by adding methyl viologen into the F430 and CH_3-S-CoM solution. Because no catalytic current was generated in the absence of F430, we can conclude that F430 can catalyze the reduction of CH_3-S-CoM with an aid of methyl viologen as a redox mediator. Constant potential electrolysis at −1.3V vs AgAgCl was conducted using carbon cloth electrode in sealed electrolysis cell. We finally analyzed the gas in the headspace generated from the electrode surface; gas chromatography analysis revealed that the gas contains not only methane, but also ethylene.

2P4 Spatial analysis of membrane coupling between ion transport and electron transport

Kazushi Minai[1], Mao Fukuyama[2], Yumi Yoshida[2], Kohji Maeda[1] ([1]Kyoto Institute of Technology, Kyoto, Japan, [2]Tohoku University, Sendai, Japan)

Introduction: In the energy-transducing membrane as mitochondria, some ion transports are coupled with electron transports. In the biological membrane, the ion transport region and the electron transport region are located separately on the membrane. Under this condition, in order to maintain the electroneutrality inside and outside the membrane, same amounts of ions and electrons should be transported through a membrane under the established membrane potential. In the present study, an artificial membrane system with separated charge transport sites is constructed, and novel coupling mechanism depending on the distance of two sites has been demonstrated.

Experimental: Two liquid membrane systems, W1/O1/W2 and W1'/O2/W2, were connected through a common phase of W2, as shown in Fig.1(a). The former is the ion transport system and the latter is the electron transport system. The organic solvent used in O1 and O2 was nitrobenzene. W1 and O1 contained the transported ion (ferricenium ion, Fc^+) as hydrophilic and hydrophobic salts, respectively. W1' contained $[Fe(CN)_6]^{4-}$. O2 contained 7,7,8,8-tetracyano-quinodimethane, TCNQ, and its anion radical, $TCNQ^{\cdot -}$. When W1 and W1' were connected through Ag/AgCl electrodes, Fc^+ was transported from W1 to W2, and an electron was transported from W1' to W2. The electric current accompanied with the coupling flowed through an outer circuit from W1' to W1. The electric current was measured simultaneously with the membrane potential between W1 and W2 and that between W1' and W2.

Results and Discussion: When two liquid membrane systems were connected, the coupling current flowed, which depended on the distance between the O1|W2 interface and the O2|W2 interface. As seen in Fig. 1(b), the current at the distance of 20 μm was larger than that at 20 mm especially for long time scale of second order. This is because Fc^+ transferred at the O1|W2 interface was diffused from the O1|W2 interface to the O2|W2 interface, which participated in the redox reaction with TCNQ, resulting in the acceleration of the coupling reaction. The coupling reaction facilitated by the common ionic species is mimicking the proton coupling in the mitochondria membrane.

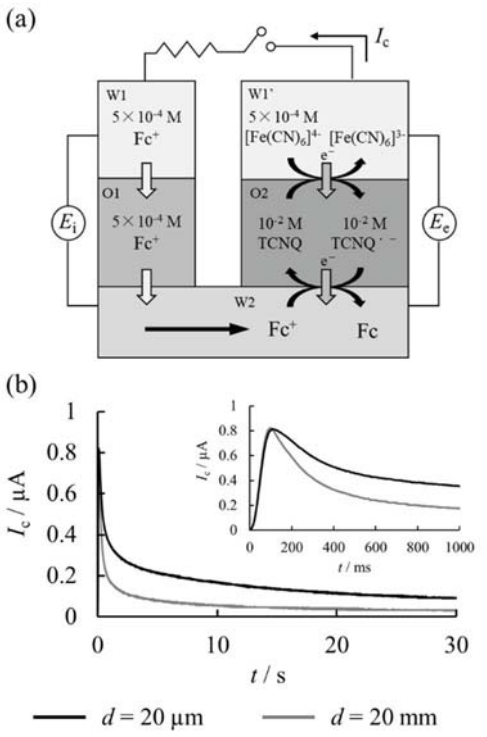

Fig. 1 Coupling reaction through same ion species. (a) Schematic model (b) Coupling current-time curve. The inset shows coupling current-time curve at mili-second scale.

2P5 The relationship between phase distance and fluoride ion intercalation kinetic properties in all-solid-state fluoride ion battery

Shuo Cao[1], Hidenori Miki[1,2], Toshiyuki Matsunaga[1], Kentaro Yamamoto[1], Hiroyuki Nakaki[1], Shinji Nakanishi[2], Hideki Iba[2], Tomoki Uchiyama[1], Koji Amezawa[3], Yoshiharu Uchimoto[1]
([1]Kyoto Univ., [2]TOYOTA Motor Corporation, [3]Tohoku Univ.)

Introduction:

Recently, fluoride ion battery using fluoride ions as carriers is quite attractive, which is capable of realizing high energy density in principle. Ruddlesden-Popper type perovskite is a promising cathode with excellent cycle and rate capability for fluoride ion batteries. Reaction of the Ruddlesden-Popper type perovskite proceeds by fluoride ion intercalation/deintercalation. The correlation between the lattice constant and diffusion rate of fluoride ion in the crystal structure has not been clearly understood, which inhibits to design high rate cathode materials. In this study, we synthesized $La_{2-2y}Sr_{1+2y}Mn_2O_7$ with different lattice constant and examined the electrochemical performance.

Experimental:

$La_{2-2y}Sr_{1+2y}Mn_2O_7$(y = 0.3, 0.35, 0.4, 0.48) were synthesized by the conventional solid state reaction from La_2O_3, $SrCO_3$ and Mn_2O_3. The obtained samples were characterized by X-ray diffraction and the crystal structure was determined by Rietveld refinement. The cathode was prepared from the composite of active materials, vapor grown carbon fiber and $La_{0.9}Ba_{0.1}F_{2.9}$ solid electrolyte. The counter electrode material consisted of PbF_2, $La_{0.9}Ba_{0.1}F_{2.9}$ and vapor grown carbon fiber. The cells were assembled in the Ar-filled glove box and the constant-current charge discharge measurements were operated at 140 °C.

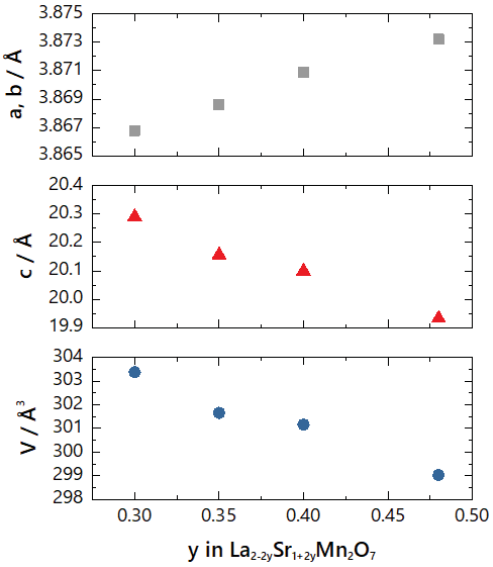

Figure 1. Lattice constant of the prepared $La_{2-2y}Sr_{1+2y}Mn_2O_7$ (y = 0.3, 0.35, 0.4, 0.48)

Results and discussion:

According to Rietveld refinement, $La_{2-2y}Sr_{1+2y}Mn_2O_7$(y = 0.3, 0.35, 0.4, 0.48) were successfully obtained with single phase and indexed to the space group of I4/mmm. Figure 1 showed the lattice constants of prepared samples. *c* showed the decrease with the partial substitution of La^{3+} by Sr^{2+}, while *a* and *b* increased with x. This might be due to the decrease of Coulomb repulsion on A-site. These materials showed the reversible insertion/extraction of fluoride ions during charge/discharge.

2P6 The effect of cation mixing on activity and durability toward oxygen evolution reaction in $LiNiO_2$

Ryusei Yamaguchi, Tomoki Uchiyama, Kentaro Yamamoto, Toshiyuki Matsunaga, Yoshiharu Uchimoto (Kyoto University, Kyoto, Japan)

Introduction: $LiNiO_2$ exhibits the high oxygen evolution reaction (OER) activity in water electrolysis [1]. However, Li^+ is expected to extract from its layered structure during electrolysis and lose its catalytic activity. Generally, $LiNiO_2$, with a rhombohedral structure(space group R-3m), has a partial cation mixing between Li (3*a*) and Ni (3*b*) sites due to the similarity of the ionic radius and Ni^{2+} at Li^+ (3*a*) site obstruct the diffusion path of the Li^+[2]. Thus, Cation mixed $LiNiO_2$ could suppress the extraction of Li from host matrix. In this study, the amount of cation mixing of $LiNiO_2$ was controlled by the synthesis conditions and their structural properties and OER activities were systematically analyzed.

Experimental: Cation mixed $LiNiO_2$ was synthesized from an aqueous solution containing $Ni(NO_3)_2 \cdot 6H_2O$, $LiNO_3$ and citric acid with molar ratio of 1:1:1.5. The solution was evaporated to dryness under stirring, followed by the calcination. For OER tests, polished glassy carbon electrode (a diameter of 5 mm, HOKUTO DENKO) was loaded with 0.30 mg/cm^2 of catalyst and ionomer (Nafion®). The electrochemical tests were performed using Bio-Logic VMP-300 with a three-electrode cell comprising a rotating disc electrode (HOKUTO DENKO) as the working electrode, a counter electrode (Pt wire), and RHE reference electrode under 0.1M KOH. OER durability test was evaluated by holding a potential at 1.8 V vs.RHE.

Results and discussion: In order to change cation mixing, the precursors were calcined by four conditions. The cation mixing amount of the synthesized $LiNiO_2$ was evaluated by X-ray diffraction and Rietveld analysis. OER durability (Figure 1) was evaluated from current persistence at 1.8 V vs.RHE. $LiNiO_2$(i) with a large amount of mixing of cation indicated the highest durability and $LiNiO_2$(iv) without cation mixing did the lowest. This high durability of $LiNiO_2$ was realized in a high cation mixing because the extraction of Li was inhibited by Ni at 3*a* site.

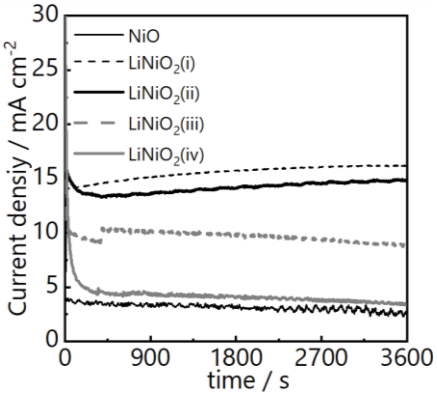

Figure 1 OER durability test

Acknowledgements: This research is based on results obtained from a project commissioned by the New Energy and Industrial Technology Development Organization (NEDO).

References: [1] G. Fu, X. Wen, S. Xi, Z. Chen, W Li, J.Y. Zhang, A Tadich, R. Wu, D.C. Qi, Y. Du, J. Cheng, K.H.L. Zhang, *Chem. Mater.*, **31** (2019) 419-428.

[2] T. Ohzuki, A. Ueda, M. Nagayama, *J. Electrochem. Soc.*, **140** (1993) 1862-1870.

2P7 Li metal dendrite growth behavior in all-solid-state battery observed by using *operando* CT analysis

Zhiwei Mu[1], Masakuni Takahashi[1], Yao Xiao[1], Hiromu Suzuki[1], Kentaro Yamamoto[1], Tomoki Uchiyama[1], Kentaro Uesugi[2], Akihisa Takeuchi[2], Atsushi Sakuda[3], Akitoshi Hayashi[3], Masahiro Tatsumisago[3], Toshiyuki Matsunaga[3], Yoshiharu Uchimoto[1] ([1]Graduate School of Human and Environmental Studies, Kyoto University, [2]Japan Synchrotron Radiation Research Institute, [3]Graduate School of Engineering, College of Engineering, Osaka Prefecture University)

Introduction: All-solid-state batteries using Li metal are attracting attention as next-generation storage batteries, but in order to use Li metal, it is necessary to suppress internal short-circuiting caused by dendrite growth of Li metal. To solve the problem, the three-dimensional non-uniform Li deposition behavior at the Li metal / solid electrolyte interface must be understood and controlled. In this study, we directly observe the three-dimensional non-uniform Li deposition behavior at the Li metal / solid electrolyte interface by using operando CT measurement.

Experimental: A symmetric cell was constructed by filling Li_2S-P_2S_5-LiCl solid electrolyte in a self-made operando CT cell and adhering Li deposited with 60 nm thick Au. CT images were acquired while performing charge / discharge measurements for a fixed time at a current density of 0.51 mA/cm^2. CT measurement was performed at a beamline BL20XU in SPring-8.

Results and discussion: Before Li deposition, there was a region that was not covered with Au in cross-sectional image. After Li deposition performed for 10 min, cracks occurred in the electrolyte starting from that region. In addition, compared to before Li deposition, the Au thickness expanded 1.58 times after Li deposition for 10 min. This value is similar to the expansion coefficient from Au to Li_3Au (1.55 times), suggesting that Au existing at the interface is alloyed. After 70 minutes of Li deposition, the cracks formed after 10 min of Li deposition expanded further. The Au at the interface was further expanded 1.1 times compared to after 10 min Li deposition, indicating that Au was dispersed after alloying. When Li precipitation was performed for 70 min and then Li dissolution was performed for 70 min, it was confirmed that cracks were reduced but did not return to the state before Li deposition (0 min).

Acknowledgement: This research was financially supported by JST, ALCA-SPRING Project.

2P8 Cation-induced ionic diode phenomenon in the microhole coated with Nafion

Ling Liu[1,2], Wataru Mizuno[1,2], Koichi Jeremiah Aoki[2],
Jingyuan Chen[1,2], ([1]Univ. Fukui, [2]Elecrochemistry museum)

Introduction: When voltage is applied between two ionic solutions which are separated with a hole in contact with an exchange membrane, the current-voltage curve exhibits ohmic variations with asymmetry for the positive voltage and the negative one, i.e. rectified variation like in a diode[1]. Although the ion exchange is obviously responsible for the rectification, rate-determining steps have not yet be known. We observed here the rectification ratio by changing the concentration of sodium and hydrogen ions by use of a cationic membrane, Nafion film.

Experimental: 0.5% Nafion solution was dropped onto a pin-holed PET film. The cell was composed of two glass funnels, of which mouths sandwiched the PET film. Some concentrations of NaCl and HCl were filled in the funnels. Two Ag|AgCl reference electrodes were inserted into the feet of the funnels. Time-scan voltage was applied to the two electrodes.

Results and Discussion: The current-voltage curves show two rising lines; the slope at in the voltage domain being larger than the other by ten times (Fig. 1). They were independent of voltage scan rates less than 0.3 V s^{-1}. The slope of the lines increased with concentrations of NaCl and HCl, but were not proportional to the concentrations (Fig.2).

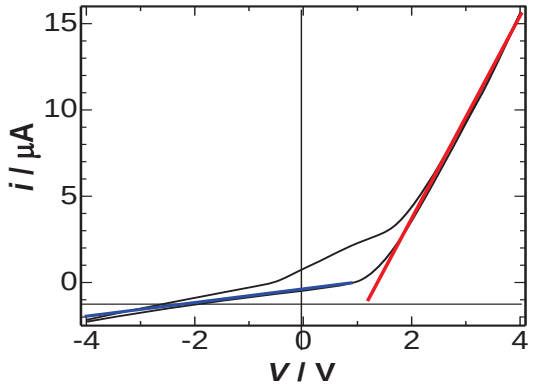

Fig. 1 Current-voltage curves in 0.1 mM NaCl solution at a hole 10 μm in diameter on a film 4.5 μm in thickness.

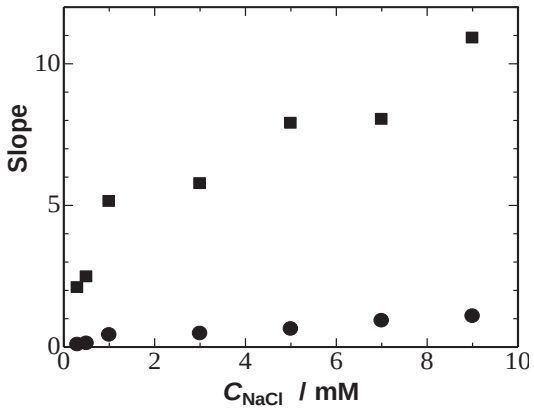

Fig. 2 Variations of the slopes of the current-voltage curves for (squares) E >1.5 V and (circles) E < 0.0 V with C_{NaCl}.

1. B. R. Putra, K. J. Aoki, J. Chen, F. Marken, A Cationic Rectifier Based on a Graphene Oxide Covered Microhole: Theory and Experiment, *Langmuir*, 35(6) (**2019**) 2055-2065

2P9 Detection of negative capacitance of redox reactions in cyclic voltammograms

Yuanyuan Liu[1,2], Bei Jia[1,2], Koichi Jeremiah Aoki[2], Jingyuan Chen[1,2], ([1]Univ. Fukui, [2]Elecrochemistry museum)

Induction: Voltammetric currents of redox reactions are conventionally regarded to be independent of double layer capacitive currents. When electrochemical oxidation generates a positive charge to relax the applied electric field, the generation of the charge would enhance the electric field in the electromagnetic sense. The enhanced field would be consumed as charging current, of which sign is negative in contrast to double layer charging current which relaxes the field. This effect has been demonstrated in ac-impedance of some redox species under the diffusion-controlled conditions. We use here cyclic voltammetry to measure the negative capacitance to find peak-potential shift by fast scan rates even under diffusion-control.

Experimental: A ferrocenyl derivative, FcTMA, was used as the redox species in 0.1 M KCl solution. A platinum thin wire 30 μm in diameter was used as a working electrode without electric shield in order to avoid floating capacitance and solution resistance. Scan rate v was varied from 0.01 V s^{-1} to 8 V s^{-1}.

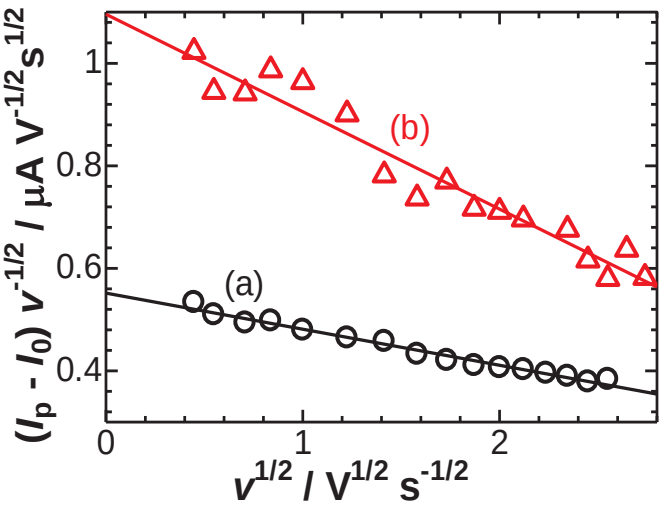

Fig. 1. Variation of $(I_p\text{-}I_0)v^{-1/2}$ with $v^{1/2}$ (a) for [FcTMA]= 1 mM and (b) 2 mM in 0.1 M KCl solution.

Results and Discussion: The currents varied linearly with $v^{1/2}$ at low scan rates and deviated below the linearity at high scan rates. The peak potentials at high scan rates were shifted linearly with log v, of which slopes were ca. ± 55mV. These values cannot be explained by heterogeneous kinetics. The peak currents can be represented by the sum of the diffusion current and the negative capacitive current: $(I_p - I_{p0})v^{-1/2} = 0.446AFc^*D(F/RTD)^{1/2} + Cv^{1/2}$. Fig. 1 demonstrates the validity of this concept. The capacitive value was -60 μF cm^{-2}, the absolute value being twice the DL capacitance.

2P10 Propagation of the action potential among multiple model cell systems

Issei Kasai[1], Yuki Kitazumi[1], Kenji Kano[1] and Osamu Shirai[1] ([1]Kyoto Univ.)

Introduction: The action potential propagation plays an important role in biological functions such as nerve conduction, constriction of muscles, etc. When muscle cells are electrically excited, the membrane potentials of whole cells change from the resting potential to the action potential one after the other. As for smooth muscles, the depolarization caused by pacemaker cells spreads to the neighboring cells via gap junctions. Since Ca^+ or K^+ flows through gap junctions between neighboring two cells, the local circulating current is generated between two cells. Thus the change in the membrane potential from the resting potential to the action potential is propagated within the tissue in succession.

In this study, the signal transmission among multiple cells was elucidated using a model cell system composed of multiple liquid-membrane cells. The liquid-membrane cells mimicking the function of K^+ and Na^+ channels were constructed. The signal transmission among respective cell units caused by activation of a given model-cell unit or application of the external electric stimulus were investigated based on the analysis of the relation among the respective membrane potentials and that among the currents flowing through the respective liquid-membrane cells.

Experimental: Two types of the electrochemical cells mimicking the functions of K^+ and Na^+ channels were constructed. W1 and W2 corresponded to the extracellular and intracellular phases, respectively. M mimicked a muscle cell membrane. The PTFE porous membrane filter impregnated with the nitrobenzene solution was used as M. The characteristics of cells were analyzed by cyclic voltammetry. Using these channel mimicking cells, model cell system was constructed. Fig. 1 shows the cell system composed of three model-cell units (1–3). The model-cell unit 1 had a switch to connect the Na^+-channel mimicking cell (Na1 cell) with the electric circuit. The Na1 cell was regarded as a source generating the action potential. The other two model-cell units had relay switches. When the membrane potentials of K^+-channel mimicking cells exceed the threshold (–50 mV), the Na^+-channel mimicking cell were connected. Thus Model cells 2 and 3 behave as signal receivers. These model cells were connected by resistors correspond to the fluid resistance and gap junction. The effect of the action potential generated at model cell 1 on model cells 2 and 3 were investigated.

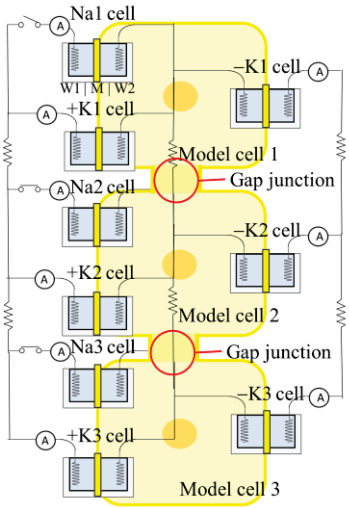

Fig. 1 Model cell system

Results and discussion: The characteristics of channel mimicking cells were similar as channels in living cell membrane. When the action potential was generated at the model-cell unit 1, the local circulating current flowed through gap junction. The influx and efflux current caused hyperpolarization and depolarization, respectively, on the surface of the neighboring cell, and the action potential was generated at the depolarized domain of the cells. The action potential spread all over the cell, and other neighboring cells were excited one after another. The propagation occurred faster because the large current passed through gap junction.

2P11 Electrochemistry of molecules bearing multiple viologen sites

Ayu Kawano, Hitomi Eguchi, Takamasa Sagara (Graduate School of Engineering, Nagasaki University, Nagasaki, Japan)

Introduction: Viologen radical cations ($V^{\bullet+}$) produced by one electron reduction of viologen dication (V^{2+}) tend to form dimers. It is an intriguing question how the electrode reactions of bis-viologen (bis-V) and tris-viologen (tris-V) depend on whether the intramolecular dimerization is allowed or forbidden. In this study, we analyze redox behavior of bis-V (Fig. 1) and tris-V, both in aqueous solution and on the electrode surface, to elucidate the factors of molecular assembling.

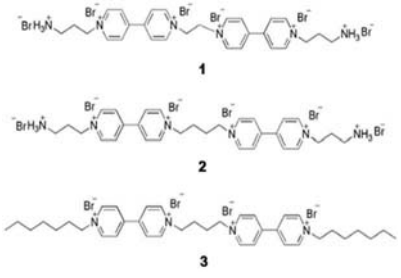

Fig. 1. Structure of viologens **1**,**2**, and **3**.

Experimental: Viologen solution was pipetted to place its droplet on an upward surface of a horizontally set HOPG electrode in an Ar gas atmosphere to measure voltammograms. A tip of an Ag/AgCl/sat'd KCl reference electrode and an Au wire counter electrode were immersed in the droplet. The bulk redox reactions were also examined at macro and micro Au electrodes using steady state voltammetry and electroreflectance methods.

Results and Discussion: On a HOPG electrode, **3** showed a phase transition between a gaseous adsorption layer of $V^{2+}$and a 2D condensed layer of $V^{\bullet+}$ (Fig. 2-a). On the other hand, highly water-soluble **1** and **2** showed no phase transition but the bulk redox reactions. In the three bis-V molecules, only **1** showed a set of reductive deposition and reoxidative dissolution (Fig. 2-b). CV data were summarized in Table 1. When **1** is reduced, $V^{\bullet+}$ dimerization occurred only intermolecularly, and much more than monolayer amount of $V^{\bullet+}$ molecules were deposited on the electrode surface. In contrast, the two-electron reduction product of **2** is an intramolecular $V^{\bullet+}$-dimer, which is still water soluble and lacking in adsorbtivity. Oxidized form of **3** can form a gaseous phase adsorption layer on the electrode surface, resulting in phase transition upon reduction (Fig. 2-a). The reduced form of **3** undergoes condensation through nucleation-growth process even after intramolecular dimerization. The results for tris-V will also be presented.

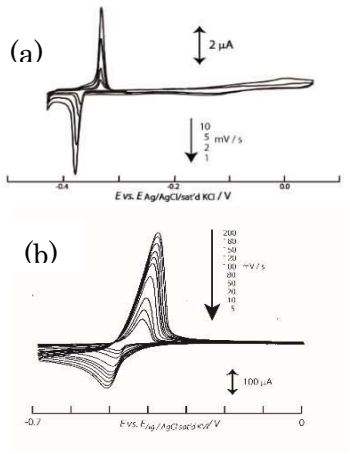

Fig. 2. CV of 1 mM (a) **3**, (b) **1** + 0.3 M KBr at HOPG electrode at various scan rates.

Table 1. Comparison of the redox behavior of three bis-viologens at HOPG electrode

bis-V	Redox process	Anodic process
1	Bulk, $E^{o'} = -554$ mV	Surface-deposited species
2	Bulk, $E^{o'} = -536$ mV	Solution species
3	Phase transition at surface, $E^{o'} = -352$ mV	$i_{pa} \propto v^{0.8}$

2P12 Development of bioelectrochemical barrier for BTEX degradation

Yung-Fu Wang (Light-Salt Testing Co. Ltd.)

Introduction:

Benzene, toluene, ethylbenzene and xylenes isomers (BTEX) that exist widely in the groundwater contaminated by gasoline and are spread by the groundwater flow. Traditional remediation methods of physical (Pump and treat) or chemical (chemical oxidation) techniques are generally costly. Biological approaches for treating BTEX in the contaminated groundwater appear to be economical and friendly environmental processes, but the supply of final electron acceptors for the microbe efficiently is still a strict problem. In our previous study, it was revealed that an electrode at a given potential could be the final electron acceptor for propionate bio-oxidation under anaerobic conditions. The goal of this research is to evaluate the possibility of BTEX bioelectrical degradation with an in-situ microbe as the biocatalyst under anaerobic conditions, as like the results under aerobic conditions.

Experimental:

The electrochemical bioreactor with a 100 mL anodic chamber was constructed to study the biodegradation of benzene with carbon felt electrode as the sole electron acceptor. The anodic potential was controlled at 0.2 V (vs. Ag/AgCl/KCl(sat.)) by a potentiostat, while a Pt wire was used as the counter electrode in the cathodic chamber. The experiments in electrochemical bioreactor were batch mode. Sterilized N2 gas was continuously flowed into the headspace of the anode chamber to maintain the anaerobic conditions during the experiment. Another soil column reactor (reaction volume was about 200 cm3) with continuous inlet was also constructed to simulate the biodegradation of BTEX in groundwater with carbon felt electrode as the sole electron acceptor. The concentrations of BTEX were measured by a GC/MS system.

Results and discussion:

The duration of the lag phase of benzene degradation was 150 hours in the first run, but it became shorter after several runs. The microbial consortia of benzene biodegradation with a carbon electrode as the electron acceptor was developed. The benzene in the anode chamber should be degraded completely by almost 100% coulombs efficiency. The degradations of BTEX were more than 95% in the soil column reactor. This result is useful for the development of a bioelectrochemical permeable reactive barrier.

2P13 Raman spectrum reveals cell-surface characteristics of *Shewanella decolorationis* NTOU1 under different pre-cultural conditions

Shiue-Lin Li[1], Yu-Xuan Liou[1], Yu-Ting Lin[1], Chi-Chang Lin[2] ([1]Department of Environmental Science and Engineering, Tunghai University, Taichung City, Taiwan, [2]Department of Chemical and Materials Engineering, Tunghai University, Taichung City, Taiwan)

Introduction:

In order to explore the extracellular-electron-transfer (EET) mechanism, Raman spectroscopy provides a way that is microscopic and non-invasive (to the bacterial cells), which possesses a high potential to analyze living cells when the current is generating. The goal of the study is to develop a platform to analyze the cell surface characteristics of EET capable microorganisms using Raman spectroscopy, and the *Shewanella decolorationis* NTOU1 was selected as a model species for analyses.

Experimental:

Raman spectroscopy was performed at room temperature using a B&W Tek's i-Raman® spectrometer (B&W Tek Inc., Newark, Delaware) equipped with a 50x objective. Different *Shewanella* strains were incubated under aerobic and anaerobic conditions respectively: under the aerobic condition, lactate and oxygen were supplied as the electron donor and acceptor, respectively; under the anaerobic condition, fumarate was supplied as the electron acceptor.

Results and discussion:

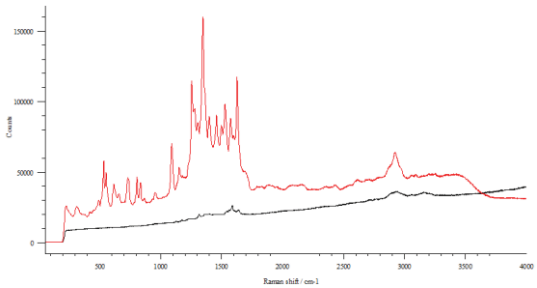

Figure . Raman spectroscopy for the analysis of the surface of *S. decolorationis* NTOU1 cell membrane. Red line, S. decolorationis NTOU1 cultured under aerobic conditions; black line, *S. decolorationis* NTOU1 cultured under anaerobic conditions.

2P14 Elimination of the diffusion limit by flowing amperometry to enhance the sensitivity of electrochemical detection

Jui-Hong Weng, Chih-Yu Lai, and Lin-Chi Chen* (Department of Biomechatronics Engineering, National Taiwan University, Taipei, Taiwan)

Introduction: Electrochemical detection in a microfluidic channel has been extensively applied in developments of various lab chips for bioassays, ranging from enzymatic to affinity-based molecular recognition. An Au electrode has well-established surface chemistry for decoration with versatile bio-recognition elements, such as antibodies, DNAs, and aptamers. Furthermore, the diffusion limit and laminar flow often show downsides in mass transfer and mixing, respectively, and both effects decrease the redox signal sensitivity in microfluidics.

Experimental: To understand how microfluidic amperometry is modulated by a flow condition, we investigate the influences of one-way flow and shuttle flow on the microfluidic amperometric detection in this work. When a forward bias is applied to the microelectrodes under a static condition, the electrode polarization results in a corresponding concentration polarization on the anode and cathode, respectively. Yet, if a one-way flow is applied to this two-electrode amperometry, a facilitated mass transfer occurs. It not only renews the surfaces of both electrodes but also increases the transfer rate in the microfluidic channel. By contrast, if the flow condition is changed to a specialized mode – a shuttle flow that moves a tiny drop of the redox couple back and forth at a certain rate for repeated reaction, the analyte will “swing” on the electrode area.

Results and discussion: One-way and shuttle flows are found especially effective for enhancing the micro-electroanalysis through exerting different flow effects. Increasing the flow rate, the one-way flow can bring in a facilitated mass transfer as evidenced by both the CV shape change from a symmetric wave-type curve to a sigmoidal I-V polarization curve and the steady-state CA response. A 24-fold enhancement of sensitivity in CA sensitivity is demonstrated. Although the shuttle flow is not as effective as the one-way flow in amperometry sensitivity enhancement and causes undesired oscillatory interference for CV, it yields a unique paired peak current pattern in CA, which can be used for not only the redox mediator quantification but also the observation of the change in flow polarization and the assessment of mixing completeness.

2P15 EIS Modeling of Symmetric Electrodes for Aptasensing

Wei-Chen Huang, Chih-Yu Lai, and Lin-Chi Chen* (Department of Biomechatronics Engineering, National Taiwan University, Taipei, Taiwan)

Introduction: Electrochemical impedance spectroscopy (EIS) applied for aptasensing using symmetric electrode systems are being extensively studied for a variety of targets. However, a single Randles circuit is often used for equivalent circuit fitting without having a detailed proof of validity of such implementation to date. This might cause erroneous parameter values being obtained. In this work, the parameter relationship between a single and symmetric Randles circuit is derived, and is verified by applying for impedimetric aptasensing of thrombin and the tumor marker MUC1 using symmetric Au electrodes.

Experimental: Symmetric electrode chips of different geometries are fabricated, and their symmetric electrochemical characteristics are verified. One-site specific binding models are used for evaluation and to further examine the applicability of theory. Aptasensing experiments with only $Fe(CN)_6^{3-}$ present and both $Fe(CN)_6^{3-/4-}$ present are verified using symmetric and three electrode setups.

Results and discussion: The parameter relationship holds when using different electrode geometries, even if finite diffusion of redox species is present when using interdigitated array (IDA) electrodes. For thrombin aptasensing with both redox species present ($Fe(CN)_6^{3-/4-}$), the relationship still holds after surface modifications and for binding events. Generality of the theory is examined using only $Fe(CN)_6^{3-}$, and a B_{max} value of 1.83kΩ and a K_D value of 129.4nM are calculated for thrombin detection. Specific EIS detection of MUC1 (3 ~ 200 nM) is performed using symmetric and three electrode setups for verification of the relationship, and K_D values of 16.31±1.44nM are obtained. Cross validation of sequence specificity is confirmed by comparing the binding affinity of S2.2 aptamer and 25mer random ssDNA sequences towards MUC1 and BSA. Thus, the feasibility of single Randles circuits applied for analyzing symmetric electrode systems is clarified, and researchers can relate the fitted and true values accordingly for obtaining important underlying parameters.

2P16 Modeling the acceleration of the redox reaction due to the heterogeneity of the electrical double layer caused by the microstructure at the electrode surface

Yuki Kitazumi[1], Seiji Nakanishi[1], Masahiro Yamamoto[2], Osamu Shirai[1], Kenji Kano[1] ([1]Kyoto University, Kyoto, Japan, [2] Konan University, Kobe, Japan)

Introduction: The facilitation of electrode reactions is an important subject for electrochemists. Acceleration of the electrode reaction due to the microstructure at the gold electrode surface has been experimentally observed. Since the electric field around the tip of the microstructure is enhanced, the electrical double layer (EDL) around the microstructure may be the origin of the acceleration. In order to demonstrate the EDL effect on the electrode reaction, a simple model based on the Poisson–Boltzmann and Butler–Volmer equations is constructed. The model shows the enhancement of the electrode reaction due to the microstructure at the electrode surface.

Model: Electric potential (ϕ) in an electrolyte solution around the microstructured conductor is calculated on the basis of the Poisson-Boltzmann equation. Electrode reaction is modeled by the Butler-Volmer equation. In order to eliminate the assumption of the reaction plane, the tunneling effect was introduced to the electrode reaction as follows,

$$v_{\mathrm{ox}} = -k^{\circ} \exp(-\beta x)\left\{c_{\mathrm{ox}} \exp\left(-\frac{\alpha F}{RT}(E-\phi-E^{\circ})\right) - c_{\mathrm{red}} \exp\left(\frac{(1-\alpha)F}{RT}(E-\phi-E^{\circ})\right)\right\},$$

where k°, x, c_{ox}, c_{red}, α, β, E, and E° are the rate constant, the distance from the electrode surface, the concentration of the oxidant, the concentration of the reductant, the transfer coefficient, the decay constant, the electrode potential, and the formal potential of the redox species, respectively. The current is calculated from the space integration of v_{ox}.

Results and discussion: Figure 1 shows the oxidation rate profile around a microstructure having a triangle shape with 5 nm height and 4 nm width at $E - E^{\circ}$ = 0.15 V. The electrode reaction is clearly enhanced at the convex tip of the microstructure on the electrode surface. The maximum value of the reaction rate shown in Fig. 1 is about twice that at the flat electrode. The origin of the rate enhancement is attributed to the compression of the EDL, which increases the difference between ϕ and E. Therefore, the oxidation reaction rate is high at a point where x is small and ($E - \phi$) has a large value.

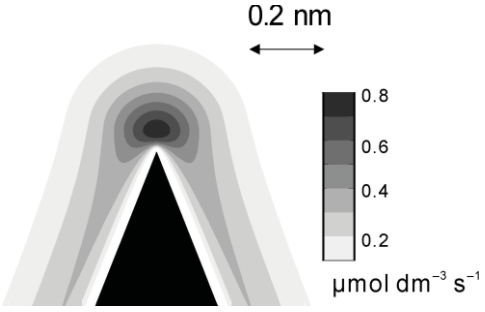

Fig. 1 Oxidation rate profile around a tip of the microstructured electrode at c^0 = 1 mM, k° = 1 ×10^6 s^{-1}, β = 1.4 Å^{-1}, and $E - E^{\circ}$ = 0.15 V.

2P17 Electrochemical behavior of uranium(IV) in ionic liquid-DMF mixtures

K. OUCHI[1], A. KOMATSU[1], K. TAKAO[2], Y. KITATSUJI[1], M. WATANABE[1]
([1] Japan Atomic Energy Agency, [2] Tokyo institute of technology)

Introduction: In fuel production of nuclear power generation, depleted uranium (U-235: 0.25%) is produced as a residue of uranium enrichment. It is a big problem that large amount of depleted uranium should be stored safely. We conceive the redox flow battery (RFB) based on the reactions of U(III)/U(IV) and U(V)/U(VI) to develop an effective utilization method of depleted uranium. The key to development is the stabilization of U(III) and U(V) which are unstable in aqueous solution. It has been reported that these ions can be stabilized in ionic liquids[1], but its high viscosity is drawback in flow systems. In this study, DMF was added to the ionic liquid to reduce the viscosity, and the electrochemical behavior of U(IV) in liquid-DMF mixtures was investigated.

Experimental: 1-Ethyl-3-methylimidazolium Bis(trifluoromethanesulfonyl)imide ($[EtMeIm^+][Tf_2N^-]$) was used for ionic liquid. UCl_4 was dissolved in 1:1 $[EtMeIm^+][Tf_2N^-]$-DMF mixture, U(VI) as an impurity was completely reduced to tetravalent by hydrogen reduction using a platinum black catalyst.

Results and discussion: The viscosity of 1:1 $[EtMeIm^+][Tf_2N^-]$-DMF mixture was 4.83 mPa/s of which the solution is easily pumped. The voltammogram of UCl_4 was measured (Fig. 1). Redox waves (Red1 and Ox1) at -1.6 and -1.5 V were observed only in the UCl_4 sample. This indicates that these waves are due to reaction of U(III)/U(IV). Further oxidation current of U(IV) was not observed at more negative potential than Cl^- oxidation; Red2 and Ox2 at 0.9 and 0.2 V were observed in the samples containing Cl^-. We conclude that U(III)/U(IV) in $[EtMeIm^+][Tf_2N^-]$-DMF mixture is applicable to the cathode reaction of RFB from these results.

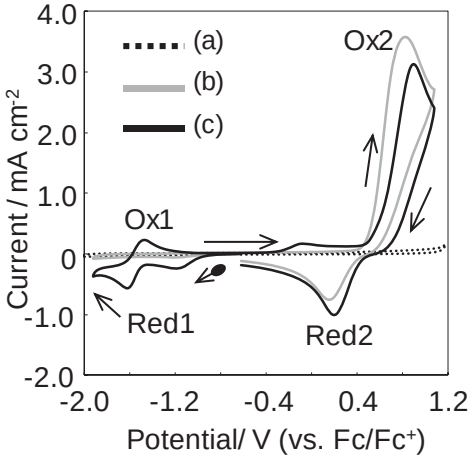

Fig.1 The voltammogram of UCl_4 in the 1:1 $[EtMeIm^+][Tf_2N^-]$-DMF mixture. (a) $[UCl_4] = 0$, $[Cl^-] = 0$. (b) $[UCl_4] = 0$, $[Cl^-] = 47$ mM. (c) $[UCl_4] = 11$mM, $[Cl^-] = 0$.

[1] C. Cannes, C. L. Naour, P. Moisy, P. Guilbaud, *Inorg. Chem.*, 52, **2013**, 11218−11227.

2P18 Non-Bornian analysis of the Gibbs transfer energy of fluorinated anions at the 2H,3H-decafluoropentane/water interface

Takeshi Kato[1], Kohei Uematsu[2], Hajime Katano[2], Kazuo Eda[1], Toshiyuki Osakai[1] ([1]Department of Chemistry, Kobe University, [2]Department of Bioscience, Fukui Prefectural University)

Introduction: Fluorous solvents are miscible with neither water nor some organic solvents, and their characteristic features have attracted the current interest in analytical and industrial sciences. Recently, our group [1] used ion-transfer voltammetry to determine the formal Gibbs energy of transfer for various ions from water (W) to 2H,3H-decafluoropentane (DFP) ($\Delta G_{\mathrm{tr}}^{\circ\prime,\mathrm{W}\to\mathrm{DFP}}$) and 1,2-dichloroethane (DCE) ($\Delta G_{\mathrm{tr}}^{\circ\prime,\mathrm{W}\to\mathrm{DCE}}$). In this study, we employed these data sets to perform multivariate regression analysis of $\Delta G_{\mathrm{tr}}^{\circ\prime,\mathrm{W}\to\mathrm{DFP}}$ and $\Delta G_{\mathrm{tr}}^{\circ\prime,\mathrm{W}\to\mathrm{DCE}}$ based on the previously proposed non-Bornian solvation model [2]. It has been found *via* energy decomposition analysis that there is a considerable repulsive interaction between DFP and non-fluorinated ions.

Calculation: Using the B3LYP hybrid DFT method with the 6-311++G(2d,p) basis set, structures of 11 highly-fluorinated anions, 12 non-fluorinated cations, and 11 non-fluorinated anions in vacuum were optimized and partial atomic charges were obtained by the Mulliken, MK (Merz-Kollman), and NPA (natural population analysis) methods. Then, the local electric field (E_i with i = 1, 2, 3, …) on the minute ionic surfaces—van der Waals (vdW) or solvent-accessible surfaces—as well as their geometric area (S_i) were evaluated. Using the experimental data sets of the Gibbs transfer energies, multivariate analyses were performed to obtain semi-empirical formulae of $\Delta G_{\mathrm{tr}}^{\circ\prime,\mathrm{W}\to\mathrm{DFP}}$ and $\Delta G_{\mathrm{tr}}^{\circ\prime,\mathrm{W}\to\mathrm{DCE}}$ based on the non-Bornian model.

Results and discussion: The number of ions in each data set was limited, so that regression analyses were successful when decreasing the number of coefficients in the regression equation from seven [1] to four:

$$\Delta G_{\mathrm{tr}}^{\circ\prime,\mathrm{W}\to\mathrm{DFP}} = \Delta A \sum S_i + \Delta B^* \sum_{E_i\le\xi} S_i E_i + \Delta B_- \sum_{\xi<E_i<0} S_i E_i + \Delta B_+ \sum_{0<E_i} S_i E_i .$$

For further details of this equation, see ref. [2]. In this study, the highest performance was generally obtained by using the combination of MK–vdW. Then, energy decomposition analysis has shown that there is a larger difference in the energy of $\Delta A \sum S_i$ (the so-called "hydrophobic" term) between highly-fluorinated and non-fluorinated ions, and has also suggested a significant repulsion of non-fluorinated ions with the fluorous solvent, DFP.

[1] H. Katano, K. Uematsu, Y. Kuroda, T. Osakai, *J. Electroanal. Chem.*, **776**, 82 (2017).
[2] T. Osakai, Y. Naito, K. Eda, M. Yamamoto, *J. Phys. Chem. B*, **119,** 13167 (2015).

2P19 Electrochemical properties of Sr_2MO_3F (M = Ni, Co, Mn) oxyfluoride cathode for all-solid-state fluoride ion battery

Zhuoran Li[1], Yanchang Wang[1], Hideonri Miki[1,2], Toshiyuki Matsunaga[1], Hiroshi Kageyama[1], Yoshihiro Tsujimoto[3], Hiroyuki Nakaki[1], Shinji Nakanishi[2], Hideki Iba[2], Kentaro Yamamoto[1], Tomoki Uchiyama[1], Koji Amezawa[4], Yoshiharu Uchimoto[1]
([1]Kyoto Univ., [2]TOYOTA Motor Corporation, [3]NIMS, [4]Tohoku Univ.)

Introduction: Recently, fluoride ion battery using fluoride ions as carriers is quite attractive, which is capable of realizing high energy density in principle. New materials, such as intercalation electrode materials, has been reported[1]. In this study, we focused on a kind of layered perovskite type structure, Sr_2MO_3F (M = Ni, Co, Mn), where the apical site is replaced by fluoride ion. Compared to Sr_2MO_4, Sr_2MO_3F is expected to improve the diffusion rate of fluoride ions. We analyzed the change of the crystal structure when insertion/desorption of fluoride ions occurs, measured electrochemical properties, and attempted to explain the kinetics of insertion/extraction reactions of F^- ions.

Experimental: Attempts were made to fluorinate Sr_2MO_3F using AgF_2 as a fluorinated reagent, and its crystal structure was measured by XRD (SPring-8 BL02B2, BL19B2) and analyzed by Rietveld method. A compacted all-solid cell was prepared using Sr_2MO_3F mixture (cathode), $La_{0.9}Ba_{0.1}F_{2.9}$ (electrolyte), and PbF_2 mixture (anode), and a charge/discharge test was conducted at 140 °C. These cells were disassembled to analyze the valence changes of elements by hard X-ray and soft X-ray XAFS. Reaction rate was also analyzed by intermittent charge/discharge measurement (GITT)[2].

Results and discussion: During charge/discharge characterization of Sr_2MO_3F, reversible insertion/extraction of fluoride ions was possible. The capacity of over two F^- per unit cell was obtained, indicating that fluorination/defluorination reaction proceeded stably up to 60 cycles. According to F^- insertion site, we continued to analyze the structure of samples by the Rietveld method. As a result (Fig. 1), when one F^- was inserted into each unit cell, both the axis lengths of *a* and *c* in crystal lattice increased, and the space group changed from I4/mmm to P4/nmm. Besides, the space group returned to I4/mmm with two F^- inserted into each unit cell during charging. From the results of XAFS measurements, we could determine the valence changes of both Mn and O when F ions were inserted/extracted.

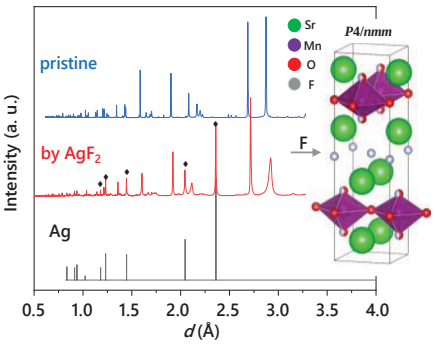

Fig. 1 X-ray diffraction patterns of cathode materials (before and after fluorination)

Reference

[1] Nowroozi, M. A.; Wissel, K.; Rohrer, J.; Munnangi, A. R.; Clemens, O., Chem Mater, 2017, 29 (8), 3441.
[2] Shen, Z.; Cao, L.; Rahn, D; Wang, C., J. Electrochem. Soc., 2013, 160 (10) A1842-A1846.

2P20 Development of *operando* techniques for investigation of catalyst-electrolyte interface by X-ray absorption spectroscopy

Kodai Kashihara, Ryusei Yamaguchi, Tomoki Uchiyama, Kentaro Yamamoto, Toshiyuki Matsunaga, Yoshiharu Uchimoto (Kyoto University, Kyoto, Japan)

Introduction: Investigating the electronic states on the electrode surface under applying potential is necessary to understand oxygen evolution activities. As the contribution of catalyst is limited to near-surface region, surface sensitive *in-situ*/*operando* measurements are required for understanding the behavior of the catalyst. In this study, we developed *operando* techniques using $La_{1-x}Sr_xCoO_{3-\delta}$ thin film model electrocatalyst for oxygen evolution in alkaline media.

Experimental: $La_{1-x}Sr_xCoO_{3-\delta}$ thin film (x = 0 - 0.4) was synthesized on 0.5 wt.% Nb-doped $SrTiO_3$ (100) substrate by pulsed laser deposition (PLD). The surface roughness was evaluated by atomic force microscope (AFM). The electrochemical tests were performed using Bio-Logic VMP-300 with a three-electrode cell comprising a thin-film fixed rotating disc electrode (HOKUTO DENKO) as the working electrode, a counter electrode (Pt wire), and reversible hydrogen electrode (RHE, reference electrode) under 0.1M KOH aqueous solution. Total reflection *operando* XAS was conducted by using home-made electrochemical cell at BL37XU, SPring-8 under 0.1M KOH aqueous solution.

Results and discussion: The onset potential of OER became smaller as increasing Sr doping level (x). This tendency was consistent with the previous report [1]. According to AFM, the surface roughness of thin films wer under 1 nm, which was small enough for total reflection XAS. Total reflection Co K-edge XAS indicated the positive shift of absorption edge of $La_{0.6}Sr_{0.4}CoO_{3-\delta}$ from 0.8 V to 1.4 V vs RHE while that of $LaCoO_3$ was not sensitive to the potential. This suggested that the surface of Co in $La_{0.6}Sr_{0.4}CoO_{3-\delta}$ had a higher oxidation state during OER as compared to $LaCoO_3$.

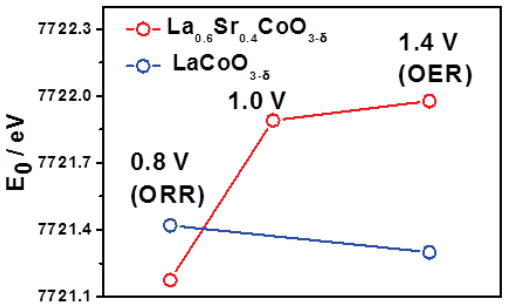

Figure 1. Co K-edge absorption edge shift for $La_{1-x}Sr_xCoO_{3-\delta}$ (x = 0, 0.4)

Acknowledgements

This research is based on results obtained from a project commissioned by the New Energy and Industrial Technology Development Organization (NEDO).

References

[1] H. Sun, X. Xu,Z Hu, L.H. Tjeng, J Zhao, Q Zhang, H.J. Lin, C.T. Chen, T.S. Chan, W. Zhou, Z. Shao, *J. Mater. Chem. A*, **7** (2019) 9924-9932.

2P21 Development of operando techniques on X-ray absorption spectroscopy under oxygen evolution reaction

Tomoya Horiguchi, Ryusei Yamaguchi, Tomoki Uchiyama, Kentaro Yamamoto, Toshiyuki Matsunaga, Yoshiharu Uchimoto (Kyoto University, Kyoto, Japan)

Introduction: Investigating the electronic states of the catalyst under electrolysis is necessary to understand oxygen evolution activities. As the bubbles from the electrode hinder the precise measurement of *in-situ*/*operando* X-ray absorption spectroscopy (XAS), we developed a new *operando* flow-cell for oxygen evolution in alkaline media. In this study, the state of Ni in $LiNiO_2$, which exhibits the high oxygen evolution reaction (OER) activity in water electrolysis [1], was investigated by operando XAS under OER potential.

Experimental: $LiNiO_2$ was synthesized from an aqueous solution containing $Ni(NO_3)_2{\cdot}6H_2O$, $LiNO_3$ and citric acid with molar ratio of 1:1:1.5. The solution was evaporated to dryness under stirring, followed by the calcination. For OER tests, polished glassy carbon electrode (a diameter of 5 mm, HOKUTO DENKO) was loaded with 0.30 mg/cm^2 of catalyst and ionomer (Nafion®). The electrochemical tests were performed using Bio-Logic VMP-300 with a three-electrode cell comprising a rotating disc electrode (HOKUTO DENKO) as the working electrode, a counter electrode (Pt wire), and RHE reference electrode under 0.1M KOH. OER durability test was evaluated by holding a potential at 1.8 V vs.RHE.

Results and discussion: According to X-ray diffraction, the synthesized $LiNiO_2$ was indexed to layered rock salt (R-3m) crystal structure. Figure 1 shows Ni K-edge *operando* XAS using flow cell under applying potential. At 1.8 V, the pre-edge peak at 8340 eV was disappeared and white line at 8350 eV was shifted to high energy. This suggested that Li^+ in crystal structure was expected to extract from its layered structure during electrolysis and lose its catalytic activity.

Acknowledgements

This research is based on results obtained from a project commissioned by the New Energy and Industrial Technology Development Organization (NEDO).

References

[1] H. Sun, X. Xu,Z Hu, L.H. Tjeng, J Zhao, Q Zhang, H.J. Lin, C.T. Chen, T.S. Chan, W. Zhou, Z. Shao, *J. Mater. Chem. A*, **7** (2019) 9924-9932.

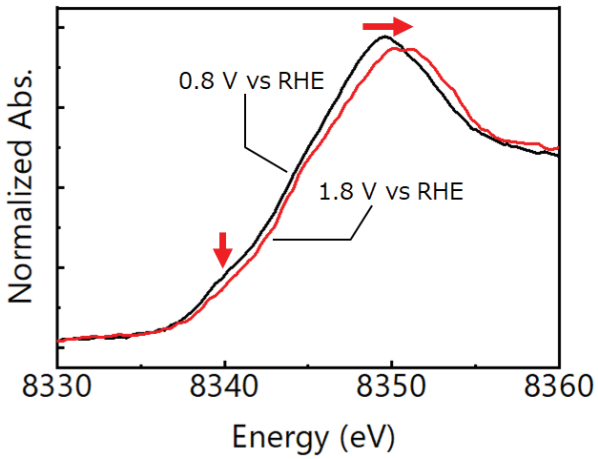

Figure 1. Ni K-edge *operando* XAS using flow cell under applying potential

2P22 Non-equivalence charges between reduction and oxidation by stripping voltammetry

Ru Wang[1,2], Kaho Imai[1,2], Koichi Jeremiah Aoki[2], Jingyuan Chen[1,2] ([1]Univ. Fukui, [2]Elecrochemistry museum)

Introduction: The deposited electric charge by stripping voltammetry should be theoretically the same in magnitude as the stripped one, but is larger than the latter actually by meticulous experiments. This effect has been explained in terms of negative capacitive current associated with the dynamically Faradaic step by the stripping[1,2,3]. It will be shown by Ag^+ and Pb^{2+} with variations of deposition times and concentrations of ionic species.

Experimental: Ag and Pb were deposited under potentiostatic conditions, and were dissolved by anodically potential scans. The deposited charge q_r and the dissolved one q_o were obtained by integration of the current –time curves as functions of deposited times, concentrations of Ag^+ and Pb^{2+} and deposited electric potentials.

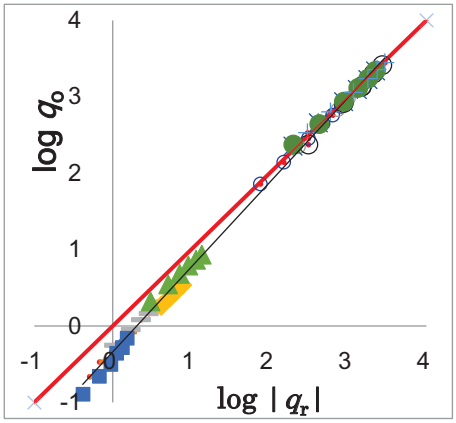

Fig. 1. Logarithmic plots of q_o against q_r for Ag^+ by anodic stripping voltammetry at several deposition times in several concentrations of $AgNO_3$, from ■ 0.2 μM to × 1.5 mM.

Results and Discussion: Double potential-step chronoamperometry showed the balance of the charge, $q_o = -q_r$. The potential scan at the dissolution revealed the unbalance $q_o > |q_r|$ (Fig. 1). A reason of the inequality is formation of positive charge (Ag^+), which blocks the Faradaic relaxation of the electric field to yield the capacitance in the negative current at the potential scan. This behavior is opposite to the double layer charging by solvent dipoles, and is satisfied with taking energy minimum.

1. K. J. Aoki, J. Chen, X. Zeng, Z. Wang, Decrease in the double layer capacitance by faradaic current, *RSC Advances*, 7 (**2017)** 22501-22509
2. K. J. Aoki, J. Chen, Effects of the dipolar double layer on elemental electrode processes at micro- and macro-interfaces, *Faraday Discussions*, 210 (**2018**) 219-234
3. K. J. Aoki, J. Chen, R. Wang, Stripped charge of Ag less than deposited one owing to negative capacitance caused by redox reactions, *Electroanalysis*, 31 (**2019**) 1-9

2P23

Electroreflectance study of cation-coated Au nanoparticles immobilized on SAM-modified Au electrodes

Risako Shiraishi, Takamasa Sagara (*Graduate School of Engineering, Nagasaki University, Nagasaki 852-8521, Japan*)

Introduction: The charge of the Au nanoparticle (Au-NP) core surface is variable by electron transfer with an electrode [1]. Fine and large-amplitude control of the charge of the Au-NPs should enable us to regulate interparticle electrostatic interaction. Thus, it is important to clarify the electrode potential dependent change of the particle charge. The dependence would be determined by the underlying SAM structure on an electrode. The aim of this study is to clearly describe the behavior of cationic trimethylammonium-terminated alkylthiol-modified Au-NPs on anionic carboxylate-terminated SAM-covered Au electrodes.

Experimental: Cationic Au-NPs were immobilized on ω-mercapto-alkanoic acid SAM-covered polycrystalline Au electrodes in ammonia buffer solution (pH = 9.2). Cyclic voltammograms (CVs) and electroreflectance (ER) spectra were measured in phosphate buffer solution (pH = 7.0). These measurements were made by the use of a Ag/AgCl/sat'd KCl reference electrode and Au wire counter electrode in a Ar gas atmosphere at room temperature.

Results and Discussion: Figure 1 shows ER spectra of the Au electrodes with Au-NPs immobilized on SAM of five different chain lengths. The positive-going bell-shaped real part ER peak indicates an increase of plasmon absorption intensity when changing the potential to more negative. Most likely, the ER response originates from charging-discharging of Au-NPs. The ER response intensity was the highest on the SAM of n = 10. In this system, the electron transfer rate constant of charging-discharging obtained by a combined use of the ER response and ac current was 8.4 × 10^3 s^{-1}. The p*K*a of the SAM-surface COOH group is lower for smaller n [2]. Therefore, we predicted that the smaller n gives rise to a greater amount of immobilized Au-NP, faster reaction rate, and greater ER response. Interestingly, the obtained results were not in line with the prediction; ER response increased with increasing the SAM chain length from n = 2 to n = 10 and decreased with n = 15 and further with n = 20. We are now in progress to see whether the n dependence originates from an optical factor or the difference in the SAM structure.

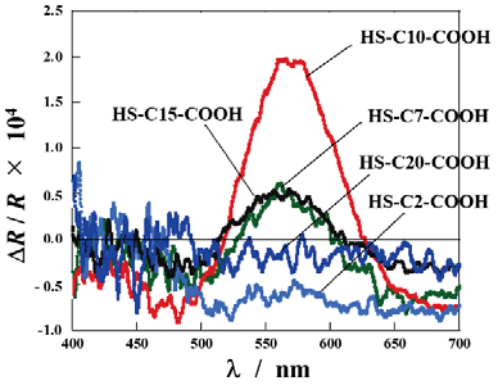

Figure 1. Real part ER spectra of the Au-NPs- immobilized Au electrodes in 50 mM phosphate buffer solution, pH = 7.0 at E_{dc} = 0.00 V with E_{ac} = 100 mV and f =14 Hz.

References: [1] A. Toyota, N. Nakashima, T. Sagara, *J. Electroanal Chem.*, **2004**, *565*, 335. [2] T. Kakiuchi, M. Iida, S. Imabayashi, K. Niki, *Langmuir*, **2000**, *16*, 5397.

2P24 Electron self-exchange (hopping) analysis of a viologen-type ionic liquid by CV and ESR

Hironobu Tahara, Akira Kitagawa, Tomoya Ikeda, Takamasa Sagara
(Graduate School of Engineering, Nagasaki University)

Introduction: Redox-active ionic liquids (RAILs) have been attracted as a functionalized ionic liquid which exhibits an electron hopping reaction between redox-active species. Electron hopping characteristics of RAILs such as viologen-type ionic liquids have been investigated but limited in electrochemical techniques.[1-3] Therefore, we have investigated electron hopping kinetics of a viologen-type ionic liquid by electron spin resonance (ESR) and cyclic voltammetry (CV) to discuss the detailed mechanism.

Experimental: A viologen-type ionic liquid $[C_4VC_7][TFSI]_2$ (Fig. 1(a)) was synthesized as our previous report.[2] CV experiments of neat $[C_4VC_7][TFSI]_2$ were performed with a two-electrode system which consists of a Au microelectrode (d = 10 μm) as a working electrode and a Pt plate as a counter electrode. ESR experiments were performed with a capillary technique. A viologen radical cation was generated by sodium borohydride as a reducing reagent.

Results and discussion: $[C_4VC_7][TFSI]_2$ produced a sigmoidal CV shape at 60 ºC (Fig.1 (b)) indicating a diffusion-limited process which is attributable to an electron hopping diffusion. At the same time, the ESR spectrum showed a singlet line shape without hyperfine resolution also attributable to an electron self-exchange (hopping) reaction. The mechanism of electron self-exchange reaction in neat $[C_4VC_7][TFSI]_2$ will be discussed with the above two experiments including the other physicochemical data.

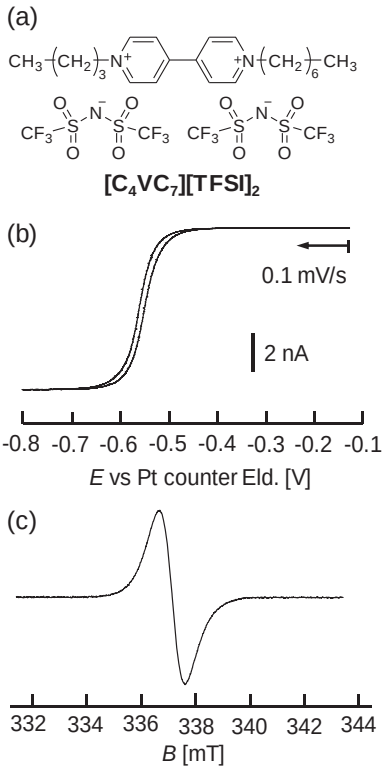

Fig. 1. (a) Chemical structure of a viologen-type ionic liquid, (b) CV of $[C_4VC_7][TFSI]_2$ at 60 ºC, (c) ESR spectrum of slightly reduced $[C_4VC_7][TFSI]_2$ at 60 ºC.

References: [1] T. Hatazawa et al., *Anal. Chem.*, 68, 597 (1996); [2] N. Bodappa et al., *J. Phys. Chem. C*, **119**, 1067 (2015); [3] N. Bodappa et al., *Electrochim. Acta*, **320**, 134559 (2019).

2P25 Effects of carbon nanostructures on direct-electron-transfer-type bioelectrocatalysis with a measure of the electrochemical effective area

Mizue Wanibuchi, Yui Takahashi, Yuki Kitazumi, Osamu Shirai, and Kenji Kano (Division of Applied Life Sciences, Graduate School of Agriculture, Kyoto University)

Introduction: Mesoporous carbons as electrode materials are often evaluated in view of weight and specific surface area. Effects of particle size, micropores, mesopores, and three-dimensional structure of carbon materials seem to be more important in the case of redox enzymes as catalysts compared with the case of inorganic metallic catalysts. In this work, three types of widely used carbon materials were compared as scaffolds for direct-electron-transfer (DET)-type bioelectrocatalysis of bilirubin oxidase (BOD): Ketjien Black EC300J (KB) with a primary particle size of 30 nm and hollow structure, vulcan (XC-72R) with a primary particle size of 30 nm, and high purity graphite SP series (JSP) with a primary particle size of 10 μm and well-developed micropores.

Experimental: An appropriate amount of carbon material suspension was mounted on polished glassy carbon (GC) electrode and dried at room temperature to evaporate the solvent. BOD was adsorbed on the carbon material-mounted GC electrode. The electrodes were left to stand in a water-saturated atmosphere. The enzyme-modified electrodes were washed with a buffer solution before electrochemical measurements. Steady-state rotating disk voltammograms were recorded in an oxygen (O_2)-saturated buffer at a rotating speed of 4000 rpm and a scan rate of 10 mV s^{-1}. A platinum wire and an Ag|AgCl|sat. KCl electrode were used as the counter and reference electrodes, respectively. Steady-state catalytic current of O_2-reduction at 0 V (i_c) were used as a measure of the DET-type activity of BOD, while non-Faradaic current (background) at 0.5 V (i_b) of the carbon material-mounted GC electrodes without BOD was used as a measure of the electrochemically active surface area.

Results and discussion: The i_c value increased with i_b and tended to be saturated for the three carbon materials. The i_c/i_b ratio at low i_b was in the following order: JSP > vulcan > KB. Micro structures of JSP seems to be very effective for DET-type reaction of BOD. Since the primary particle sizes of vulcan and KB are almost identical with each other, parts of the electrochemically active surface of KB, most probably inside faces of partially broken KB particles, are not effective as scaffolds for BOD.

2P26 Easy-to-use electrochemical endotoxin sensor

Kentaro Ito, Kumi Y. Inoue, Kosuke Ino, Yuji Nashimoto, Tomokazu Matsue, Hitoshi Shiku (Tohoku University, Japan)

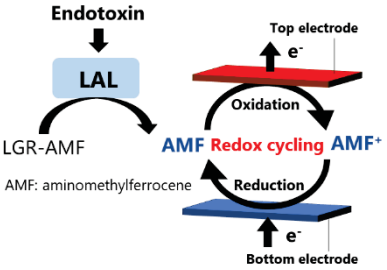

Fig. 1. Principle of endotoxin assay

There are many approaches to improve the sensitivity of electrochemical sensor. Among them, redox cycling is a especially powerful tool for a highly sensitive sensor, amplifying amperometric current by repeating reduction and oxidation of redox molecules at neighboring electrodes applied different potentials. We applied the redox cycling in a nano-space to the endotoxin sensing[1)] which requires ultra-high sensitivity for medical safety. Previously, we successfully quantified endotoxin concentration with detecting *p*-aminophenol (pAP) liberated from peptide-conjugated pAP (LGR-pAP) by *Limulus* amebocyte lysate (LAL) reaction. But, electrode surface was fouled with polymerized pAP. In this study, we characterized peptide-conjugated aminomethylferrocene (LGR-AMF) as a novel substrate for LAL based endotoxin sensing with redox cycling (Fig. 1).

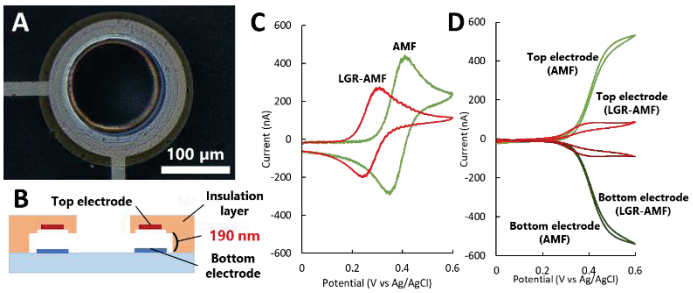

Fig. 2 (A) Optical image of the device. (B) Cross-sectional illustration of the device. CVs of AFM and LGR-AFM using the GC electrode (C) and the device (D). Adapted with reference (1).

First, we fabricated a device with a pair of electrodes facing each other across a 190 nm gap using photolithography and sputtering (Fig. 2A and B). Then, we characterized the electrochemical properties of LGR-AMF and AMF with cyclic voltammetry (CV) at a scan rate of 20 mV/s. When using the device, the potential of the top electrode was swept with 20 mV/s while the bottom electrode was biased at 0.0 V. CVs obtained with a GC disc electrode (1.0 mm in diameter) show that redox reactions of LGR-AMF and AMF are reversible with the formal potential of 0.29 V and 0.38 V, respectively (Fig. 2C). CVs obtained with the device show amplified current by redox cycling (Fig. 2D). The steady-state current of LGR-AMF and AMF are 83 and 520 nA, respectively, the difference of which is derived from the difference of diffusion coefficient of LGR-AMF and AMF. The half wave potential of LGR-AMF and AMF are 0.32 V and 0.41 V, respectively, when using the device. The formal potential shift using the device was due to the inhibition of formation of electric double layer in nano space because of the restriction of ion movement. The shape of CVs shows less electrode fouling characteristics of LGR-AMF than LGR-pAP. But further study indicated that this new substrate hardly be hydrolyzed with LAL reaction. We are now modifying the LGR-AMF substrate to more readily react with LAL.

Reference: 1) K. Ito *et al.*, *Analyst*, 2019, **144**, 3659.

2P27 Quantifying impact of cathode biofouling in the bioelectrochemical wastewater treatment system: analysis of electrochemical performance and microbial commuity

Chao-Chin Chang [1], Chang-Ping Yu [2]

Introduction:

Due to the essential functions of nutrient removal and energy harvesting, developing biofilm growth on the cathode may be beneficial both to pollution control and energy output enhancement in the microbial fuel cells (MFCs). However, biofilm could be not only beneficial but harmful to cathode performance.

Experimental:

In this study, we evaluated the influences of biofilm fouling on the scale-up of membrane-free air-cathode microbial fuel cells by utilizing electrical and electrochemical methods, including power density and polarization curves, cyclic voltammetry and electrochemical impedance spectroscopy. In addition, microbial component and morphology were analyzed by 16S rRNA and SEM.

Results and discussion:

Electrical results operated in an eight-unit air-cathode system indicated that FePc-coated cathode performance gradually declined with a nonlinear scale up of power densities. Electrochemical impedance spectroscopy showed a higher ohmic resistance on the surface of cathode, and cyclic voltammetry demonstrated a lower onset potential on these biofouled cathodes. 16S rRNA demonstrated Bacteroidetes (40%) and Proteobacteria (40%) took higher relative abundance of different phyla with *Pseudomonas* (10%), *Chlorobium* (9%) and *Dechlorobacter* (7%) as predominant genera on these cathodes.

2P28 High spatial-temporal electrochemical imaging system using closed bipolar electrode array and observation of biological phenomena

Tomoki Iwama[1], Kumi Y. Inoue[1], Hiroya Abe[2,3], Tomokazu Matsue[4] and Hitoshi Shiku[1] ([1]Graduate School of Environmental Studies, Tohoku Univ., Sendai, Japan, [2]Frontier Research Institute for Interdisciplinary Sciences, Tohoku Univ., [3]Advanced Institute for Materials Research, Tohoku Univ., [4]Center for Promotion of Innovation Strategy, Tohoku Univ.)

Introduction: Electrochemical imaging using multi-electrode array has been used for various bio-sample observations. For these observations in a smaller area of a biological sample, a higher density electrode array is required. However, conventional arrays require the presence of connecting lines between the voltage supplier and individual electrodes, which severely limits the spatial resolution of the resulting image. To overcome this problem, we have employed a closed bipolar electrode (cBPE) with electrochemiluminescence (ECL) detecting system as a new platform for bioimaging system, focusing on its feature that each cBPE need no connecting lines.

Experimental: Figure shows the schematic of cBPE imaging system. Two driving electrodes (Counter electrode, reference electrode, working electrode) were inserted to the sample cell and the detection cell. By applying a driving voltage, reduction reaction of sample molecule and oxidation reaction of the luminophore molecules occurs simultaneously, therefore, ECL signal generates on the surface of the cBPEs in the detection cell. To monitor the MCF-7 respiration activity, living MCF-7 spheroid and a dead MCF-7 spheroid treated with paraformaldehyde was put on a cBPE array. Driving voltage was applied while observing the ECL signal by CCD camera.

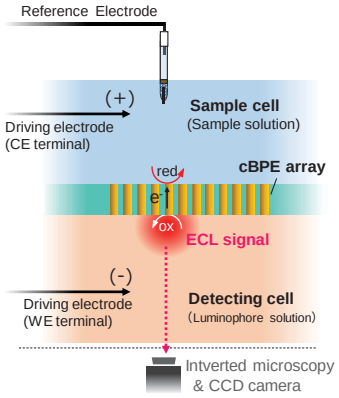

Figure Schematic of cBPE imaging system

Results and discussion: As a result of applying a driving voltage while a living MCF-7 spheroid and a dead MCF-7 spheroid was on cBPE array, a larger ECL signal decrease was observed at the position where the live cell spheroid was placed. The results indicate that the cBPE imaging system can be applied in the observation of biological activities. In future, various biological phenomena will be observed by enhancing the target molecules by using enzyme modification on cBPE array.

2P29 Monitoring the K^+ insertion/extraction process of Prussian Blue with a Solid-contact Ion-selective Microelectrode

Wei-Li Shih[1], Yi-Min Wu[1], Lin-Chi Chen[1*], Cheng-Lan Lin[2*] ([1]Department of Biomechatronics Engineering, National Taiwan University, Taipei, Taiwan, [2]Tamkang University)

Introduction: In this work, a K^+ solid-contact ion-selective microelectrode (SCISME) is fabricated and investigated as a probe for monitoring the K^+ activity variation. PEDOT is chosen as the solid contact material. To verify the idea of combination of the solid-contact ion-selective electrode (SCISE) technique and a microelectrode, the insertion/extraction process of Prussian Blue (PB) is chosen as the monitoring target.

Experimental: The K^+ SCISME fabrication process is described as follows. Firstly, a PEDOT thin film was electrodeposited on a Pt microelectrode by cyclic voltammetry. The PEDOT thin film served as the ion-to-electron transducer (IET) layer to transfer an ion-signal into an electrical signal. The K^+ ion-selective membrane (ISM) was then dip-coated on top of the PEDOT thin film, which enabled the selective detection potassium ions. For the monitoring verification, the PB thin film was electrodeposited on the substrate by amperometry. When monitoring, the PB was applied 0.6V and -0.3V vs. Ag/AgCl alternatively.

Results and discussion: Our prepared K^+ ISME exhibit a detection limit of 10^{-4} M, a sensitivity of 59.4 mV/dec, and a noise of 0.703mV/s (measured with open circuit potential method). This K^+ SCISME successfully detects the signal of K^+ insertion/extraction process of PB.

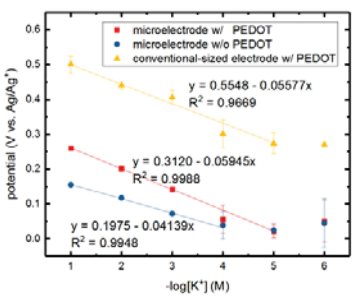

Fig.1. Comparison of the calibration lines

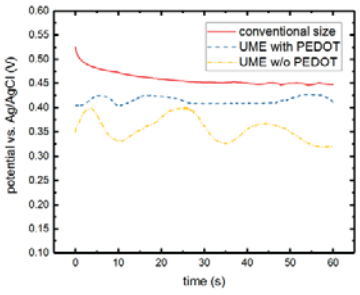

Fig.2. Comparison of the noise of the ISEs

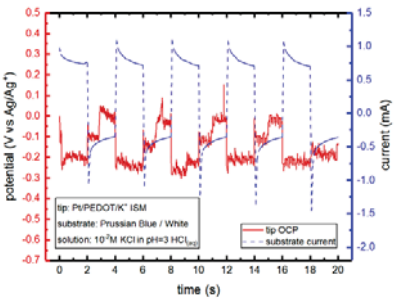

Fig.3. K^+ activity variation signal when PB conduct redox reaction

2P30 Investigation of electrochemical reaction mechanism during flash sintering of yttria-stabilized zirconia

Ho-Wei Chan[1], Hsun-Yi Chen[2] ([1,2]Department of Biomechatronics Engineering, National Taiwan University, Taiwan)

Introduction: Flash sintering is a new method to rapidly densified ceramic, which could lower sintering temperature of YSZ from 1400℃ to 850℃ and shorten sintering time from hours to seconds. Flash sintering has attracted many literatures on its mechanism due to saving lots of energy consumption during ceramics fabrication. Electrochemical reduction mechanism is one of the proposed mechanism involved in flash sintering, but less directly evidence of mass transport. In this work, we aim to investigate the electrochemical reactions during flash sintering of YSZ in atmosphere and vacuum environment. A systematic comparison of sintering results, including grain size distribution, microstructure under different atmosphere and sintering duration, were demonstrated by SEM imaging. Furthermore, we proposed different electrochemical reactions in atmosphere and vacuum environments via electrochemical impedance spectroscopy (EIS), which were conducted at initial stage of flash sintering.

Experimental: Powders were purchased from commercially available 3 mol% yttria stabilized zirconia powder with particle size of 60 nm and pressed into rectangular shape with two holes, in length of 20 mm, 15 mm in gage length, and cross section of 5 mm x 2 mm. The condition for flash sintering of YSZ was at 900℃ with $100 Vcm^{-1}$ and upper limit current at 50 $mAmm^{-2}$ in air or vacuum of 10^{-5} atm. Density and grain size of samples were measured by Archimedes' method and Image J, respectively. EIS was conducted with flash sintered YSZ at 1400℃ with 0.5 $mAmm^{-2}$, at the state just before flash event, and used potentialstatic methods, setting with 1 V and with amplitude potential of 0.2 V in frequency from 1 to 100000 Hz under atmosphere or vacuum environment.

Results and discussion: Flash sintering could be completed without external oxygen involved, but blackening region appeared on the surface of flash sintered YSZ under vacuum environment. Blackening region was occupied by partially reduced zirconia, which was confirmed by Raman analysis, and accompanied with small grains, which was predicted as ZrO_2 by EDS analysis. Therefore, we proposed oxygen anions and precipitated zirconium dominantly enhanced the diffusion rate under atmosphere and vacuum environment from the bode plot, respectively.